Rheological properties of biological materials: from cell suspensions to tissues

Andreea L. Iordan

UNIVERSITE JOSEPH FOURIER – GRENOBLE I

N° attribué par la bibliothèque

- - - - - - - - - -

THESE

pour obtenir le grade de

DOCTEUR DE L'UJF

Spécialité : Physique pour les sciences du vivant

préparée au Laboratoire de Spectrométrie Physique

dans le cadre de l'Ecole Doctorale de Physique

par

ANDREEA LUMINIȚA IORDAN

soutenance le 15 décembre 2008

—

Rheological properties of biological materials: from cell suspensions to tissues

Propriétés rhéologiques de matériaux biologiques : des suspensions cellulaires aux tissus

—

Jury :

Patrice FLAUD,	Examinateur
Lazhar BENYAHIA,	Rapporteur
Luigi PREZIOSI,	Rapporteur
Alain DUPERRAY,	Examinateur
Claude VERDIER,	Directeur de Thèse

Acknowledgement

I did not know Dr. Claude Verdier when I asked for a PhD position in his group. Now, three years later, I do not regret having become his student and I think I could not have chosen a better advisor for my PhD studies. Claude has always been there to respond to any of my queries and he gave me the freedom to develop self-responsibility. I am very thankful for his support. It has been a pleasure working together with him.

Without the help of Dr. Alain Duperray, I would have been lost many times. I have benefited much from the experience of Alain in the field of Biology. Indeed, he taught me a lot. He certainly deserves very special thanks for everything he has done for me.

I would like to thank Prof. Luigi Preziosi for having organized the Marie Curie Network and for the interest he has shown in my work. Also, I am indebted to the European Community for its financial support through the Marie Curie Research Training Network.

I would like to thank Alexei Grichine for he helped me carrying out important experiments using confocal microscopy.

I wish to thank Yves Usson, which provided me with the Edit3D_quanti software.

Furthermore, many thanks to the people at Spectro: Cécile and Shirin for the nice time we have spent sharing the same office; all the other PhD students (Valentina, Badr,

Jos, Christoph, Giovanni, David) for having created a special atmosphere; and everybody at Spectro for contributing to a stimulating and cooperative working atmosphere.

Many thanks to my special friends: Livia, Monica, Ioana, Helga, Magalie, Anne-Marie and Maur, Raul, Olivier, Mihai, François. I also would like to acknowledge David Basanta for his precious advice.

Thanks to my former colleagues from Romania (IFIN-HH): Nenea, Bogdan, Titi, Victorița, Diana, Adriana, Ileana, Mihai, Nae, Caly.

I would not have gone through all the ups and downs of PhD, and life also, if I had not had Benoît and my family at my side constantly. I therefore wish to express my deepest gratitude to them for their confidence, encouragements and appreciation.

Contents

This thesis is divided into five chapters. **Chapter 1** is an introduction to the subject. **Chapter 2** reminds some basic concepts of rheology of cell tissues and some already existing models describing the viscosity of suspensions. **Chapter 3** presents the techniques and software used for data processing. The experimental results on the rheology of CHO cell suspensions are presented and discussed in **Chapter 4**. **Chapter 5** presents the main results obtained with CHO cells in a 3D collagen network. Finally, **Chapter 6** draws conclusions.

Sommaire

Cette thèse est divisée en cinq chapitres. Le **chapitre 1** est une introduction au sujet. Le **chapitre 2** rappelle certains concepts de base de la rhéologie des tissus cellulaires et de certains modèles déjà existants décrivant la viscosité des suspensions. Le **chapitre 3** présente les techniques et les logiciels utilisés pour le traitement des données. Les résultats expérimentaux sur la rhéologie des suspensions de cellules CHO sont présentés et discutés dans le **chapitre 4**. Le **chapitre 5** présente les principaux résultats obtenus avec les cellules CHO dans un réseau 3D de collagène. Enfin, le **chapitre 6** tire les conclusions.

Contents

1. Introduction

This work has been carried out within the framework of a Marie Curie Network (RTN) entitled "Modelling, Mathematical Methods and Computer Simulations of Tumour Growth and Therapy" (2004-2008) [1], regrouping twelve Universities. The network has been coordinated by the Politecnico di Torino (Profs N. Bellomo, L. Preziosi). This network is concerned with modelling of biological problems related to cancer. Several teams from different countries are involved in this network and have worked on:

- tumour growth (Fig. 1.1),
- angiogenesis (development of capillary vessels to provide tumours with oxygen),
- competition between cells within blood,
- metastasis (development of a secondary tumour after escape of cells from a primary tumour).

Fig. 1.1: Sketch showing tumour cell metastasis. Invasive cancer cells migrate and grow from the primary tumour site into the surrounding tissue towards blood vessels.

The network activities are concerned with all the different scales. At the *subcellular level*, certain cancer cells lost their ability to control their fate, therefore they divide very rapidly due to gene alteration. Then such cells interact with each others and compete with the immune system (within blood or within tissues) or migrate, this is the *cellular level*. Finally cells form tumours or suspensions (*macroscopic scale*), but they also migrate through tissues, therefore, it is also important to control the relevant mechanical properties at this scale.

The south French team (France S, coordinator: C. Verdier) was in charge of experimental aspects at the cellular and macroscopic scale, and has paid attention to cell interactions, in relation with the development of metastases. It has been shown that during cancer metastasis, after cells have escaped from a primary tumour, they can penetrate within the blood flow (intravasation) and they are transported over long distances (Fig. 1.1). Some of them survive, can eventually adhere to the endothelium and manage to extravasate, i.e. penetrate through the (small) inter-endothelial junctions, while undergoing very large deformations (Fig. 1.1). In order to do so, cells need to possess special rheological properties [Verdier 2003] and must be able to modulate them [Mollica 2007],[Preziosi 2003],[Bellomo 2003]. This work actually belongs to the microscopic scale.

On the other hand, it is also important on our part to consider the macroscopic scale. Indeed, tumours are viscoelastic systems which are not so well characterized yet. Then cells migrating within tissues (Fig. 1.1.) are also affected by the mechanical properties of these tissues (environment) and it is of importance to determine these precise rheological properties. Finally, cells which are carried out within the blood can affect the flow conditions, therefore models of blood or cell suspensions are precious to understand the complex behaviour of biological tissues. Our final aim is to provide models

describing the behaviour of cells, their interactions and their collective behaviour (suspensions and tissues).

In the present work, we will focus mainly on the mechanical properties that cell suspensions possess, and we will also study the effect of the environment. This will allow us to start from *cell suspensions* and then include other components (such as extra cellular matrix) in order to reconstitute a *model tissue.*

A good starting model is blood (ensemble of red blood cells and a few white cells) where cells can aggregate to form "rouleaux" [Chien 1967a], [Coussot & Grossiord 2002]. It is of particular interest to consider the viscoelastic behaviour of such suspensions because they can give rise to interesting behaviours under flow (yield stress, plug flow, blood clothing). This serves as an initial model to understand the particular properties of cell suspensions.

The second point is the understanding of tissue properties, in order to come up with rheological models capable of describing their behaviour. The four processes essential for the construction of a tissue are:

1. Proliferation: from one single cell, new cells are produced.
2. Differentiation: cells acquire different functions, at determined locations.
3. Interactions: cells coordinate their behaviour with that of their neighbours.
4. Motion: cells are rearranged in order to structure tissues, then organs.

Tumours, in particular, are caused by abnormal proliferation.

Fig. 1.2 sketches a tumour as compared to a normal organised tissue. Tumour has a large number of dividing cells, which occurs in an uncontrolled manner, thus leading to variations in cell size, shape and loss of normal tissue organization. The extracellular space can be filled with a network of cross-linked proteins (collagen, laminin,

fibronectin, etc.) known as the extracellular matrix (ECM), which form the structure of tissue.

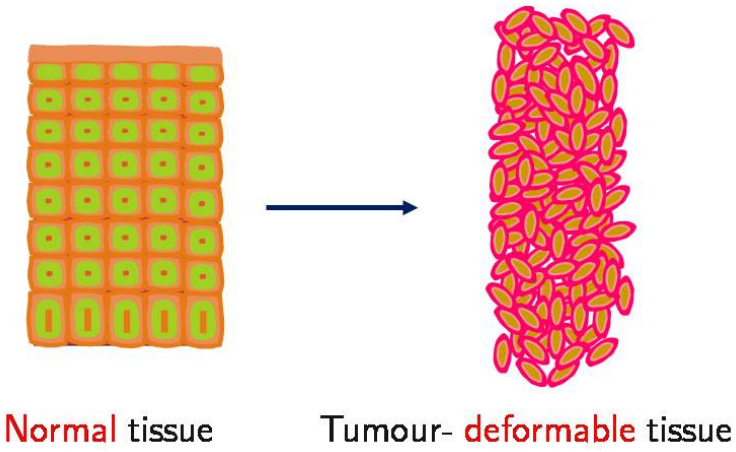

Fig. 1.2: Comparability between normal tissue and tumour.

This helps hold cells and tissues together, and provides an organized environment within which migrating cells can move and interact. Previous works (for example [Hamilton 1998]) have shown that typical tumours grow like spheroids, with a necrotic part in the centre and that the outer part keeps proliferating (while fed by nutrients) and therefore the tumour increases in size. Tumours can be also affected by the environment, in particular its rigidity [Helmlinger 1997]. In any case (normal tissue or tumour) interactions between cells and the ECM are very complex. Cells continuously remodel the ECM by digesting part of it and at the same time they rebuild it by making their own ECM. This process can also be affected by the stress applied to the tissue [Mollica 2007].

The object of this PhD thesis is concerned with the biomechanical properties [Fung 1996] of suspensions and tissues, and is based on the following strategy :

1. To study the microstructure of the tissue, using microscopy or relevant techniques, in order to determine the geometry and complex organisation of the systems at hand.
2. To determine the tissue rheological properties in normal living conditions using rheometry.
3. To propose theoretical models and compare them with experimental data, and determine scaling laws (viscosities, moduli, yield stress) to provide new tools helpful for modelling suspensions, tissues and tumours.
4. To analyze the effect of cell interactions and their interactions with the environment (i.e. the ECM).

Note that we will only pay interest in the latest two cell processes of the construction of a tissue, which were described previously: interactions and motion of the cells within the tissue and in particular the results of these two processes, deformation. We will neglect grow as this has been studied by other groups [Byrne & Preziosi 2003], [Drasdo & Hohme 2005].

In our work, we sought to characterize, using mechanical devices, the behaviour of cell suspensions and tissues. Rheological experiments on cell suspensions were first conducted. We changed the concentration of these suspensions over a wide range: from dilute to concentrated solutions. In particular, we were able to characterize the flow properties of cells as well as their viscoelastic properties. It should be noted that these experiments were carried out using a particular animal cell line (CHO, Chinese Hamster Ovary) [Zhao 2006]. Two characteristics of CHO cells motivated our choice: they belong to the fibroblasts family, a usual cell class also present in tissues (e.g. connective tissues), and it is possible to modify them genetically. This is the first part of the present work.

In the second part of the thesis we designed a tissue model and measured its viscoelastic properties, to see the difference between cell aggregates and tissues. This involves combining cells together with collagen fibres, in a culture medium, as described in Fig. 1.3.

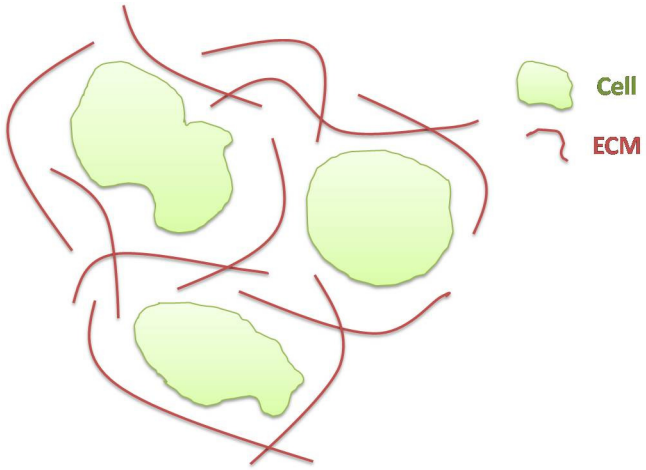

Fig. 1.3: Sketch of a model tissue including cells and ECM.

We realized, when carrying out microscopy visualisation, that cells play a very active role by remodelling the ECM matrix (collagen here). Finally we tried to understand the rheological properties of such systems by proposing a microstructural reorganisation process which controls the mechanical properties.

This model system can serve as a basis for new experimental approaches for validating theoretical models (in particular tumour growth models [Preziosi 2008]). Moreover, it may also serve as a model system for testing therapies.

Résumé français

Le chapitre 1 est une introduction au sujet. Ce travail de thèse a été réalisé dans le cadre d'un réseau européen Marie Curie traitant de la modélisation des problèmes biologiques reliés au cancer. Les activités de ce réseau se font à plusieurs échelles : subcellulaire, cellulaire et macroscopique. Au niveau subcellulaire, les cellules cancéreuses perdent leur capacité à contrôler leur rythme biologique. Elles se divisent alors anarchiquement, conséquemment à des défauts subis par leur ADN. Ceci mène à une prolifération donnant naissance à des tumeurs malignes. Au niveau cellulaire, les cellules cancéreuses interagissent entre elles ou avec d'autres cellules et certaines parviennent à s'échapper de la tumeur initiale par perte d'adhésion. Elles pénètrent alors dans le sang (grâce à l'angiogenèse, c'est-à-dire la formation de néo-vaisseaux qui vont alimenter la tumeur en oxygène) et entrent en compétition avec le système immunitaire. Les cellules qui survivent peuvent parfois réussir à passer au travers de la paroi vasculaire pour aller former une tumeur secondaire. A l'échelle macroscopique, les cellules forment des tumeurs ou des suspensions dont les propriétés ne sont pas toujours bien maîtrisées en termes de rhéologie. C'est pourquoi, l'équipe française coordonnée par C. Verdier a choisi de s'intéresser aux échelles cellulaire et macroscopique, en ce qui concerne les interactions cellulaires et les propriétés rhéologiques.

L'objectif de cette thèse consiste en l'étude des propriétés rhéologiques des suspensions et des tissus, et se base sur la stratégie suivante:

- déterminer les propriétés mécaniques, par rhéométrie, des suspensions et des tissus, en passant de l'un à l'autre par l'ajout de composants de la matrice extracellulaire (MEC),
- étudier la microstructure des matériaux biologiques, en utilisant principalement la microscopie optique,

- enfin, proposer des modèles théoriques et les comparer avec les données expérimentales, afin de déterminer les lois de comportement (viscosité, modules visqueux et élastique, contrainte seuil) pour fournir de nouveaux outils utiles à la modélisation des suspensions, des tissus et des tumeurs.

2. Rheological properties of suspensions

Nature and industry provide us with a vast range of materials composed of complex elements in suspension: emulsions, foams, and suspensions of solid particles, etc. A suspension or dispersion consists of discrete particles randomly distributed in a fluid medium. Generally we divide suspensions in three categories: solid particles in liquid medium (suspension), liquid droplets in a liquid medium (emulsion), and gas in a liquid (foam).

For a better understanding of the behaviour of cell suspensions and model tissues (cell suspension embedded into collagen extracellular matrix), we review in this chapter the rheological properties of suspensions of particles in a liquid medium. Section 2.1 and 2.2 present some basic concepts of viscosity of suspensions and viscoelasticity, Section 2.3 describes the yield stress and Section 4 is a review of already existing models predicting the viscosity of suspensions.

2.1 The concept of flow and viscosity

What is rheology? The term "rheology" is due to Bingham in 1920 and comes from the Greek verb *rheos,* to flow. Thus rheology means the study of flow and deformation. In principle, it should include everything dealing with the flow behaviour. However, in practice rheology has usually focused on the study of fundamental relations, called *constitutive relations*, relating forces and deformation of materials, primarily liquids.

The simplest and probably first relation between force and deformation (the first constitutive equation) is Hooke's law: the force is proportional to the deformation or

$$\tau = G\gamma_0$$

Here τ is the shear force per unit area or *stress* (expressed in Pa.) and γ_0 is the relative length change or *strain* (dimensionless). G is the constant of proportionality called *elastic modulus.* It is an intrinsic property of a material. For liquids, the simplest constitutive equation is Newton's law: the stress is proportional to the rate of straining (shear rate), or $\dot{\gamma} = d\gamma/dt$,

$$\tau = \eta\dot{\gamma}$$

where η, the Newtonian *viscosity,* is the constant of proportionality.

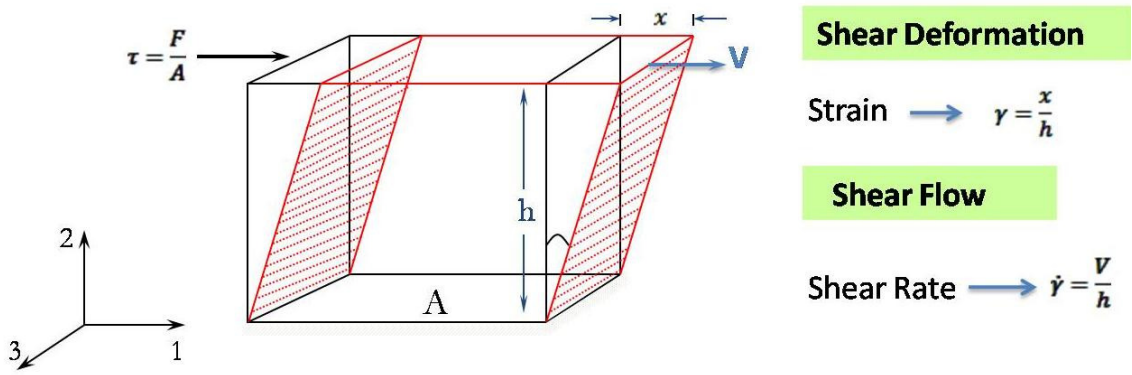

Fig. 2.1: Velocity profile in steady simple shear flow.

Steady simple shearing flow is shown in Fig. 2.1: the resistance which arises from the absence of slip between the liquid parts, other things being equal is proportional to the velocity with which the parts of the liquid are separated from one another (Newton). The upper plane moves with relative velocity V and the length of deformation between the planes is equal to x. The force per unit area required to produce the motion is F/A and is proportional to the shear rate V/h. The strain is defined by $\gamma = x/h$. For more

details of the steady simple-shear flow associated with Newton's postulate (Fig. 2.1), we can conveniently express the velocity V in the mathematical form:

$$V_1 = \dot{\gamma} x_2, \;\; V_2 = V_3 = 0$$

where V_1, V_2, V_3 are the velocity components in the 1, 2 and 3 directions, where $V = V_1$ in Fig. 2.1.

An instrument designed to measure viscosity is called a *viscometer*. A viscometer is a special type of *rheometer* (defined as an instrument for measuring rheometrical properties) which is limited to the measurement of viscosity. The current unit (SI) of viscosity is the Pascal-second, abbreviated to *Pa.s*. In Chapter 3 we give general examples of the relevance of the viscosity to a number of practical situations; we discuss its measurement using various rheometer geometries; in the following discussion we study its variation with experimental conditions such as shear rate, time of shearing and temperature.

2.1.1 The shear-dependent viscosity of non-Newtonian liquids

Definition of Newtonian behaviour- Because we concentrate on non-Newtonian viscosity behaviour in this section, it is important that we first emphasize what a Newtonian behaviour is, in the context of the shear viscosity. Newtonian behaviour in experiments conducted at constant temperature and pressure has the following characteristics:

1. The only stress generated in simple shear flow is the shear stress σ, the two normal stress differences being zero. In the case of a Newtonian liquid, the stress distribution for such a flow can be written in the form:

$$\sigma_{21} = \eta\dot{\gamma}, \;\; \sigma_{13} = \sigma_{23} = 0, \qquad \sigma_{11} - \sigma_{22} = 0, \qquad \sigma_{22} - \sigma_{33} = 0,$$

and there would be little purpose in considering anything other than the shear stress σ_{21}, which we denoted as σ in Newton's law. It is usual to work in terms of normal stress differences rather than normal stresses themselves, because it allows eliminating the pressure term.

2. The shear viscosity does not vary with shear rate.
3. The viscosity is constant with respect to the time of shearing and the stress in the liquid falls to zero immediately after the shearing has stopped.

A liquid showing any deviation from the above behaviour is called a *non-Newtonian fluid*.

2.1.2 The shear-thinning non-Newtonian liquid

When viscometers became available to investigate the influence of shear rate on viscosity, scientists found departures from Newtonian behaviour for many materials, such as suspensions, emulsions and polymer solutions. In the majority of cases, the viscosity was found to decrease with increasing shear rate, giving rise to what is now generally called *shear-thinning* behaviour. For shear-thinning materials, the general shape of the curve representing the variation of viscosity with shear stress is shown in Fig. 2.2. An equation that predicts the shape of the general flow curve is the power law model. For steady shear the power law becomes: $\sigma_{12} = \sigma_{21} = k\dot{\gamma}^n$ or $\eta = k\dot{\gamma}^{n-1}$. For $n < 1$, the fluid shows shear-thinning behaviour.

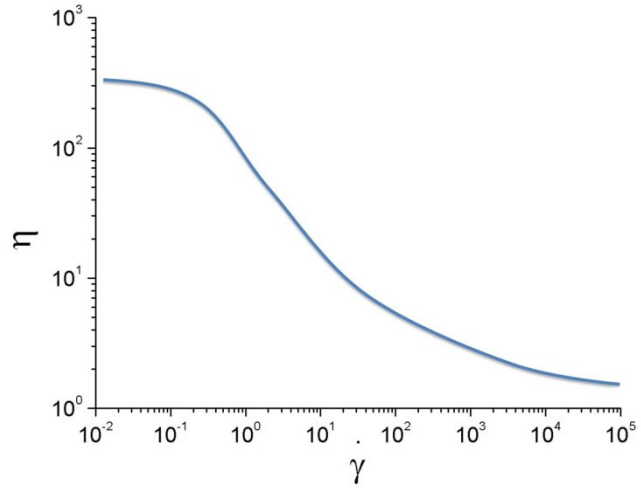

Fig. 2.2: Viscosity versus shear rate (log-log scale) for a shear-thinning non-Newtonian liquid.

For $n < 1$, the fluid shows shear-thinning behaviour.

2.1.3 The shear-thickening non-Newtonian liquid

It is possible that during deformation of a material some rearrangements of the microstructure take place such that the resistance to flow increases with shear rate. Typical examples of the shear-thickening phenomenon are given in Fig. 2.3.

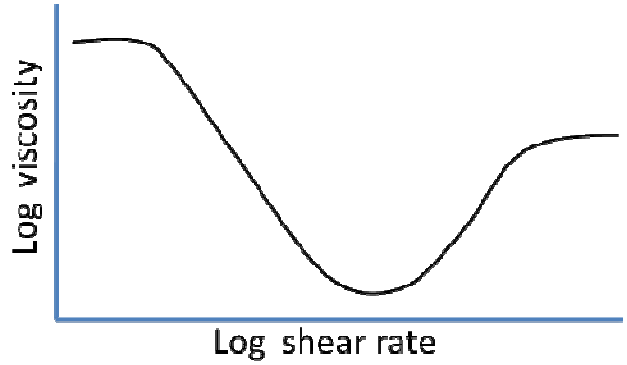

Fig. 2.3: Viscosity versus shear rate with shear-thickening behaviour at high shear rates.

It will be observed that the shear-thickening region extends only for high shear rates. If we assume again that $\eta = k\dot{\gamma}^{n-1}$, the power-law model can usually be fitted to the data in the high shear region (right part of the curve) with a value of n greater than unity.

2.1.4 Time effects in non-Newtonian liquids

Transient shear stress (Fig. 2.4.a) - we have assumed that for a given shear rate results in a corresponding shear stress, whose value does not change as long as the value of the shear rate is maintained. In fact the previous curves (Fig. 2.2 and Fig. 2.3) were obtained for the limiting steady state. Usually, the measured shear stress, and hence the viscosity, changes (increase or decrease) after application of a given shear rate. This is shown in Fig. 2.4.

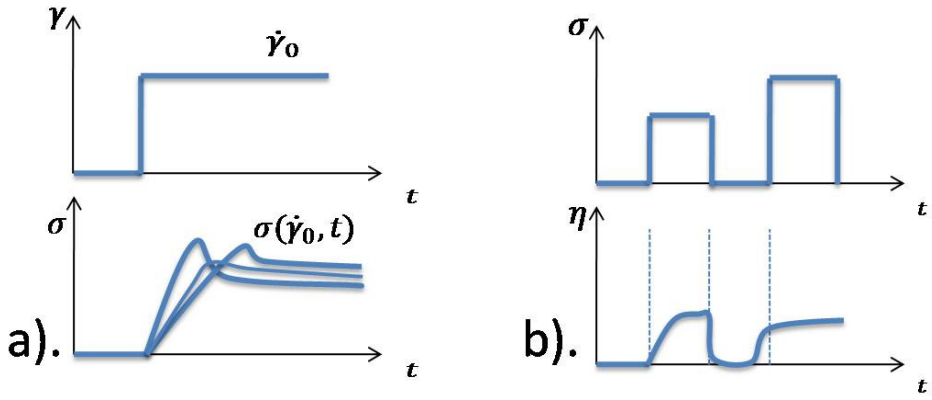

Fig. 2.4: a). Transient shear stress with possible overshoot; b). Thixotropy.

In all curves, the steady shear stress is obtained for large times and corresponds to the value to be used for calculation of the viscosity.

Thixotropy (Fig. 2.4.b) - according to the general definition, a gradual decrease of the viscosity under shear stress is followed by a gradual structure recovery when the stress is removed. This viscosity effect is linked to the yielding character of suspensions. Indeed, thixotropy is often correlated with the presence of a yield stress, but not necessarily the other way. A yield stress fluid has a certain internal structure which can break when flow occurs. At rest this structure generally recovers rapidly. In practice the typical rheological properties of thixotropic fluids are viscosity decrease in time and increase of apparent yield stress with time when at rest. Both effects are related to the competition between the destructing and restructuring effects.

2.1.5 The general form of the viscosity curve for suspensions

Typical viscosity/shear rate curves for suspensions of solid particles (at different concentrations) are shown schematically in Fig. 2.5.

The first Newtonian plateau at low shear rates is followed by the power-law shear-thinning region (at moderate concentrations ϕ) and then by a flattening effect until a second Newtonian plateau is reached (difficult to measure). When concentration increases, there is an increase in the viscosity of suspensions of solid particles. The important parameter here is ϕ the volume fraction (or the amount of material suspended in the liquid). The reason why volume fraction is so important is that the rheology depends to a great extent on the hydrodynamic forces which act on the surface of particles or aggregates of particles, as we will see when describing the models.

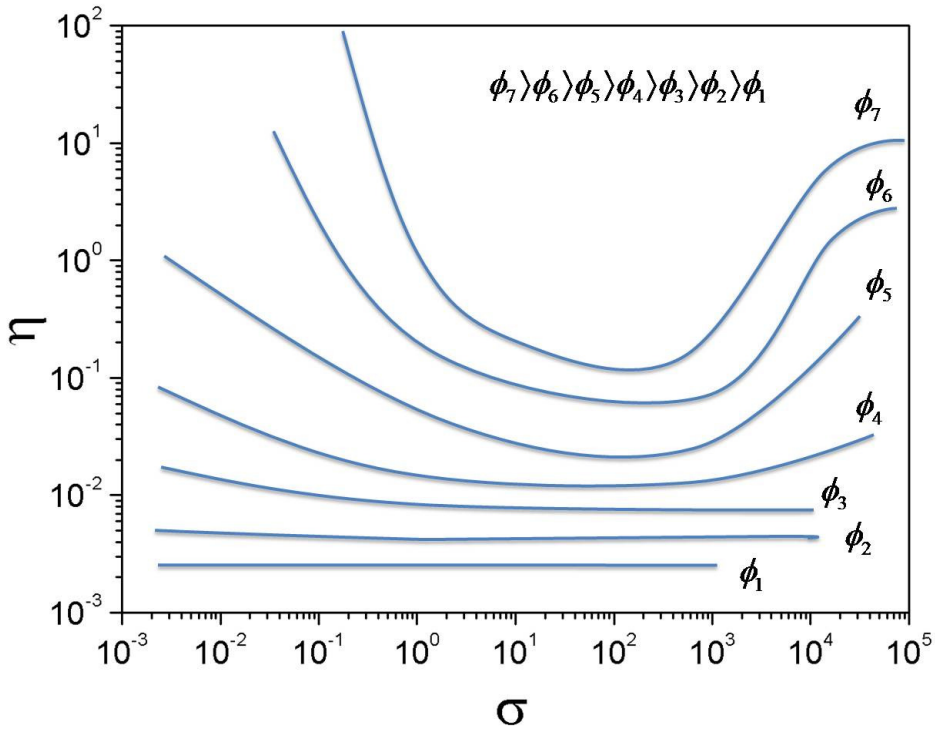

Fig. 2.5: Viscosity versus shear stress for aqueous suspensions of charged polystyrene copolymer spheres at various volume fractions ϕ, redrawn from [Larson 1999].

Fig. 2.5 shows that for large enough concentrations, the viscosity can increase with shear rate (shear thickening). Finally, Fig. 2.5 also shows that for higher concentrations ϕ , at small shear rates (or large viscosities), the shear stress reaches a limiting value called the yield stress, as will be explained in Section 2.3.

2.1.6 Summary of the forces acting on particles suspended in a liquid

In flowing suspensions three kinds of forces usually coexist to various degrees. First, there are those of colloidal origin that arise from interactions between the particles.

These are controlled by the properties of the fluid such as polarizability, but not by viscosity. These forces can result in an overall repulsion or attraction between the particles. The former can arise, for instance, from like electrostatic charges or from entropic repulsion of polymeric or surfactant material present on the particle surfaces. The latter can arise from the van der Waals attraction between the particles or from electrostatic attraction between unlike charges on different parts of the particle. If the net result of all the forces is an attraction, the particles flocculate. Contrarily, total repulsion means that they remain separate (i.e. dispersed or deflocculated). Each colloidal force has a different rate of decrease from the surface of the particle and the estimation of the overall result of the combination of a number of these forces operating together can be quite complicated. Fig. 2.6 shows the form of some single and combined forces [Barnes 1989].

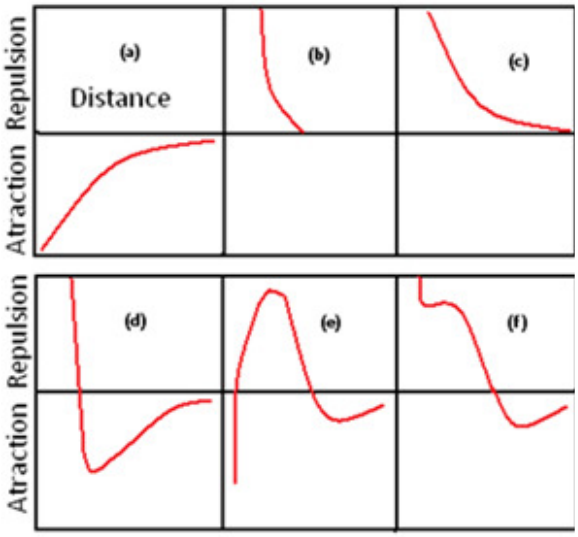

Fig. 2.6: Examples of the typical interaction Forces between a pair of sub-micron particles: (a) van der Waals attraction; (b) Repulsion due to adsorbed macromolecules; (c) Electrostatic repulsion due to the presence of like charges on the particles and a dielectric medium; (d) A combination of (a) and (b); (e) A combination of (a) and (c); (f) A combination of (a), (b) and (c). Redrawn from [Barnes 1989].

Secondly, we must consider the Brownian (thermal) randomising force. This force is strongly size-dependent, so that below a particle size of 1 μm, it has a big influence. This force ensures that the particles are in constant movement and any description of the spatial distribution of the particles is a time average.

Thirdly, we must take into account the viscous forces acting on the particles. The viscous forces are proportional to the local velocity difference between the particle and the surrounding fluid. Hence the way these affect the suspension viscosity enters via the viscosity of the continuous phase which then scales all such interactions. Thus an important parameter is the *relative viscosity* η_r defined as the ratio of the viscosity of a solution to that of the solvent.

The presence of isolated particles means deviation of the fluid flow lines and hence an increased viscosity. At higher concentrations, more resistance arises because particles have to move out of each other's way. When particles form flocculated structures, even more resistance is encountered because of the flocs, by enclosing and thus immobilising some of the continuous phase; this has the effect of increasing the apparent phase volume, thus again giving a higher than expected viscosity.

2.1.7 Maximum packing fraction

The influence of particle concentration on the viscosity of the concentrated suspensions is best determined in relation with the maximum packing fraction. There must come a time, as more and more particles are added, which gives continuous three-dimensional contact throughout the suspension, thus making flow impossible, i.e. the viscosity tends to infinity. This will be also correlated with the existence of the yield stress discussed later.

The volume fraction at which this happens is called the maximum packing fraction ϕ_m and its value will depend on the arrangement of the particles. Maximum packing fractions thus range from approximately 0.5 to 0.75. The maximum packing fraction, as

well as being controlled by the type of packing, is very sensitive to particle-size distribution and particle shape. Geometrically, considering that particles are spherical and identical in size, the limiting theoretical maximum packing fraction can be calculated assuming packing types: Face-centred cubic ($\phi = 0{,}74$), Simple cubic ($\phi = 0{,}52$), etc.

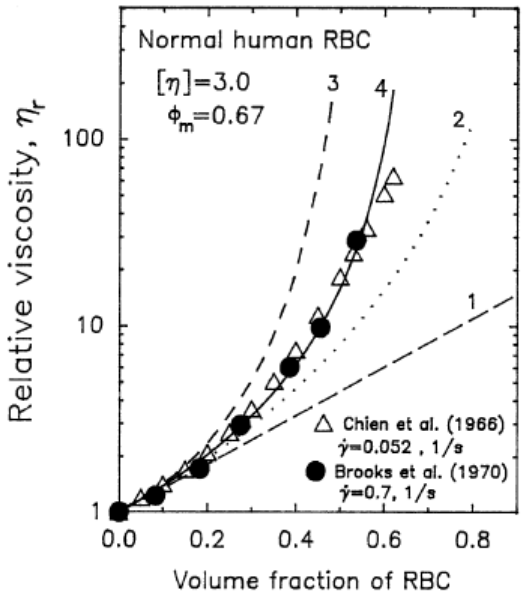

Fig. 2.7: Behaviour of a suspension of normal RBCs as a function of concentration [Pal 2003].

Fig. 2.7 shows how the relative viscosity can depend on volume fraction, in particular in the vicinity of ϕ_m.

The comparison between the experimental data of normal RBC suspensions at low shear rate and predictions of various models are shown [Pal 2003] . We can see that for small concentrations of cells, at constant shear rate, the viscosity is linear. For higher concentrations, the interactions between particles are stronger and viscosity is increasing quickly. Finally at concentrations close to ϕ_m, the viscosity becomes very high (possibly infinite).

2.2 Viscoelasticity

Viscoelastic properties of suspensions arise from particle interactions of all kinds. Elasticity comes from the elasticity of the deformable objects, whereas viscous effects are mainly due to the interstitial fluid. If these require a preferred arrangement of the particles at rest in order to fulfil some minimum energy requirement, there will always be a tendency for the suspension to return, or relax, to this arrangement. This return is due to the relaxation time, a characteristic time (λ) of the system. We compare it with a typical experimental time (t_{exp}):

- As $t_{exp} \ll \lambda$ (short times or high frequencies) the system behaves elastically,

- As $t_{exp} \gg \lambda$ (long times or small frequencies) the system behaves in a viscous way.

It is possible to make small perturbations, i.e. to impose *small-amplitude oscillatory shearing* in order to measure the combined response of the material. This is another way to explore the rates of structural rearrangement within a complex fluid, and one that does not significantly deform the fluid's microstructure. The sample is deformed by an applied sinusoidal strain:

$$\gamma = \gamma_0 sin\omega t$$

For small enough γ_0, the stress can be assumed to be sinusoidal at the same frequency.

$$\sigma = \sigma_0 \sin(\omega t + \varphi)$$

where φ is the phase angle.

Such data is analyzed by decomposing the stress wave into two waves of the same frequency ($sin\,\omega t$) and one 90 degree out of phase with this wave ($cos\omega t$).

$$\sigma(t) = \gamma_0[G' \sin(\omega t) + G'' \cos(\omega t)]$$

This composition suggests two dynamic moduli, G' is called the *storage modulus* and G'' is called the *loss modulus*.

The storage modulus represents storage of elastic energy, while the loss modulus represents the viscous dissipation of that energy. The ratio G''/G' , which is called the loss tangent $\tan\delta$, is high ($\gg 1$) for materials that are *liquid-like*, but is low ($\ll 1$) for materials that are *solid-like.* The *complex modulus* G^* is defined by $G^* = G' + iG''$, where i is the imaginary number ($i = \sqrt{-1}$).

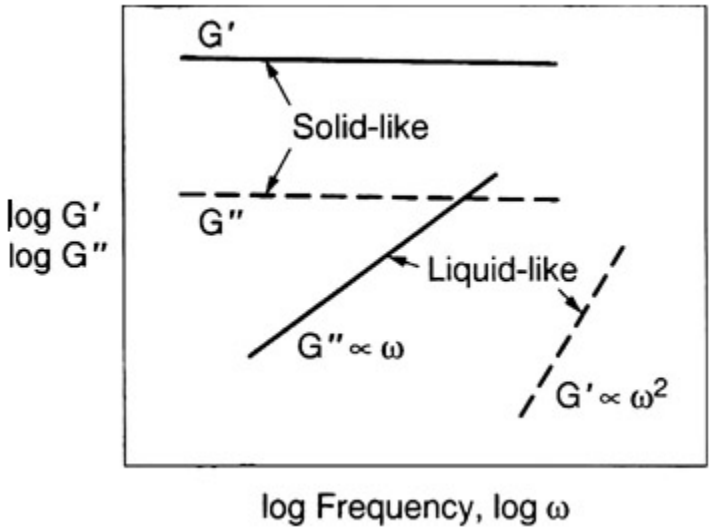

Fig. 2.8: Illustrations of frequency-dependent storage and loss moduli G' and G'' for prototypical "liquid-like" and "solid-like" material [Larson 1999].

The storage and loss moduli G' and G'' for our prototypical *liquid-like* and *solid-like* fluids are shown in Fig. 2.8. For the *liquid-like* fluid, the storage modulus is much lower than the loss modulus, and it scales with frequency as $G' \propto \omega^2$, the loss modulus is linear in frequency, $G'' \propto \omega$. The low-frequency *liquid-like* region in which G' and G'' obey these power laws is called the terminal region (i.e. Newtonian region). For the *solid-like* fluid, $G' \gg G''$, and G' is nearly frequency-independent. For other types of complex materials such as cell suspensions we will pay attention to two things:

- the order of magnitude of (G', G''),
- the typical slopes of (G', G'') versus ω in log-log scale .

2.3 Yield stress

When solids, or very viscous liquids, are subjected to stresses that are not high enough to cause them to flow, a process known as *yield,* or *plastic deformation*, can occur. This phenomenon strongly resembles the dislocations that may occur in a crystalline solid structure. Yield is especially important in metals, they have a crystalline arrangement of atoms and they deform irreversibly under high stresses, rather than fracturing [Hirsch & Mott 1975]. Yield is also important in glassy solids [Bowden 1973] and in liquids near their glass transition points. Yielding occurs at stresses above the *yield stress* σ_s, which depends weakly on strain rate and temperature. At stresses below σ_s the material is elastic, deforms reversibly and recovers its original shape when the stress is removed. Above σ_s, the material deforms irreversibly so that there is only partial recovery.

Fluids that do not flow unless they are subjected to a certain load (stress) are widely used in both cosmetic and industrial applications; well-known examples are mayonnaise (an emulsion), shaving foam, wet and dry sand and toothpaste. Examples well known to the rheologist include many polymer gels like carbopol [Magnin & Piau 1990] and colloidal gels like oil drilling fluids [Moller 2006]. The most important characteristic of these materials is that they can behave as solids under small applied stresses, and liquids at high stresses. In spite of the macroscopic similarity of these materials, the microscopic mechanism for their behaviour is quite different.

Yield stress fluids can be defined as fluids that can support their own weight to a certain extent i.e. can support shear stresses without flowing as opposed to Newtonian fluids. As a consequence, a yield stress fluid on an inclined plane will not flow if the slope is below some critical angle, but will flow as soon as the angle becomes large enough. One of the simplest constitutive equation (1D) capturing this phenomenological behaviour is given by (Bingham):

$$\sigma = \sigma_s + \eta\dot{\gamma} \quad \text{if } \sigma \geq \sigma_s \text{ and}$$

$$\dot{\gamma} = 0 \text{ if } \sigma \leq \sigma_s$$

with σ being the applied shear stress, σ_s the yield stress and $\eta\dot{\gamma}$ a function of the shear rate $f(\dot{\gamma})$. This law is called the Bingham law. It is fairly well verified experimentally, in the case of suspensions, pastes, gels. An alternative of this law is Casson's model, which was used to model blood [Fung 1996], considered as a suspension of red blood cells and white cells in a Newtonian fluid (plasma). The behaviour of blood follows the law of Casson quite well,

$$\sqrt{\sigma} = \sqrt{\sigma_s} + \sqrt{\eta\dot{\gamma}} \quad \text{if } \sigma \geq \sigma_s$$

$$\dot{\gamma} = 0 \quad \text{if } \sigma \leq \sigma_s$$

and the viscosity as well as the yield stress σ_s are both functions of the hematocrit H (volume percentage of cells in the presence). Fig. 2.9 shows the dependence of viscosity η versus shear rate $\dot{\gamma}$ for real Red Blood Cell (RBCs) suspensions:

- At low shear rates, σ is close to yield stress σ_s, therefore $\eta \sim {}^{\sigma_s}/_{\dot{\gamma}}$ and varies with the slope -1 (log-log),
- At higher shear rates, the viscosity varies like $\eta_0(H)$, a constant independent of the shear rate.

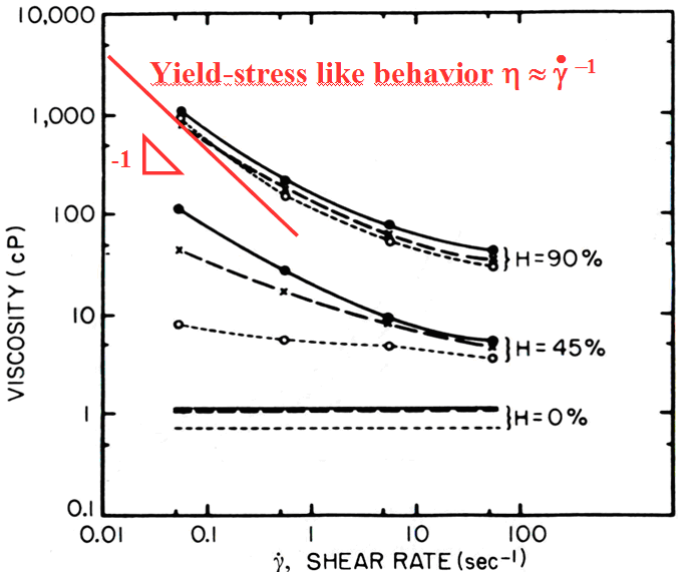

Fig. 2.9: The viscosity-shear rate relations in whole blood at various hematocrit H [Chien 1966].

Shear stress is difficult to measure and is only obtained here at small enough $\dot{\gamma}$ for concentrated systems, or by extrapolation to low shear rates.

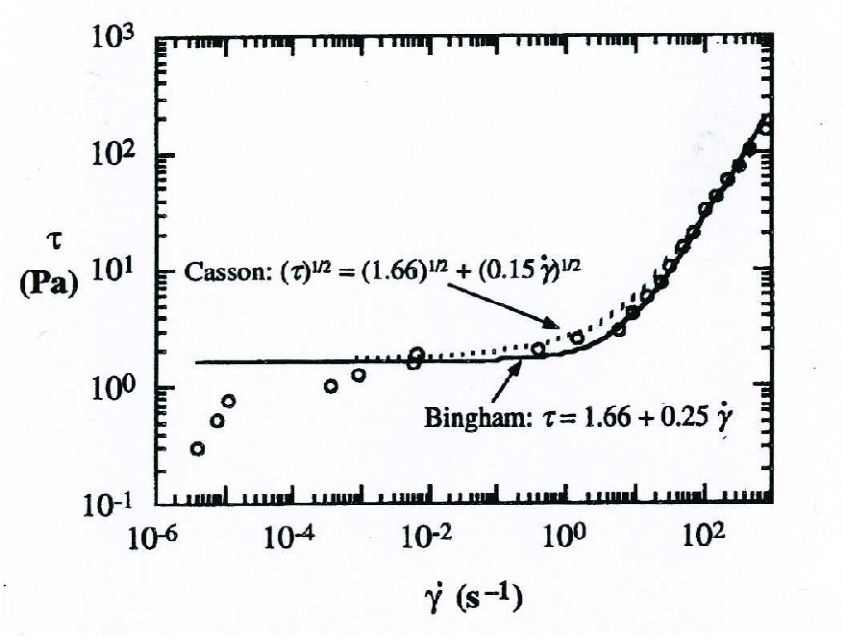

Fig. 2.10: Comparison of the law of Bingham and Casson for a suspension of iron oxide [Macosko 1994].

An example of Casson versus Bingham is given in the Fig. 2.10. A comparison between Bingham and Casson fits is made for the iron oxide suspension data. Parameters for

Bingham are $\eta = 0.25\, Pa.s$ and $\sigma_s = 1.66\, Pa$, while for Casson's model they are $0.15\, Pa.s$ and $1.66\, Pa$, respectively. The low values of the shear rates used show the deviation from the yield stress behaviour due to evaporation.

Another typical model of this behaviour is the so-called Herschel–Bulkley model:

$$\sigma = \sigma_s + M\dot{\gamma}^n$$

where M and n are positive constants. If $\sigma_s = 0$ and $n = 1$ the Herschel–Bulkley fluid degenerates to a Newtonian fluid.

2.4 Rheological models

Cell suspensions often lead to unexpected flow behaviours and to understand how suspended particles affect the overall suspension flow, it is important to review successful past models.

2.4.1 Einstein (1906)

The study of homogeneous suspensions has a long history beginning with the seminal work of Einstein showing that the effective viscosity η of a dilute suspension of hard spheres grows linearly with the volume fraction of particles ϕ according to:

$$\eta = \eta_0 \left(1 + \frac{5}{2}\phi\right), \qquad (2.1)$$

where η_0 is the solvent viscosity and η is the viscosity of the suspension. We notice immediately that in equation (2.1), there is no effect of particle size, nor of particle interactions, because the theory neglects the effects of other particles [Einstein 1906] .

Thus, Einstein's formula is only valid when the suspension is dilute enough, so that the flow field around one sphere is not appreciably influenced by the presence of neighbouring spheres.

2.4.2 Batchelor, Green (1972)

When interactions between particles are included, the situation becomes more complex. The presence of other particles is accounted for by higher-order terms in ϕ. However the only tractable theory is for extensional flow, because only in this type of flow can the relative position of the particles be accounted for analytically. Such interactions between two spheres lead to a contribution to η that is proportional to ϕ^2, three-body hydrodynamic interactions produce a term proportional to ϕ^3, and so on. The effect of two-body interactions on η was computed by Batchelor [Batchelor 1977]. Batchelor combined his calculations with Einstein's results and gives the viscosity in this case as:

$$\eta = \eta_0(1 + 2.5\phi + 5.2\phi^2). \qquad (2.3)$$

2.4.3 Krieger, Dougherty (1959)

In 1959, Krieger and Dougherty proposed that for hard spheres the rheological properties are directly related to the volume occupied by the particles [Krieger & Dougherty 1959], this formula applies also for large concentrations.

$$\frac{\eta}{\eta_0} = \left[1 - \frac{\phi}{\phi_m}\right]^{-q}, \qquad (2.2)$$

where $q = [\eta]\phi_m$, $[\eta]$ is the intrinsic viscosity of the suspension (the limiting value of the reduced viscosity as the concentration approaches to zero, $[\eta] = \lim_{\phi\to 0}\frac{\eta-\eta_0}{\eta_0\phi}$), and

ϕ_m is the maximum volume fraction. For these dependences $\eta(\phi)$, Krieger and Dougherty gave the correct solution of Mooney's approach [Mooney 1951], where ϕ_m is observed close to the Random Close Packing ϕ_{RCP}=0.637, not the theoretical value ϕ_{FCC}=0.74 (the Face Centered Cubic packing). Equation (2.2) has been chosen so that is reduces to the Einstein equation (2.1) when ϕ is small and $[\eta] = 2.5 = 5/2$.

2.4.4 Snabre, Mills (1996)

While the previous relations were for the zero-shear steady viscosity, to describe the steady state viscosity of weakly aggregated suspensions of rigid particles, a rheological law was derived [Snabre & Mills 1996]. The shear viscosity only involves the volume fraction and the maximum packing concentration of particles. Particle aggregation can influence the parameters of the reference viscosity law. The rheological behaviour of aggregated suspensions shows a yield stress below which the infinite spanning network no longer flows and displays solid-like behaviour.

In the case of concentrated systems of hard spheres in a viscous fluid, the relative shear viscosity can be estimated from the formula:

$$\eta_r(\phi, \phi_m) = \frac{\eta(\phi, \phi_m)}{\eta_0} = \frac{1-\phi}{(1-\frac{\phi}{\phi_m})^2}\ , \qquad (2.4)$$

where ϕ_m is the maximum packing fraction. In the case of a suspension of aggregated particles, the interparticle attractive forces between particles and/or clusters contribute to make the pair distribution isotropic and to inhibit the shear-induced clustering. The atomic pair distribution function describes the density of interatomic distances in a material. Moreover, the polydispersity and the flexibility of irregularly shaped particles or clusters, as well as sedimentation effects are limiting factors for shear-induced

ordering [Wagner & Russel 1990]. In the following and for volume fraction not too close to the maximum packing concentration ϕ_m, equation (2.4) is therefore assumed to be the reference rheological law for a random concentrated suspension of particles or permanent clusters, without dependence of the structure parameter ϕ_m upon the shear rate. They take into account that aggregates are organized in a fractal way (Fig. 2.11) and that the size of aggregates R_f is characterized at rest by the following relationship:

$$\frac{R_f}{a} = N^{1/D}\,, \tag{2.5}$$

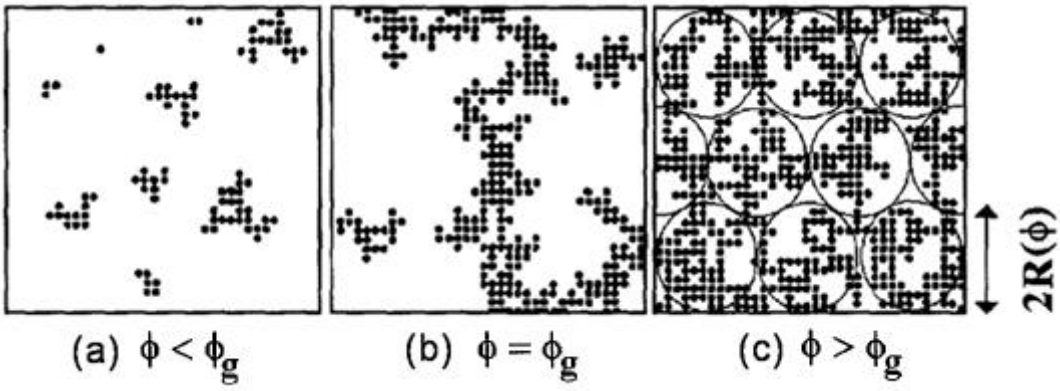

Fig. 2.11: Structure of flocculated suspension at rest (ϕ_g is the critical gelation concentration) a).$\phi < \phi_g$: finite size cluster; b). $\phi = \phi_g$: isolated aggregates; c). $\phi > \phi_g$: packing of fractal aggregates of dimension $R_f(\phi)$ [Snabre 1996].

where N is the number of particles in the cluster, $\boldsymbol{a}$ is the characteristic radius of elementary particles and D is called the fractal dimension. The mean particle volume fraction $\phi_f(N)$ in a fractal cluster is:

$$\phi_f(N) = \frac{Na^3}{R_f^3} \approx N^{\frac{D-3}{D}} \approx \left(\frac{R_f}{a}\right)^{D-3}, \tag{2.6}$$

and decreases with particle number belonging to the structure. For $\phi_f(N) < \phi_g$ (critical gelation concentration), the suspension consists only of isolated particles (see Fig. 2.11.a) and finite sized cluster. An increase in the concentration leads to interpenetration of clusters (see Fig 2.11.c). Hence, for the concentrated suspensions the maximum radius of fractal cluster can be expressed as follows:

$$\phi = \phi_f \phi_m \approx \frac{N a^3 \phi_m}{R_f (N)^3} \approx \phi_m \left(\frac{R_f}{a}\right)^{D-3}, \tag{2.7}$$

which finally gives:

$$\frac{R_f}{a} = \left(\frac{\phi}{\phi_m}\right)^{-\frac{1}{3-D}}. \tag{2.8}$$

In a flowing suspension, clusters can grow until they reach a maximum stable size, which is an equilibrium between the formation and breakup of aggregates.

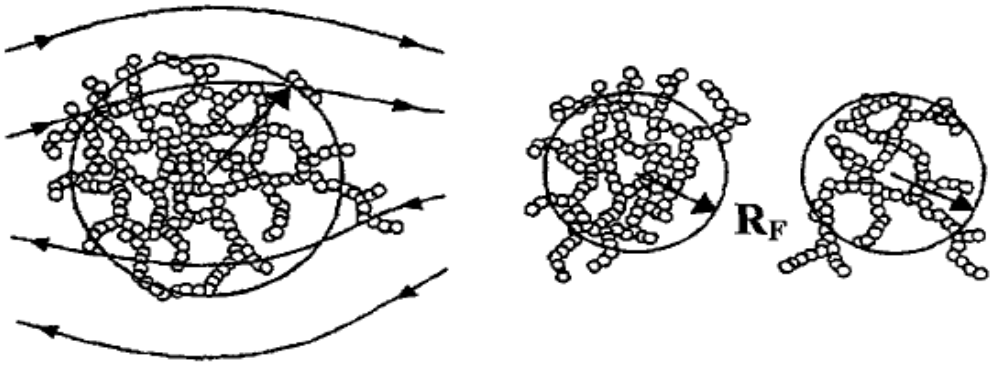

Fig. 2.12: Shear break-up of a fractal cluster into approximately equals parts [Snabre 1996].

An aggregate is destroyed by the shear stress and can break up into approximately equal parts (Fig. 2.12).

Equilibrium radius $R_f(\sigma)$ of an isolated fractal cluster decrease with increasing shear stress σ in the form of a power law assumed to be:

$$\frac{R_f(\sigma)}{a} = 1 + \left(\frac{\sigma^*}{\sigma}\right)^m, \tag{2.9}$$

where σ^* is a characteristic shear stress and m is a dimensionless parameter. The characteristic shear stress σ^* is related to the surface adhesive energy Γ :

$$\sigma^* = \frac{\Gamma}{a} . \tag{2.10}$$

For the hydrodynamic conditions close to the shear yield stress σ_s, the maximum stable radius $R_f(\sigma_s)$ of aggregates is equal to the dimension $R_f(\phi)$ of the filling space. Relations (2.4) and (2.5) together with the condition $R_f(\sigma_s) = R_f(\phi)$ then gives an expression of the yield stress:

$$\sigma_s = \sigma^* \left[\left(\frac{\phi}{\phi_0^*} \right)^{\frac{1}{D-3}} \right]^{-\frac{1}{m}} . \tag{2.11}$$

2.4.5 Snabre, Mills (1999)

Later, Snabre and Mills presented a new model starting with the motion of deformable particles in a shear flow [Snabre & Mills 1999].The particle is assumed to follow a Kelvin-Voigt model. The first order deformation-orientation of a viscoelastic sphere in a shear flow can be described by a rotating Kelvin-Voigt element (Fig. 2.13).

In concentrated suspensions, hydrodynamic interactions enhance shear gradients and particle deformation, thus leading to a decrease in suspension viscosity (shear-thinning effects). Therefore, the non-Newtonian behaviour of the suspension is essentially due to the non-linear relation which exists between the suspension viscosity and the particle deformation.

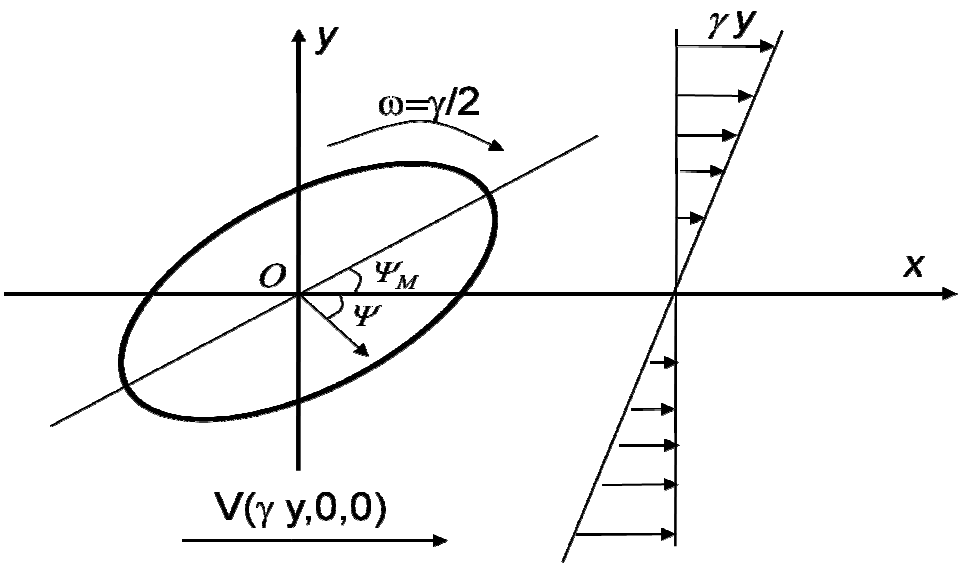

Fig. 2.13: Deformation and orientation of an initially spherical viscoelastic particle in a simple shear flow. The spherical particle of radius R centered at the origin O in the xy-plane parallel to the fluid velocity vector $V(\gamma y, 0, 0)$ was considered. The particle rotates with an angular velocity $\omega = \gamma/2$.

By introducing the shear rate dependence of the maximum packing concentration in the reference law described previously in equation (2.4), an equation for the relative shear viscosity $\eta_r(\phi, \Omega)$ can be obtained:

$$\eta_r(\phi, \Omega) = \frac{1-\phi}{\left[1 - \frac{\phi}{\phi_0^*}\left(1 + \eta_r(\phi, \Omega)\frac{\beta\Delta^{-1}\Omega^2}{1+\Omega^2}\right)^{-1}\right]^2}, \qquad (2.12)$$

where β = a constant related to flow type, $\Omega = \gamma\theta$ is Deborah number (the ratio of a characteristic relaxation time of a material θ to a characteristic time of the relevant deformation process γ) and Δ= viscosity ratio between effective viscosity and η_0 the solvent viscosity). For equation (2.12) an implicit method is required to obtain the relative viscosity. This model accounts for shear rate dependence of viscosity and shows the shear thinning behaviour.

2.4.6 Quemada (1998)

In this work, complex fluids are considered as mixtures of Structural Units (SUs) and individual elements (as primary particles or likely irreductible flocs, called IFs), in dynamical equilibrium under steady flow conditions [Quemada 1998]. As a group of IFs (or a cluster of these groups), any SU contains some amount of immobilized fluid which depends on its compactness C. This approximate description leads to a new, more realistic definition of the effective volume fraction (EVF):

$$\phi_{eff} = [1 + CS]\phi \,, \tag{2.13}$$

where S is a constant defined as the *aggregated* fraction and $C = \varphi^{-1} - 1$, with $\varphi = \phi_{eff}/\phi$. The effective volume fraction ϕ_{eff} of IFs and SUs depends on two variables:

- S, the fraction of individual particles embedded in all the clusters,
- C the compactness of the clusters.

A kinetic equation governs the time evolution of S under steady or unsteady shear conditions, leading to a shear-dependent EVF.

The kinetic processes involved during formation and breakdown (or reduction) of SUs are supposed to be relaxation processes with mean relaxation times, t_A and t_D, respectively.

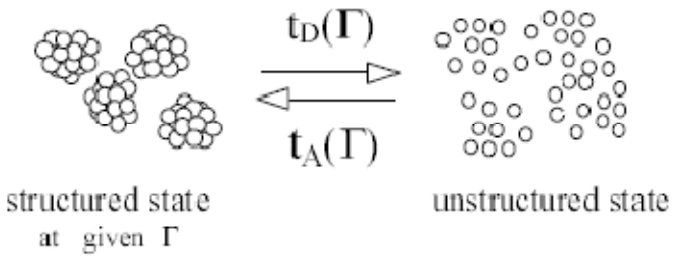

Fig. 2.14: Dynamical equilibrium under steady conditions at given Γ (reduced shear stress).

In other words, the above-defined number fraction of aggregated particles S is governed by:

$$\frac{\mathrm{dS}}{\mathrm{dt}} = \mathrm{k_A}(\mathrm{S_0} - \mathrm{S}) - \mathrm{k_D}(\mathrm{S} - \mathrm{S_\infty})\,, \tag{2.14}$$

with $k_A = t_A^{-1}$ and $k_D = t_D^{-1}$ as shear-dependent kinetic constants of formation and rupturing of SUs, and where S_0 and S_∞ are the limits of S at very low and very high shear, $\Gamma \ll 1$ and $\Gamma \gg 1$ respectively (Fig. 2.14).

The steady state ($dS/dt = 0$) solution of equation (2.14) is given by:

$$S_{eq} = \frac{S_0 + S_\infty \theta}{1 + \theta}\,, \tag{2.15}$$

where θ is defined by:

$$\theta = \frac{k_D}{k_A} = f(\Gamma) \tag{2.16}$$

This solution corresponds to the equilibrium structure the system reaches under constant shear, characterized by Γ.

Finally a model of hard sphere suspensions equation (2.17), is generalized to complex fluids, arguing that clustering of particles is also present in hard sphere suspensions and may mask their differences from complex fluids, mainly by the broad particle distributions in size and in shape of the latter.

$$\eta_r = \left\{1 - \left[1 + \frac{C(S_0 + S_\infty \theta}{1 + \theta}\right]\frac{\phi}{\phi_m}\right\}^{-2} \tag{2.17}$$

This model of viscosity predicts all kinds of behaviours: Newtonian, shear-thinning, shear-thickening, Bingham or Casson fluid.

2.4.7 Pal (2003)

Starting from the viscosity equation for a dilute suspension of deformable elastic particles, four new models have been developed for the viscosity of concentrated suspensions of deformable elastic particles, using the DEMA- differential effective medium approach [Pal 2003]. The author developed four models in this work:

- two models predict the relative viscosity of suspensions to be a function of two variables: shearoelastic number, defined as the ratio of shear stress to elastic shear modulus of particle, and volume fraction of particles,
- two models include an additional parameter, that is, the maximum packing volume fraction of particles.

The proposed models are capable of describing the rheological behaviour of unaggregated suspensions of human erythrocytes. A decrease in relative viscosity and an enhancement of shear-thinning behaviour are predicted when either the particle rigidity is decreased or the continuous phase viscosity is increased. These predictions are similar to those observed in the case of un-aggregated suspensions of RBCs. The proposed models are evaluated using the data from the literature on relative viscosity of normal and hardened human RBC suspensions in protein-free saline [Pal 2003].

The already existing models of suspension are resumed in the following table (2.1):

Theory	System	Results
Einstein, 1906	-dilute suspensions -rigid spheres -explicit method	$\eta = \eta_0\left(1+\frac{5}{2}\phi\right)$
Batchelor-Green, 1972	-dilute suspensions -rigid spheres -hydrodynamic interactions -explicit method	$\eta = \eta_0\left(1+2.5\phi+6.2\phi^2\right)$
Krieger-Dougherty, 1959	-concentrated suspensions -rigid spheres -explicit method	$\frac{\eta}{\eta_0} = \left[1-\frac{\phi}{\phi_m}\right]^{-q}$ $q = [\eta]\phi_m$
Snabre-Mills, 1996	-dilute & concentrated suspensions -fractal structure of agreggate -yield stress -shear thinning -implicit method	$\sigma_s = \sigma^*\left[\left(\frac{\phi}{\phi_0^*}\right)^{\frac{1}{D-3}}\right]^{-\frac{1}{m}}$
Snabre-Mills, 1999	-dilute & concentrated suspensions -viscoelastic particles -shear thinning fluid	$\eta_r(\phi,\Omega) = \frac{1-\phi}{\left[1-\frac{\phi}{\phi_0^*}\left(1+\eta_r(\phi,\Omega)\frac{\beta\Delta^{-1}\Omega^2}{1+\Omega^2}\right)^{-1}\right]^2}$
Quemada 1998	-concentrated suspensions -SUs (system unitis) -predicts all type behaviors : shear thinning, shear thickenning -explicit method	$\eta_r = \left\{1-\left[1+\frac{C(S_0+S_\infty\theta}{1+\theta}\right]\frac{\phi}{\phi_m}\right\}^{-2}$ C=compactness

Pal, 2003	- concentrated suspensions -4 models developed -shear thinning -implicit method	$\eta_r = \left(1 - \frac{\phi}{\phi_m}\right)^{-[\eta]\phi_m}$

Table. 2.1: Already existing models of viscosity of suspensions.

2.4.8 A model for visco-elasto-plasticity applied to cell suspensions

In a recent work to be submitted for publication [Preziosi 2008], the authors consider a new model for analysing the behaviour of cell suspensions. The basic idea is to consider continuum mechanics applied to a body which undergoes a transformation. It is possible that this body grows as in a tumour spheroid [Ambrosi & Preziosi 2008], but this is not considered here. Another possible property of this model is that it can allow that, during deformation, part of the stresses can relax elastically whereas another part of the transformation will allow cell reorganization, related to plastic deformations. The body configuration can therefore be divided into two parts, one elastic (large deformations can occur) and another one for plastic irreversible motion. Following the approach by Ambrosi et al. (2008) using the concept of multiphase materials (one phase containing cells and another phase being the fluid), the equations of motion can be obtained and the result is a constitutive equation for the traceless stress $\mathbb{T}'$:

$$\frac{\mathcal{D}\mathbb{T}'}{\mathcal{D}t} + \frac{1}{\lambda}\left[1 - \frac{1}{\tilde{f}(\mathbb{T}')}\right]_+ \left(\mathbb{T}'\mathbb{B}_n - \frac{1}{3}tr(\mathbb{T}'\mathbb{B}_n)\mathbb{I}\right) = \frac{2}{3}\mu[tr(\mathbb{B}_n)\mathbb{D} - tr(\mathbb{B}_n\mathbb{D})\mathbb{I}]$$

Where the derivative on the left is one preserving frame invariance (here the upper convected one), $\mathbb{D}$ is the symmetric part of the velocity gradient tensor, $\mathbb{I}$ is the identity tensor, λ is a relaxation time and $\mathbb{B}_n = F_n F_n{}^T$ is the finger tensor with F_n the deformation gradient corresponding to the elastic part of the motion. The expression in

brackets is the positive value (i.e. 0 or the positive number) of the expression, and $\tilde{f}(\mathbb{T}')$ is a function of the invariants of $\mathbb{T}'$, μ is the shear elasticity coefficient. For small transformations of the elastic state, this equation reduces to:

$$\lambda\dot{\mathbb{T}}' + \left[1 - \frac{1}{\tilde{f}(\mathbb{T}')}\right]_+ \mathbb{T}' = 2\eta\left(\mathbb{D} - \frac{1}{3}tr\mathbb{D}\mathbb{I}\right)$$

where η is the viscosity. One can then consider steady shear, oscillatory shear and relaxation following an applied deformation. This has been tested for example in the case of compression [Preziosi 2008] in reference to previous data from Forgacs [Forgacs 1998] on cell aggregates in compression. The previous formula can include a yield stress since the positive valued function can exist or be equal to zero. When it is zero, we recover the case of elasticity. When it is non zero, it can give rise to yield stress behaviour. In the 1D case, we can use a power function for $\tilde{f}$ and this leads to:

$$\dot{T} + \frac{1}{\lambda}\left[1 - \left(\frac{\hat{\tau}}{|T|}\right)^{\alpha}\right]_+ T = \mu\dot{\gamma}$$

where $\hat{\tau}$ is the yield stress. In particular, for steady shear $\dot{\gamma} = \dot{\gamma}_0$, that we will only consider here, we find the viscosity-gradient relationship:

$$\dot{\gamma}_0 = \frac{\hat{\tau}}{T/\dot{\gamma}_0}\left(1 - \frac{\eta}{T/\dot{\gamma}_0}\right)^{-1/\alpha}$$

where $\eta(\dot{\gamma}_0) = T/\dot{\gamma}_0$ is the viscosity given in implicit form, but this can be solved since $\dot{\gamma}_0$ is given explicitly as a function of $\eta(\dot{\gamma}_0)$. Finally, we show the result of the computed viscosity, or its reduced form in terms of the shear rate, for different values of the parameter α (Fig. 2.15).

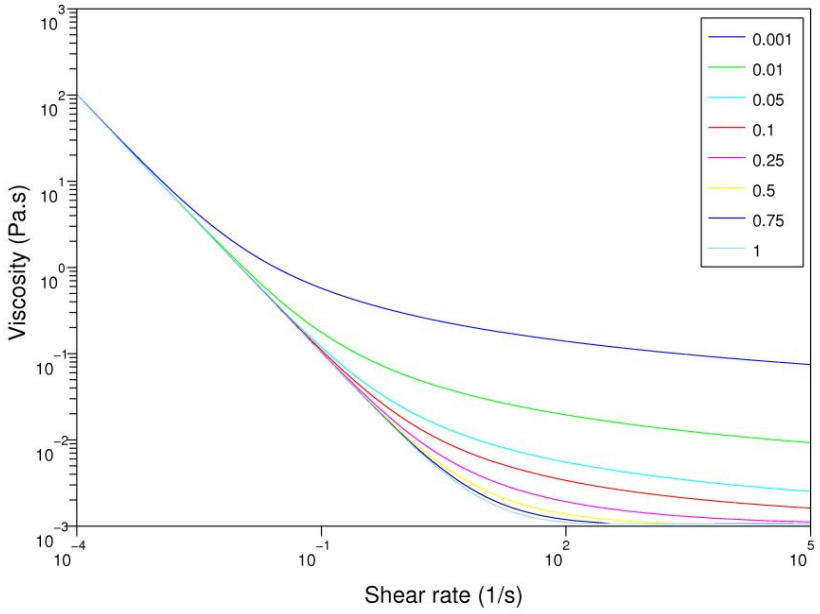

Fig. 2.15: a). Viscosity vs. shear rate at different values of the parameter α (listed on the graph).

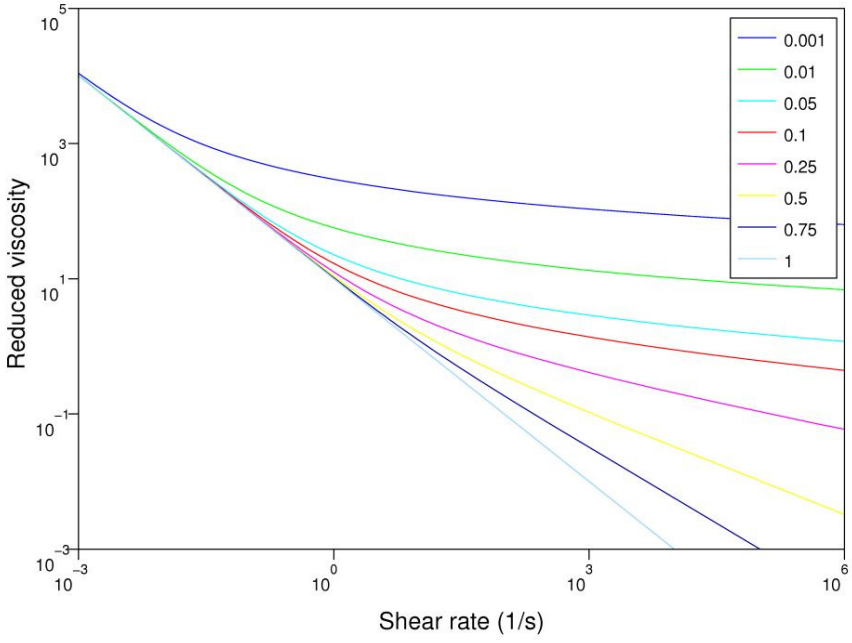

Fig. 2.15: b). Reduced viscosity $(\eta(\dot{\gamma}_0) - \eta)/\eta$ vs. shear rate at different values of the parameter α (listed on the graph).

The behaviour of the viscosity is the following:

- at low shear rates the viscosity varies like $\eta(\dot{\gamma}_0) \approx \sigma_s/{\dot{\gamma}_0}^{-1}$ (slope -1) which is the signature of a yield stress fluid,
- at intermediate rates it changes slope gradually,
- at high shear rates, the limiting η value is reached [Fung 1996]. On the other hand, the reduced viscosity has a limiting slope exactly equal to $-\alpha$.

Résumé français

Ce chapitre rappelle certains concepts de base de la rhéologie des suspensions et de certains modèles déjà existants décrivant la viscosité. Les suspensions de particules ont été largement étudiées et de nombreux modèles théoriques ont été proposés pour prédire leur caractère rhéo-fluidifiant, rhéo-épaississant ou de fluide à seuil. L'étude des suspensions a une longue histoire qui commence avec les travaux d'Einstein. Plusieurs modèles décrivant la viscosité des suspensions sont présentés (Batchelor et Green, Krieger et Dougherty, Snabre et Mills, Quemada, Pal).

Preziosi, Ambrosi et Verdier utilisent un nouveau modèle visco-élasto-plastique pour analyser le comportement des suspensions cellulaires.

3. Tools of investigation

To carry out the steps for the determination of the rheometrical properties of cell suspensions and tissue model systems, proper tools are needed. In this chapter we describe the experimental techniques used (Rheometry and Microscopy).

Special attention has been paid for processing images obtained during microscopy experiments.

3.1 Rheometry

A rheometer is an instrument used to study rheological properties of a material by imposing a shear stress (σ) and observing the resulting shear strain (γ) or shear rate ($\dot{\gamma}$) and vice versa. In this study, we use a stress-controlled Bohlin rheometer (Gemini 150) equipped with temperature control and a home-built vapour chamber to create a stable humidity controlled environment.

This rheometer uses an air bearing system where the rotor of the drive and the motor axis float in air due to the continuous supply of compressed air. The rheometer uses the air bearing system to minimize the bearing friction. Usually, it is common to carry out experiments in a rotational rheometer when dealing with biological fluids or materials. This instrument allows us to have access to stresses (or torque) and strains or strain rates. The basic idea is that operating in a circular geometry allows us to keep the fluid (material) in the same device, whereas capillary rheometry requires systems that push the fluid, therefore requiring a larger amount of material.

Usual rotational rheometers include different geometries such as the plate-plate, cone-plate, and Couette geometry (used for less viscous fluids). There are different macroscopic tests that can be carried out with cells and tissue model. They are classified in two categories: the ones giving access to shear properties, or the ones giving access to tensile or elongational properties.

We performed shear experiments. Classical definitions of such shear tests are given first.

3.1.1 Transient Motions

In classical rheometry, one applies a steady shear rate $\dot{\gamma}$ (in fact, start up from 0 to $\dot{\gamma}$) and the shear stress $\tau = \sigma_{12}$ is measured. Then the transient viscosity $\eta^+(t,\dot{\gamma})$, the first and second normal stress coefficients $\psi_1^+(t,\dot{\gamma})$, and $\psi_2^+(t,\dot{\gamma})$, can be determined:

$$\eta^+(t,\dot{\gamma}) = \frac{\sigma_{12}(t,\dot{\gamma})}{\dot{\gamma}} ,$$

$$\psi_1^+(t,\dot{\gamma}) = \frac{(\sigma_{11} - \sigma_{22})(t,\dot{\gamma})}{\dot{\gamma}^2},$$

$$\psi_2^+(t,\dot{\gamma}) = \frac{(\sigma_{22} - \sigma_{33})(t,\dot{\gamma})}{\dot{\gamma}^2}.$$

They are named the viscosimetric functions. If these behaviours correspond to typical viscoelastic materials, one expects a rise of $\eta^+(t,\dot{\gamma})$, $\psi_1^+(t,\dot{\gamma})$, and $\psi_2^+(t,\dot{\gamma})$, until a plateau is reached.

The limiting values will then be $\eta(\dot{\gamma})$, $\psi_1(\dot{\gamma})$, $\psi_2(\dot{\gamma})$. When elastic effects are important at high shear rates, for example, there might be an overshoot in the time evolution of the previous functions until the steady state is found [Bird 1987].

3.1.2 Steady-state functions

The steady-state functions $\eta(\dot{\gamma})$, $\varphi_1(\dot{\gamma})$, $\varphi_2(\dot{\gamma})$ are the limits of time-dependent functions as time becomes large. These limits are usually reached after a time inversely proportional to the velocity of deformation (shear rate $\dot{\gamma}$ here).

Materials or fluids with decreasing $\eta(\dot{\gamma})$ are said to be shear thinning where as the opposite is the shear-thickening behaviour, as observed for certain concentrated suspensions of particles. When the stress goes to a limit at small vanishing shear rates, the material exhibits a so-called yield stress as explained previously for the Bingham fluid [Verdier 2002].

The first and second normal stress differences are important, because they are related to elastic effects, not usually encountered with Newtonian fluids. They correspond to the fact that the application of shear in the 1-2 plane can give rise to normal stresses σ_{11}, σ_{22} and σ_{33} allowing to explain strange non-Newtonian behaviours (rod-climbing effect, die swell, etc.).

3.1.3 Dynamic Rheometry

This is one of the most common test used for characterizing biological materials, when small quantities of materials are available (collagen solution, actin, etc.).

In shear, one applies a sinusoidal deformation $\gamma(t) = \gamma_0 sin(\omega t)$ as described previously.

The stress σ is assumed to vary like $\sigma(t) = \sigma_0 sin(\omega t + \varphi)$. One of its components is in phase with γ (elastic response), and the other one varies like $\dot{\gamma}$ (viscous part). One

defines, respectively, the elastic and viscous moduli G' and G''. They are defined by $G'\gamma_0 = \sigma_0 cos\varphi$ and $G"\gamma_0 = \sigma_0 sin\varphi$.

The loss angle φ is given by $tan\varphi = \frac{G''}{G'}$. In complex variables, the complex modulus G^* is $G^* = G' + iG''$. The dynamic complex viscosity is $\eta^* = \frac{G^*}{i\omega} = \eta' - i\eta'' = \frac{G''}{\omega} - \frac{iG'}{\omega}$. Moduli G' and G'' are determined for small deformations (linear domain), i.e. the domain where they remain constant for small enough γ_0.

Other recent studies deal with the use of large deformations, but we did not use such approaches here.

For our measurements we used two geometries, parallel disks and cone-plate, which are briefly described below. There is a different working formula for each one.

3.1.3.1 Cone and plate rheometer

It presents the advantage to impose a constant shear rate when the angle of the cone is small (typically 2 to 4 degrees). A sketch of the cone and plate geometry is shown in Fig. 3.1.

In this set-up, the sample is placed between a plate and a cone; the bottom flat plate is generally stationary while the top cone rotates. For this cone and plate geometry, we can calculate the shear stress (σ), the shear strain (γ), and the shear rate $(\dot{\gamma})$ from the applied torque (M) and measured angular velocity (Ω) using the following equations [Macosko 1994] :

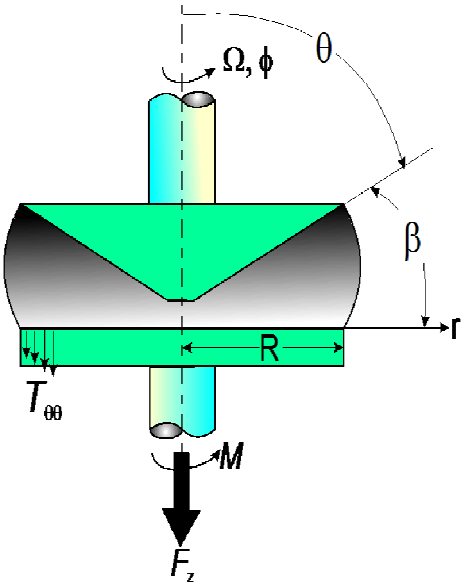

Shear stress

$$\tau_{12} = \tau_{\phi\theta} = \frac{3M}{2\pi R^3}$$

Shear strain $\gamma = \frac{\phi}{\beta}$

Shear rate $\dot{\gamma} = \frac{\Omega}{\beta}$ (homogeneous)

Normal stress $\tau_{11} - \tau_{22} = \tau_{\phi\phi} - \tau_{\theta\theta} = \frac{2F_z}{\pi R^2}$

Fig. 3.1: Schematic cone-plate rheometer.

Where M is the torque applied to the sample, R and β are the radius and the angle of the cone respectively, ϕ is the angular displacement and Ω is the angular velocity.

3.1.3.2 Plate-plate rheometer

For most of our measurements, the Bohlin Gemini set-up was parallel plate geometry. This is essentially the same design as the cone-plate instrument, except that a plate replaces the upper cone. A constant torque is applied to the upper plate, and the angular deflection or rate of strain is measured. Sample preparation and loading is simpler for viscoelastic materials. The geometry is sketched in the Fig. 3.2 with the working equations [Macosko 1994].

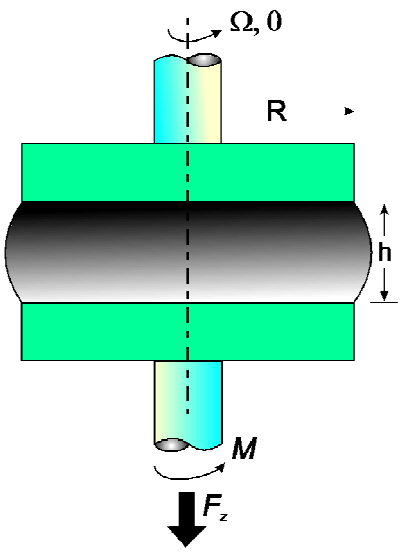

Shear strain: $\gamma = \frac{\theta r}{h}$

(nonhomogeneous, depends on position)

Shear rate at r = R $\dot{\gamma}_R = \frac{R\Omega}{h}$

Shear stress:

$$\tau_{12} = \tau_{\theta z} = \frac{M}{2\pi R^3}\left[3 + \frac{d\ln M}{d\ln \dot{\gamma}_R}\right]$$

Fig. 3.2: Schematic plate-plate rheometer.

Apparent or Newtonian shear stress: $\tau_a = \frac{2M}{\pi R^3}$

Representative shear stress: $\eta(\tau) = \eta_a(\tau_a) \pm 2\%$

For $\tau = 0.76\tau_a$ and $\frac{d\ln M}{d\ln \dot{\gamma}_R} < 1.4$

Normal stress: $N_1 - N_2 = \frac{F_z}{\pi R^2}\left[2 + \frac{d\ln F_z}{d\ln \dot{\gamma}_R}\right]$

$(F_z)_{inert}$ = Inertia force (tend to pull the plates together rather than push them apart)

$$(F_z)_{inert} = 0.075\pi\rho\Omega^2 \mathrm{R}^4.$$

This geometry is more suitable for our experiments but because we had samples in small quantities (difficult to have cells in large quantities and short term) we had to use more frequently this plate-plate geometry with a small gap and a low value of the radius.

3.1.4 Techniques of rheometry in the case of cell suspensions

During the experiments several problems may appear which are briefly described below.

3.1.4.1 Evaporation

In rheometrical tests with rotational geometries there is generally a sample free surface, which is an interface between the suspension and air. This is the first reason for evaporation. The liquid within the sample may then evaporate into the air. Since the rate of evaporation increases with relative velocity of the system, the sample may dry much faster than if it were left at rest. For simple liquids, the consequence of such a phenomenon is simply a decrease in the sample volume. But for suspensions, a decrease of the volume can change the volume fraction ϕ and therefore affect their rheological properties.A second reason of evaporation is the increase of sample's temperature. To prevent evaporation, a device was build which is similar to a circular ring with a water chamber, as seen in Fig. 3.3.

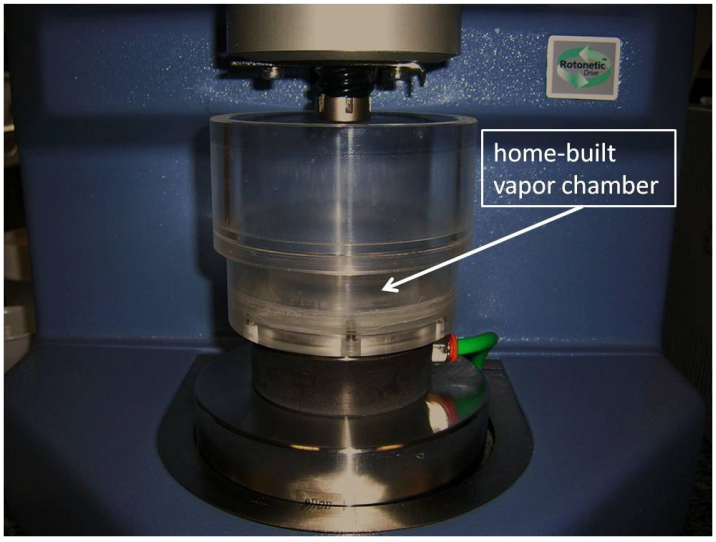

Fig.3.3: Water chamber to prevent evaporation.

As the liquid evaporates, the ambient air will saturate with liquid vapor (water here) to eliminate evaporation.

3.1.4.2 Slip

Problems are encountered when using rotational rheometry usually due to the presence of particles at the surfaces of the measuring devices. This phenomenon known as *slip* is of particular relevance at low shear rate levels [Magnin 1990], [Coussot 2005]. Slip at the wall occurs when fluids having a dispersed particulate phase become in contact with the solid walls of the rheometer. These effects reduce the viscosity and hence lower the value of the yield stress if it exists [Picart 1998]. A number of methods have been suggested to eliminate slip during measurements, all of which appear to be equally valid. These methods include the use of an adhesive at the interface between the sample and the measuring device or pasting sand paper to the wall surface.

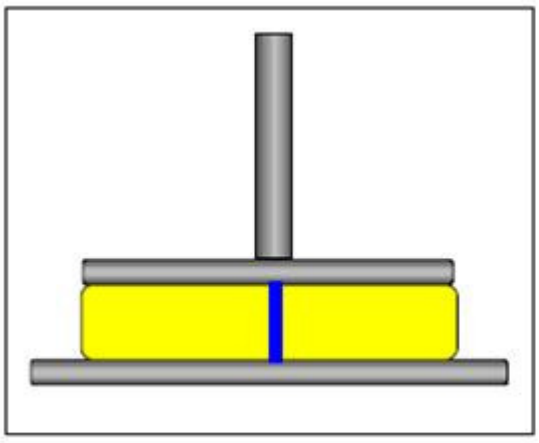

Fig. 3.4: Plates 1 illustrate the effect of slippage [2], [Magnin 1990], [Coussot 2005].

A sample of yellow ink was placed between the plates and a vertical blue line of ink was drawn onto the surface of the ink, Plate 1 (Fig. 3.4).

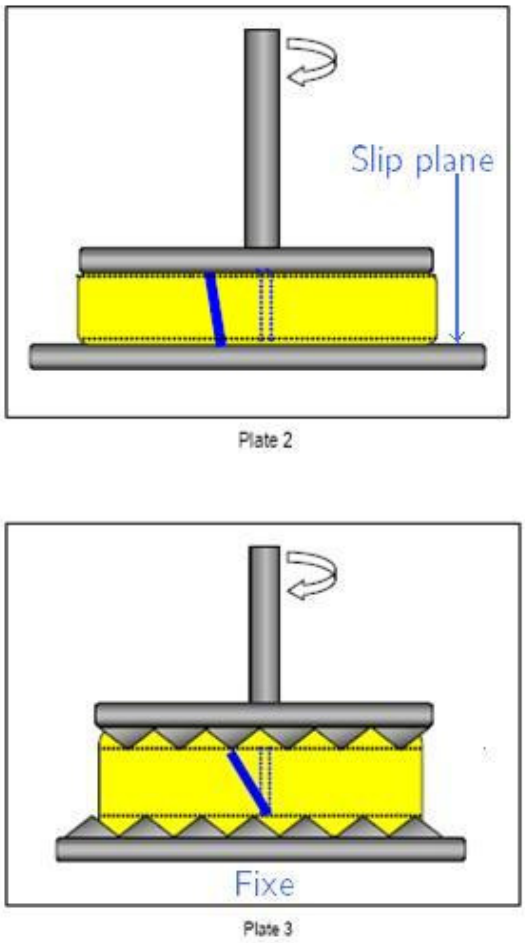

Fig. 3.5: Plates 2 - 3 illustrate the effect of slippage [2], [Magnin 1990], [Coussot 2005].

The material was subjected to a constant stress for a period of time and the blue line was observed (Fig. 3.5). Plate 2 shows the distortion of the line after 5 minutes. The line indicates that slippage is located at the lower plate, since it does not exhibit linear flow between the two plates. However, when using rough plates to do the same experiment, linear flow between the plates is observed (Plate 3) with no apparent slip at the lower plate. For our cell suspensions the slip phenomenon was not noticed for very low shear rates, due to the good adhering properties of the cells, unlike in the case of solid particles. Note that we also never used very small shear rates to avoid this phenomenon.

One of the most important requirements for a particle suspension is that the dispersed phase remains stable in time (microstructure does not change when the sample is subjected to stress). Cell suspensions are rheologically complex fluids that have combined viscous and elastic behaviours, which can be described by a viscoelastic spectrum (G' and G'' versus frequency in log-log scale). A complete spectrum must

cover frequency dependence of the material functions. The microstructure of the suspensions will depend upon the balance of the repulsive and attractive forces which the particles experience as they approach one another. For experimental rheology to play a significant role in predicting particle stability, the measurement technique must be sensitive to extremely small viscoelastic differences or structural changes. This effectively allows investigation of the sample. The first test to perform on an unknown sample is the amplitude sweep (viscoelastic properties versus shear strain γ_0). The purpose of this test is to determine the linear viscoelastic region (the amount the sample can be strained without changing its structure). Experimental rheology is capable of rapidly identifying the important material functions that control the stability of suspensions providing the viscoelastic spectrum. To ensure validity of the analysis, it is necessary to make all measurements in the linear viscoelastic region well below the critical strain. Our suspensions were tested in order to find the linear domain (Fig. 3.6) and the viscoelastic

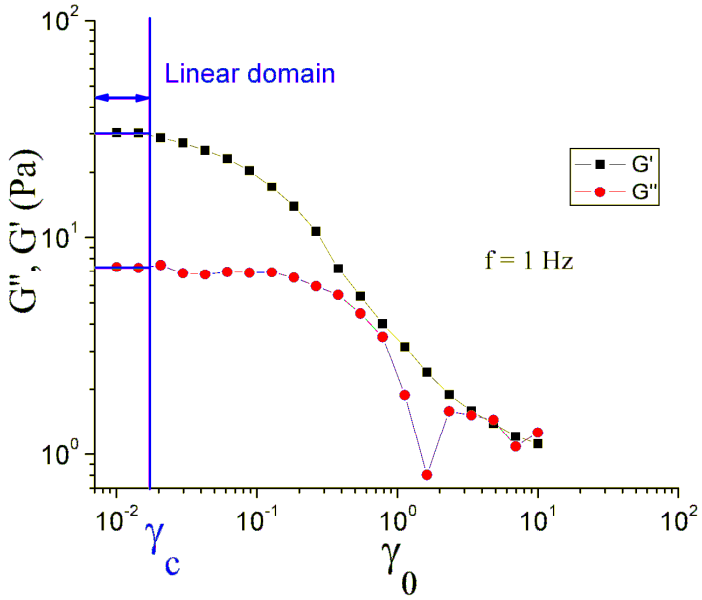

Fig. 3.6: Amplitude sweep for collagen type I solution (c= 0.95 mg/mL).

regions were found. Fig. 3.6 shows an example for collagen solution (c= 0.95 mg/mL) and we can see that below 1% ($\gamma < \gamma_c$) we are in the linear domain.

The next test is the frequency sweep. This test is of primary interest because G' is related to elastic particle interactions. Results for cell suspensions and collagen solutions will be presented in the next chapters.

3.2 Microscopy

While rheometrical measurements can give us important information in a macroscopic sense, they are generally not adapted for studying the microstructure. This is because in rheological experiments, structural changes responsible for the measured behaviour remain hidden, because samples are usually opaque. However, a few experimental devices have been built in order to look at the simultaneous microstructural changes [Snabre 1999], but this will not be the case here. Thus, rheometry is often most useful when supplemented by other experimental methods that characterize structural changes, like microscopy in this work.

Since the objects that we are studying are of the order of the micron, the observations during our experiments require the use of a microscope. Several techniques have been used preferentially to match with the observation needed. In fact, the cells used in this study are easy to observe using phase-contrast microscopy but the study of cells in a collagen matrix requires the use of Confocal Reflection Microscopy.

Phase-contrast microscopy, Reflection Microscopy and Confocal Microscopy are presented in the next section.

3.2.1 Phase Contrast Microscopy

We used Phase Contrast Microscopy to determine the shape, dimensions and numbers of cells. We used an upward microscope (Olympus BX51). This type of light microscopy enhances contrasts of transparent and colourless objects by changing the optical path of light. The phase contrast microscope is able to show most components in a cell (i.e. nucleus, organelles, cytoplasm, and membrane) which would be very difficult to see using ordinary bright field microscopy. Therefore, one of the major advantages of phase contrast microscopy is that living cells can be examined in their natural state without being fixed or stained.

The principle of the phase contrast microscopy is shown in Fig. 3.7. Phase-contrast is a widely used technique that shows differences in refractive index in a specimen as the difference in contrast. The system consists of a circular annulus in the condenser (condenser annulus) which produces a cone of light.

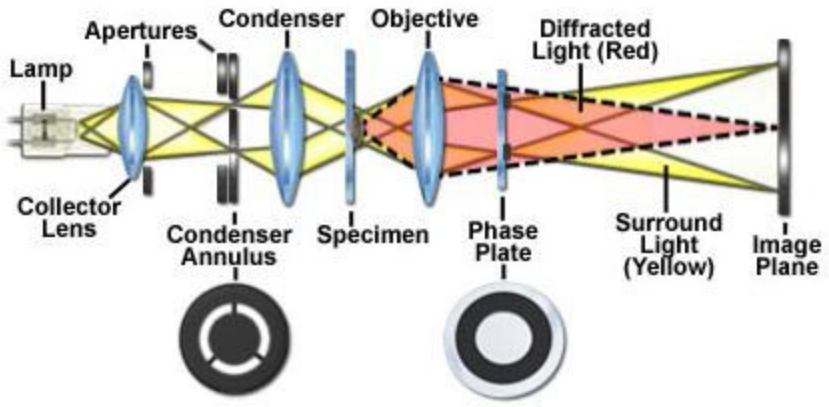

Fig. 3.7: Principle of the phase contrast microscopy [3].

This cone is superimposed on a similar sized ring (phase plate) within the objective. The ring in the objective has special optical properties: first of all, it reduces the direct light in intensity, but more importantly, it creates an artificial phase difference of about

1/4 wavelength. As the physical properties of this direct light have changed, interference with the diffracted light occurs, resulting in the phase contrasted image.

3.2.2 Confocal Imaging

The Confocal Imaging Facility at the "Institut Albert Bonniot" (Service de Microscopie, Alexeï Grichine) was used in order to make quantitative and qualitative measurements of 3D collagen gels together with cells. To visualize the cells and collagen, two techniques were combined: Confocal Fluorescence and Reflection Confocal Microscopy.

For fluorescence microscopy, the sample is the light source itself. The technique is used to study specimens, which are fluorescent when excited properly. The fluorescence microscope is based on the phenomenon that certain material emits energy detectable as visible light when irradiated with the light of a specific wavelength. The sample can either be fluorescent in its natural form like collagen, or treated with fluorescent chemicals.

The facility has a Zeiss Laser Scanning Microscope (LSM 510) with the following details:

- Microscope: Zeiss Axiovert 135M LSM 510 (Carl Zeiss), inverted design, infinity-corrected optics.
- Objectives: C-Apochromat 40X, water immersion;
- Fluorescence excitation: Argon laser lines: 488nm;
- CRM excitation: HeNe laser linearly polarized: 633 nm;
- Temperature control: A temperature-controlled stage kept cells at 37°C in CO_2 controlled atmosphere

The confocal principle microscopy is presented in Fig. 3.8.

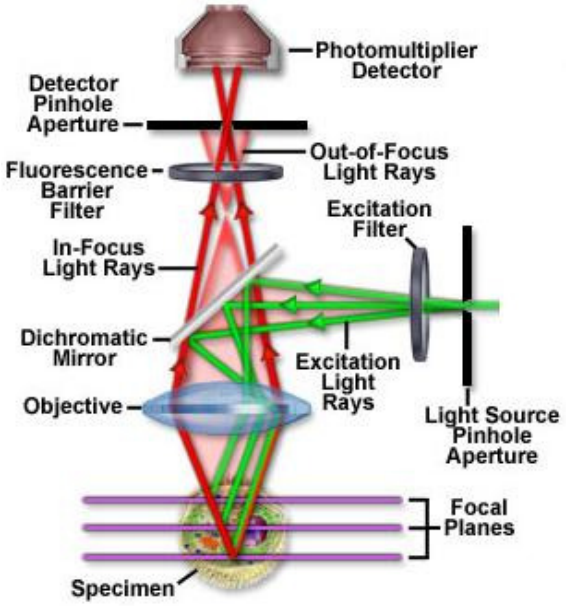

Fig. 3.8: Principle of confocal microscopy [5].

Coherent light emitted by the laser system (excitation source) passes through a pinhole aperture that is located in a conjugate plane (confocal) with a scanning point on the specimen and a second pinhole aperture positioned in front of the detector (a photomultiplier tube). As the laser is reflected by a dichromatic mirror and scans across the specimen in a defined focal plane, secondary fluorescence emitted from points on the specimen (in the same focal plane) pass back through the dichromatic mirror and are focused as a confocal point at the detector pinhole aperture.

3.2.3 Confocal Reflection Microscopy

When we think "confocal microscopy", we usually have fluorescence imaging in mind. A majority of the common biomedical applications of the confocal microscope have

utilized its optical sectioning power, combined with fluorescence to produce improved images of cells and tissues. Confocal reflection microscopy can be utilized to gather additional information from a specimen with relatively little extra effort, since the technique requires minimum specimen preparation and instrument re-configuration. In addition, information from unstained probes like collagen is readily available with confocal reflection microscopy if the specimen reflects light. The method can also be utilized in combination with more common classical fluorescence techniques, and that is our case. To see the interactions between cells growing in collagen gels we used a technique termed confocal reflection microscopy. In our case, the adhesion between the cell and its matrix was visible at the interface of the glass coverslip and the "apical side" of the cell. The cells marked with GFP were analyzed using fluorescence and collagen, including the contacts between cells and collagen, was viewed using confocal reflection microscopy. The cell-substratum interface can be difficult to locate in the confocal microscope, but the highly reflective coverslip can be employed as an aid in focusing. This interface was located by focusing in fast scan mode, and the collagen fibres appear just after the bright flash of the coverslip when penetrating the cell layers. A polarization analyzer (PA) was placed in front of a photomultiplier tube (PMT) and blocked reflected light with unchanged polarization. Using this method, collagen was reconstructed in three dimensions with a resolution better than that of conventional microscopy techniques, such as confocal microscopy.

Collagen gels with and without cells were polymerized in a Lab-Tek chamber with coverglass and imaged using a Zeiss Axiovert (135M LSM 510 model) microscope, inverted design. The method was performed to visualize matrix fibres and cells using a C-Apochromat 40X, (water immersion) objective lens. During the experiments, samples are placed in a temperature and CO_2 controlled stage (37°C, 5% CO_2).

Two lasers are coupled to the microscope (Fig. 3.9):

- Argon laser at 488 nm was used to see the GFP-marked cells,
- HeNe laser at 633 nm to visualize collagen matrix.

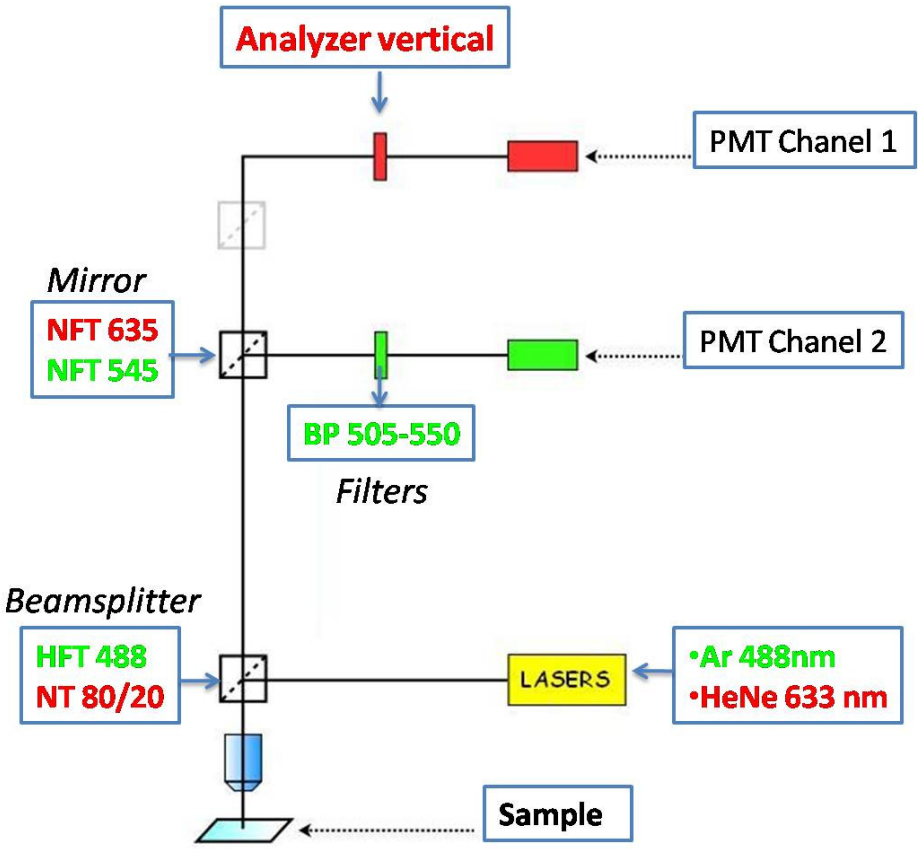

Fig. 3.9: Confocal and fluorescence Microscopy setup.

Fig. 3.9 depicts the microscopy setup employed to simultaneously collect confocal reflectance and fluorescence images. Lights enters in the inverted mode and is directed to the objective by a beamsplitter (NT 80/20) for confocal reflectance, or a shortpass (SP) dichroic mirror (at 488 nm) for fluorescence. Light reflected from the sample passes through the beamsplitter, and is deflected by a dichroic mirror (at 635 nm), through a pinhole, and to a photomultiplier tube (PMT1).

In the case of fluorescence, cells are irradiated and then emit fluorescence which is collected through a specific beamsplitter, dichroic mirror (at 545 nm) and vertical analyzer to a PMT2.

The quantification of signal intensity was done on 8 bits (256 gray level values). For each sample, the optical sections were stored as two series of digital images, one corresponding to the sections of the cells and the other corresponding to the sections of collagen.

The setup was driven by the AIM software imaging system. An HBO lamp was used as the light source.

3.2.4 Image Analysis

For the experiments obtained with Phase Contrast Microscopy we performed image analysis. To do so we used ImageJ - freely available on the web [4].

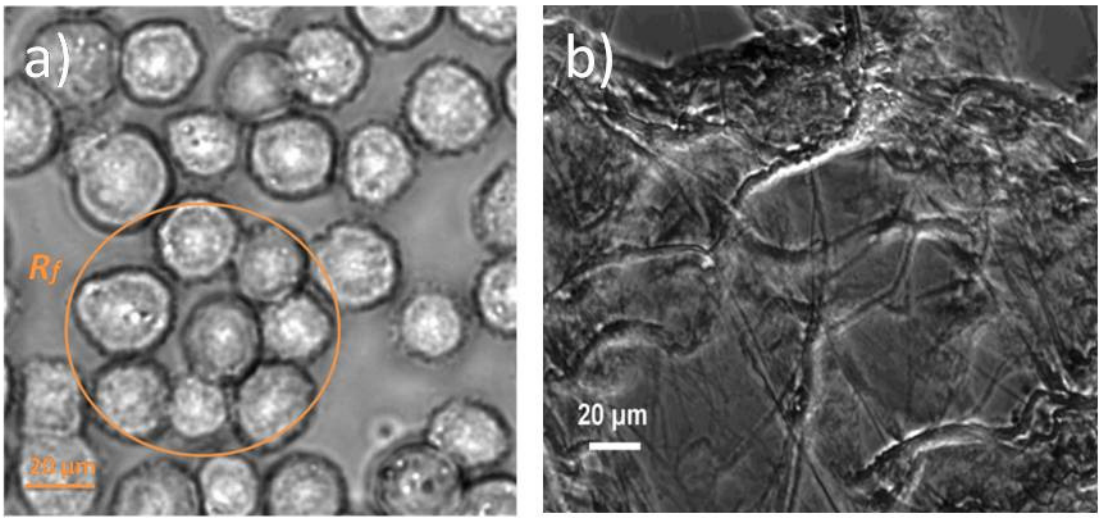

Fig. 3.10: a) Image J allows measuring the size and number of the clusters or cells. b) Amount of polymerization of collagen fibres.

This program was used to determine several parameters such as the typical dimensions (radius of cells, size of clusters), the orientation of collagen fibres, as illustrated in Fig. 3.10.

To process the data obtained from the confocal microscope we used the AIM software. This software can be used online with the microscopes or offline. It has image processing capabilities, including 3D visualization. A free version called Image Browser with reduced functionality is available. All images are saved as *.lsm files. Typically they are accessed through a *.mdb database. The imaging parameters are stored within the image file as well as in the database. Images not associated with a database can be opened using the "File $\rightarrow$ Import" command. The images can be exported in a variety of file formats, including *.tiff, *.jpg and *.avi. Once images have been acquired, we used MetaMorph Offline 7.5.4 to cut off the cells from entire Z-series from the confocal microscope (Fig.3.11). Files are exported in the *.lsm form and saved as a *.stk file. The 3D measurement module facilitates the visualization of multidimensional data sets, stacks (a series of images that share a single window) and sequential images. We can simultaneously view multiple Z sections in a single image, as well as binarize multidimensional image data into discrete objects. Because we wanted to find out the orientation of cells within collagen matrix, a special program "Edit 3D_quanti" by Yves Usson was used [Parazza 1993], [Parazza 1995], [Wozniak 1996]. The images with cells were exported in Edit 3D_quanti. The data was treated using several levels of image processing as explained in Appendix 1.

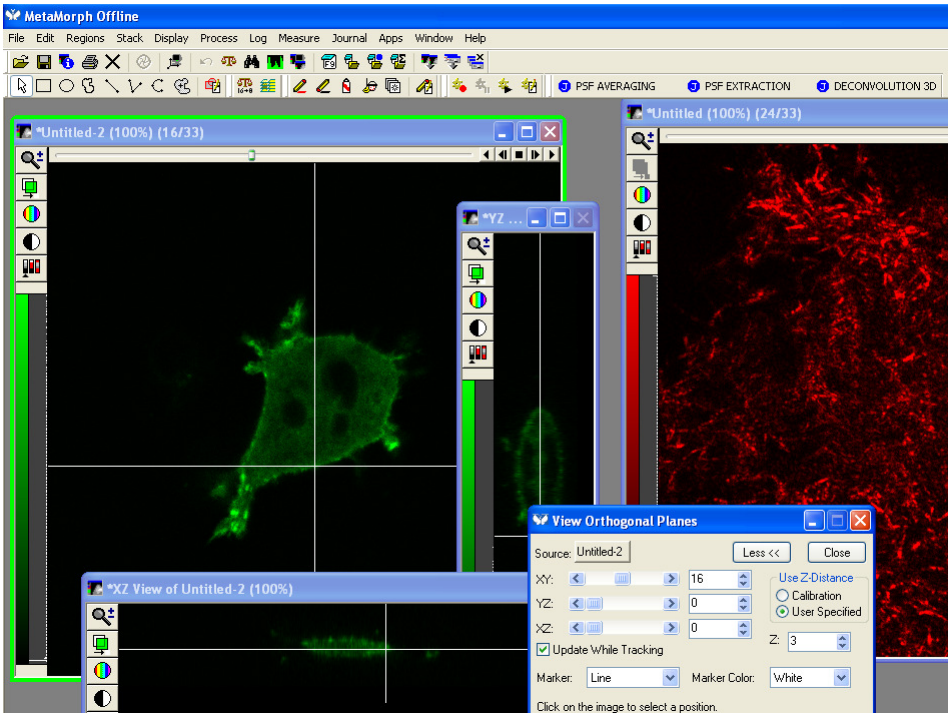

Fig. 3.11: MetaMorpfh Offline was used to split the channels.

Fig. 3.11 shows a cell in green, its projections XZ, YZ and collagen in red. The cell was made fluorescent whereas the red part (collagen) is obtained by the reflection technique.

Résumé français

Le chapitre 3 présente les techniques et les logiciels utilisés pour le traitement des données. Dans un premier temps nous présentons le rhéomètre, les méthodes de rhéométrie utilisées et les précautions prises pour contrôler l'évaporation et éviter le glissement. Dans une seconde partie, nous passons en revue les différentes méthodes de microscopie (contraste de phase, réflexion et confocale) et les logiciels utilisés pour le traitement des données.

4. Rheology of concentrated suspensions[1]

4.1 Introduction

The rheology of complex fluids has been studied extensively over the past decades [Larson 1999] and has revealed very intriguing behaviours, in particular properties of suspensions, either micronic or colloidal, are still a subject of interest [Coussot 1995], [Flatt & Bowen 2006], [Alexandrou 2007], [Brader 2007].

Classical behaviours of suspensions usually reveal shear-thinning effects, but other unusual ones like shear-thickening [Laun 1984] (i.e. viscosity increase with shear rate) or yield stress have been observed [Coussot 2005], [Flatt 2006]. The yield stress is the critical value of the shear stress needed to induce flow for a given fluid. It is closely related to the internal structure of the fluid therefore its ability to form (or break) particle clusters under flow. In this respect most studies have focused on solid sphere suspensions.

[1] *The contents of this chapter have been published (see appendix 3):*
A. Iordan, A. Duperray, C. Verdier, Fractal approach to the rheology of concentrated cell suspensions, Phys. Rev. E 77, 011911 (2008)

On the other hand, there are much less works dedicated to suspensions of deformable particles, such as biological cell suspensions. The main works can be found in the field of blood rheology. Suspensions of Red Blood Cells (RBC) within plasma were first investigated by Chien [Chien 1967a], [Chien 1967b] and revealed a shear-thinning behaviour, but a more detailed inspection of the viscosity-shear rate diagrams showed that at low shear rates, the stress level is close to a constant σ_s (Pa), called the yield stress.

The well-known Casson's model [Casson 1959] relating the shear stress σ to the shear rate $\dot{\gamma}$ (μ being a constant viscosity) can be used to determine the yield stress:

$$\sqrt{\sigma} = \sqrt{\sigma_s} + \sqrt{\mu\dot{\gamma}} \tag{4.1}$$

Chien and co-authors obtained σ_s for a large range of hematocrit (H), i.e. the RBC volume concentration [Chien 1966].

They showed a relationship of the type $\sigma_s \sim (H-b)^3$ (b being a constant hematocrit). It is still not known yet whether this type of behavior is universal, or if it could depend on cell type, cell shape or other biological effects such as cell adhesion or cell elasticity. In particular, one proposed explanation of the yield stress in RBCs suspensions is based on the existence of "rouleaux" which build due to cell interactions and exhibit large shape aspect ratios [Chien 1967b] and a fractal dimension D. Therefore it is necessary to apply strong enough stresses in order to break such aggregates, in close relation with the yield stress.

In this work we propose to investigate the rheology of a new cell suspension, consisting of CHO cells (Chinese Hamster Ovary cells) in a large range of concentrations. Such cells are commonly used in biology, easy to culture, and can be genetically modified to induce different adhesive properties. These cells are spherical when suspended in a

culture medium, and organized in a specific manner leading to particular aggregation patterns of fractal type. This leads to the determination of scaling laws based on fractal exponents (for the yield stress σ_s and elastic modulus G_0) which are seen to be non universal but cell type dependent.

The flow curves constitute a basis to test classical empirical models (Bingham, Casson, Herschel-Bulkley models) and other ones [Snabre 1996] [Snabre 1999] based on kinetic theories describing the rupture and formation of particle clusters. The latter ones successfully relate macroscopic effects to microscopic parameters, such as the cell-cell adhesion energy and the cell's elasticity. The microscopic parameters that we find match well the ones found in the literature using other techniques. This is important in the context of recent studies related to tumour growth [Drasdo 2005],[Galle 2005] which consider cell assemblies with interactions as well as cell elastic deformations. Furthermore, this study emphasizes the relationship between the dynamic rheological properties of suspensions [Verdier 2003] and the single cell properties.

The chapter is organized as follows. In Section 4.2, the materials and methods of investigation (i.e. mainly rheometry and microscopy) are described. Then steady shear and dynamic oscillatory shear results are presented in Section 4.3. In the light of the typical scaling laws obtained, we suggest the use of the model of Snabre and Mills [Snabre 1996] presented in Section 4.4 to analyze our data, and find the corresponding microscopic parameters. Finally, two alternative approaches based on structural similarity [Coussot 1995] and a recent model [Preziosi 2008] are presented. Section 4.5 draws some conclusions.

4.2 Materials ad Methods

4.2.1 CHO cell line

Chinese Hamster Ovary cells (CHO cells) are an established line of fibroblasts. They are often used in biological and medical research [Zhao 2006] .

4.2.1.1 Cell culture

In our model system, adherent CHO cells are grown in culture medium (DMEM containing 10% Fetal Calf Serum) using standard T75 boxes under proper conditions (37°C, 5% CO2) in a cell incubator, until they reach 70% confluence. The suspensions, with different concentrations are made from CHO cells and culture medium. Medium is then replaced and the cells are diluted (after detaching them first from the support with trypsin, 1 ml for each flask). We dilute 12 such flasks with cells until we obtain 30-40 mL (medium+cells). The suspension is well homogenized and separated in 2-3 small tubes, 15 ml each. Suspended cells are centrifuged at 1200 rpm, a high enough velocity to get a concentrated suspension, but slow enough in order to maintain the cells alive.

Fig. 4.1.a shows the flask with adherent CHO cells in culture medium. By centrifugation of suspensions, cells are separated from the medium (Fig.4.1.b).

a) 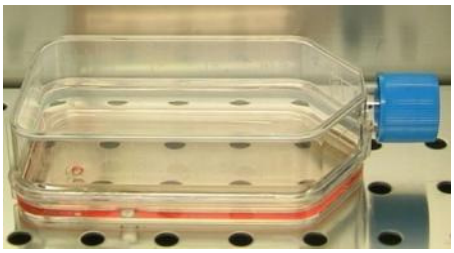 b) 

Fig. 4.1 : a) Adherent CHO cells in culture medium (T = 37 ° C, 5% CO2) in a T75 Flask. b) Results obtained after centrifugation, about 0.2 ml of cells at the bottom.

From 12 flasks we obtain approximately 0.3-0.5 mL cells, depending of the culture condition. The compacted CHO cells (highly concentrated), are recombined with the medium up to approx 1-3 ml= V_0 (suspension volume) to obtain the desired concentration, as explained below.

4.2.1.2. Determination of cell concentration

Accurate concentration determination is performed in glass capillary tubes (length 75 mm, diameter 1.3-1.4 mm, volume 60 µL). The tubes are filled with a 10 µL micropipette containing the cell suspension, avoiding the formation of air bubbles and sealed first with wax and then with glue at both ends (Fig. 4.2).Then tubes are centrifuged at 1200 rpm for 5 min.

l= cells

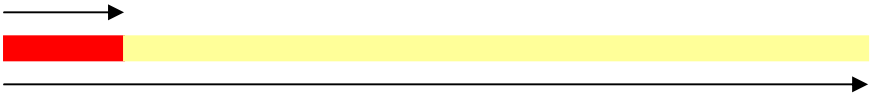

L= tube's length

Fig. 4.2: Measurement of l (after centrifugation) giving access to cell concentration $C = l/L$.

To obtain the required concentration, we remove carefully a know volume of medium (V). For calculating the concentration, the following formula is used:

$$C^* = C\frac{V_0}{V_0 - V}$$

$C* =$ Suspension concentration

$V_0 =$ Suspension volume

$V =$ Medium volume removed

4.2.2 Rheological measurements

Rheological measurements were conducted using a stress–controlled Rheometer (Bohlin) with temperature control. The special device with vapor chamber (see Section 3.1.6.1) was used to avoid evaporation of the medium from suspension during measurements.

Two types of measurements were performed: steady state and oscillatory experiments.

Both measurements were made at T=20° C.

4.2.2.1 Viscosimetry

In the case of viscosimetry measurements, two geometries (plate-plate and cone-plate) were used. Due to the large amount of cells needed (we usually require twelve T75 flasks in order to obtain a volume at least 0.3 mL of cells), we chose to use a plate-plate geometry (20 mm diameter) with a small gap (between 400 μm and 1 mm) for the concentrated suspensions whereas the smaller concentrations (below 10%) and the

medium were tested using the 60 mm cone-plate geometry (2° angle). Typically in our fluid, the suspended cells are spherical and monodisperse with a radius a~10 μm.

Since the size of suspended cells was much smaller than the width of the gap (h) in the case of plate-plate geometry, the suspensions could be considered homogeneous (h≥20 (2a)) and continuum mechanics theories can hold.

The viscosity was measured as a function of shear rate. The viscosity of the suspension was obtained for each value of shear rate, at 20°C.

A sample volume of 0.157 mL was needed for plate-plate geometry and 1.97 mL for cone-plate one. The shear rate was increased step by step. Moreover, since the total suspension shearing time was less than 8 min., it was found that not sedimentation occurred.

In some cases, we limited ourselves to the higher shear rates because of experimental reasons (i.e. steady state not reached).

4.2.2.2 Oscillations

The measurements of the moduli G' and G'' were made as a function of frequency.

The effects of volume fraction on the viscoelastic properties were studied at 20°C in a frequency range between 0.1 and 5 Hz.

4.3. Results

4.3.1 Rheometry

Fig. 4.3 shows the curves $\eta(\dot{\gamma})$ for nine different suspensions. Special attention is made for concentrated systems (40-60%). By a first inspection of the curves, we recognize the signature of a yield stress fluid as depicted by the slope close to -1 in the viscosity-shear rate diagram (or equivalently a constant shear stress at low shear rates), especially at the largest concentrations ϕ. The existence of this yield stress is attributed to weak interactions which can exist after preparation of the system.

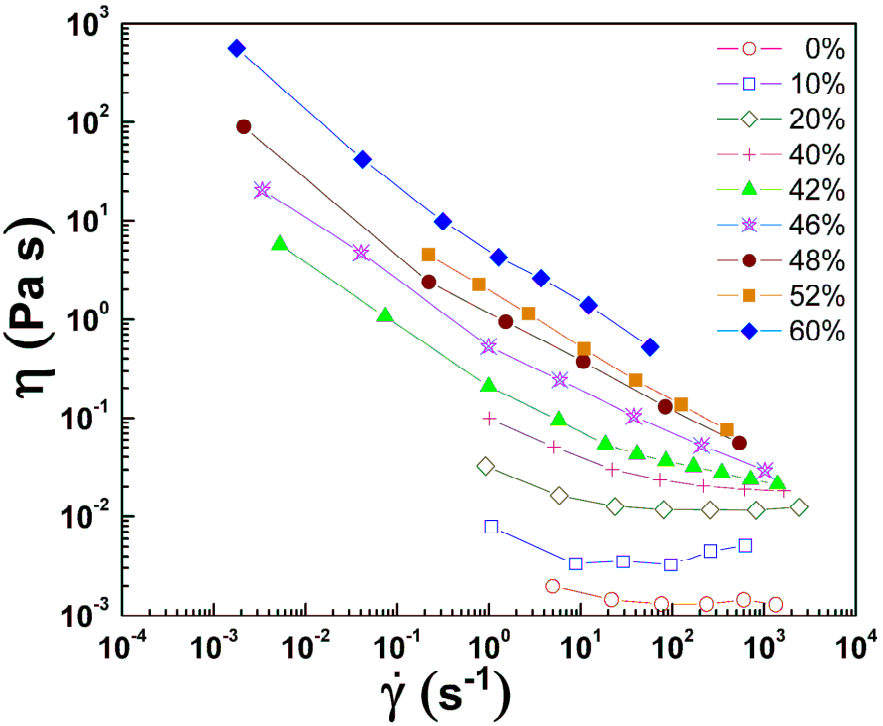

Fig. 4.3: Viscosity η (Pa.s) vs. shear rate $\dot{\gamma}(s^{-1})$ at different volume concentrations ϕ from 0 to 60%.

Already existing proteins are available on cell membranes and can be recruited to form bonds, leading to particular structure arrangements. This explains the presence of a yield stress related to the formation of such structures. The yield stress is found to depend on volume concentration ϕ in a manner to be discussed later.

A second series of experiments was carried out in order to study the systems under oscillatory strains at frequency f. Small deformations (1%) within the linear regime were performed in order to characterize the elastic modulus $G'(f)$ and the loss modulus $G''(f)$. The frequency values were limited to the narrow range corresponding to fast modes, in order to limit a possible time-dependence of the results, due to sedimentation, protein expression, or cluster formation-destruction.

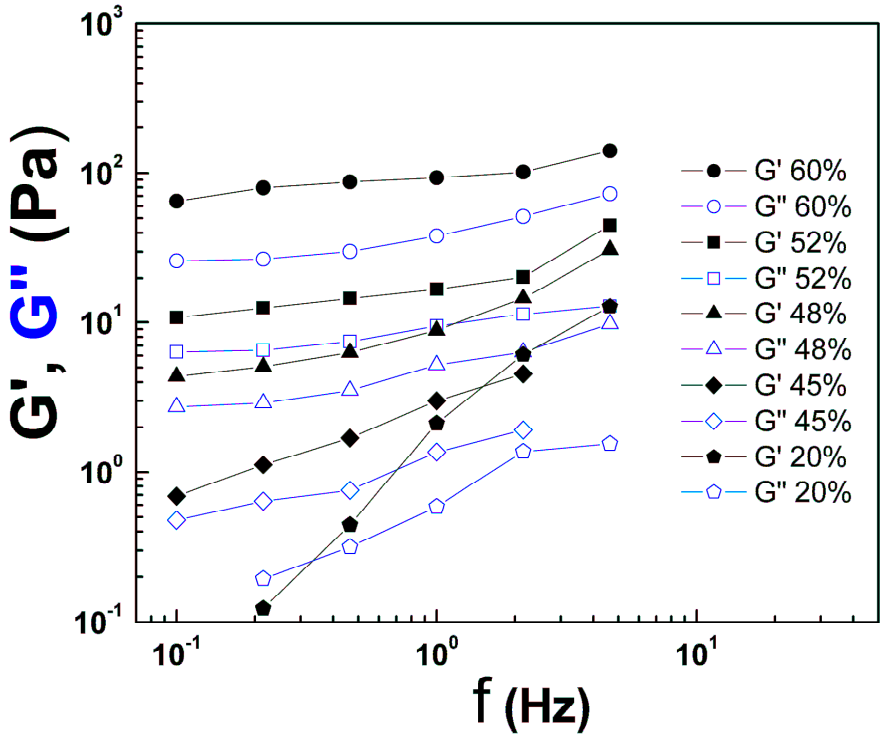

Fig. 4.4: Shear moduli G′ and G″ (Pa) vs. frequency f at different volume concentrations ϕ ranging from 20% to 60%.

We find an interesting behaviour as shown in Fig. 4.4. Moduli $G''(f)$ usually prevails over $G'(f)$ at small concentrations (e.g. $\phi = 0.2$), but as ϕ increases, the system becomes elastic with a much larger $G'(f)$. This behavior is the signature of a viscoelastic medium, due to the fact that interactions between elastic cells become effective at large concentrations ($\phi \geq 0.4$) .

The slow increase of the elastic modulus G' against frequency reveals the presence of a so-called 'elastic plateau' modulus (G_0) determined by the value of $G'(f)$ at intermediate frequencies (1 Hz typically).

The presence of elasticity has been observed previously for RBC suspensions [Thurston 1972], above a critical volume fraction around $\phi = 0.2$, and is believed to come from the elasticity of the cells as they are packed more closely at large concentrations such as the ones also encountered in tumour spheroids [Galle 2005]. Finally, we observe that the trends in the $G' - G$" plots for large concentrations ($\phi \geq 0.5$) are remarkedly similar to previous microrheological results obtained on single cells [Fabry 2001], [Alcaraz 2003],[Hoffman 2006]. Indeed, they show a slowly increasing G' and G'' (increasing slightly faster at frequencies above 1 Hz), where the elasticity dominates ($G' \geq G''$).

As in the case of suspensions, we define a maximum packing fraction ϕ_m (which is usually 0.64 or even 0.74 for solid spheres in a face-centered-cubic crystal), depending on cell elasticity, i.e. their compactness [Quemada 1998]. Due to the presence of soft spherical cells, it is expected that the value of ϕ_m will be in this range. ϕ_m is determined using the reduced viscosity plot η/η_0 as a function of ϕ (η at a shear rate of 10^{2} s^{-1}, η_0= 0.0013 Pa.s the solvent viscosity). In our case, this data is found to match the well-known equation proposed by Krieger and Dougherty [Krieger 1959], this providing the value $\phi_m = 0.65$ (Fig. 4.5).

$$\frac{\eta}{\eta_0} = \left(1 - \frac{\phi}{\phi_m}\right)^{-2.5\phi_m} \tag{4.2}$$

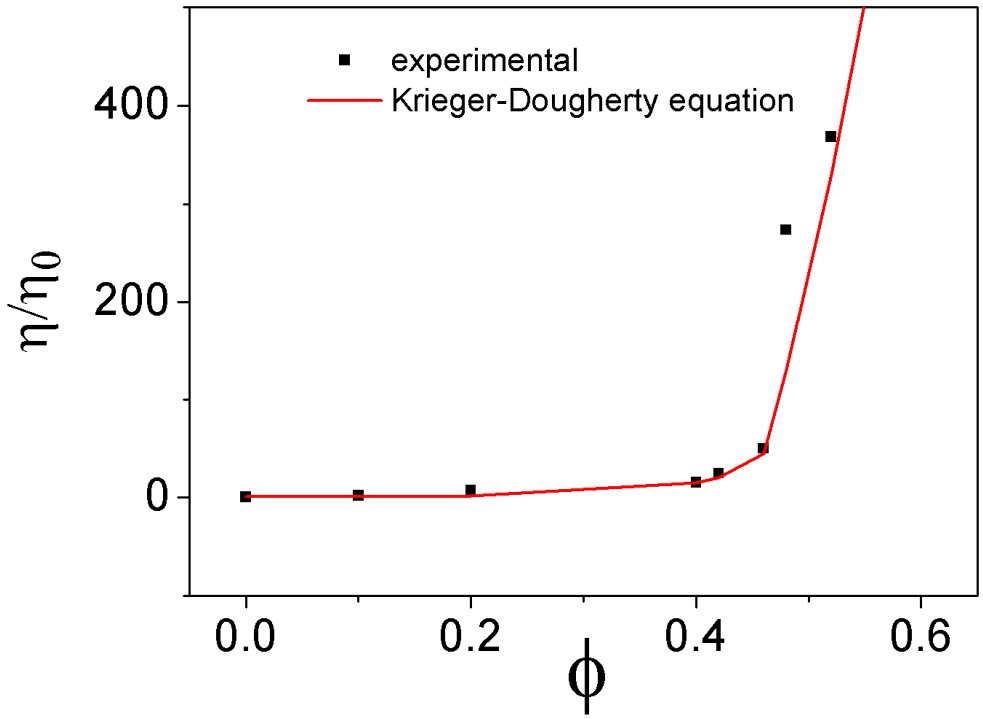

Fig. 4.5: Reduced viscosity versus concentration ϕ. Experimental data were fitted with Krieger-Dougherty equation.

Note that this relationship is interesting because it matches Einstein's viscosity for hard spheres [Einstein 1906], [Einstein 1911] $\eta/\eta_0 = 1 + 2.5\phi$ as well as Batchelor's correction for non colloidal spherical particles [Batchelor 1972] $\eta/\eta_0 = 1 + 2.5\phi + 5/2\phi^2$ (here an expansion of equation (4.2) for small ϕ gives a second coefficient in the expansion of roughly 5 instead of 5.2, when using $\phi_0 = 0.65$). Finally, equation (4.2) diverges as expected when $\phi \to \phi_0$, the limiting packing fraction.

In order to investigate the effect of the volume concentration ϕ, we first need to obtain the flow curve $\sigma(\dot{\gamma})$ of the suspensions, as well as the relevant parameters, such as the

yield stress σ_s. From the viscosity curve in Fig. 4.3, we plot the stress $\sigma = \eta(\dot{\gamma})\dot{\gamma}$ vs. shear rate $\dot{\gamma}$ in Fig. 4.6, and fit the data with the Herschel-Bulkley law [Coussot 2005]

$$\sigma = \sigma_s + M\dot{\gamma}^n \tag{4.3}$$

where M is a constant, and n is a shear-thinning exponent ranging between 0 and 1 (1 is for a Bingham fluid, and the case of the Newtonian fluid is recovered for n=1, $\sigma_s = 0$). Parameters have been optimized using a standard Newton-Raphson method (numerical analysis for finding successively better approximations to the zeros of a real-valued function). The parameter n is found to be very close to 1 at small concentrations (0, 10, 20%) and decreases with concentration, taking respective values of 0.89, 0.71, 0.57, 0.55, 0.47, 0.47 for concentrations of 40, 42, 46, 48, 52 and 60% respectively (Fig. 4.7). This point will be further discussed.

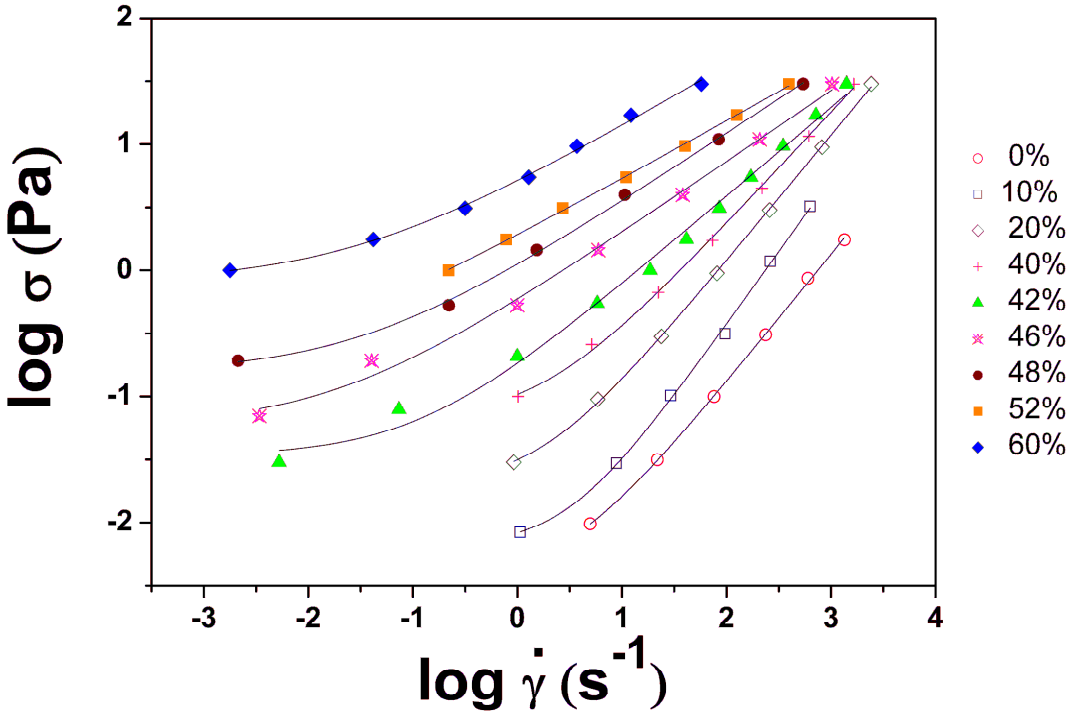

Fig. 4.6: Determination of the yield stress σ_s using Herschel-Bulkley's model.

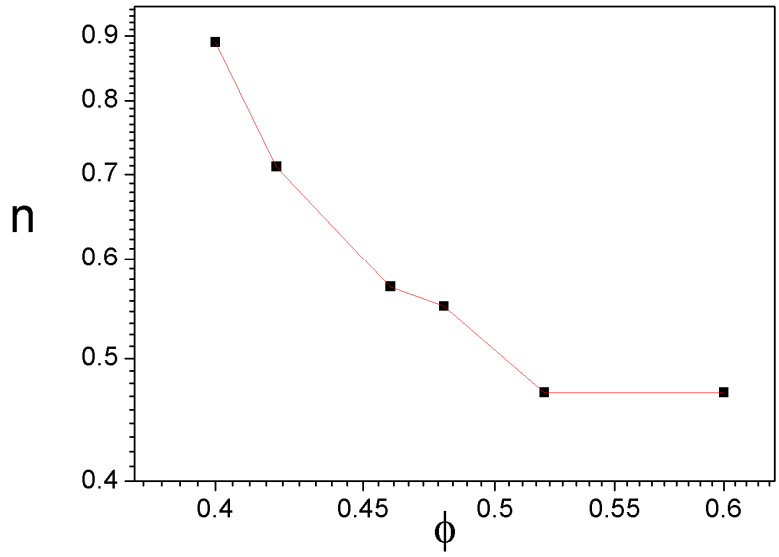

Fig. 4.7: Shear-thinning exponent n versus concentration ϕ in log-scale.

This leads to the determination of the yield stress σ_s as a function of volume fraction ϕ.

Such measurements are usually difficult [Chien 1966] because of possible slip, sedimentation and evaporation [Fung 1996]. Care has been taken to avoid such problems, therefore only shear rates larger than $2 * 10^{-3} s^{-1}$ (lowest value) are considered. The empirical Herschel-Bulkley model (involving a yield stress) is then used when sufficient data points are available. The fits are in satisfactory agreement with the data which gives good confidence in the values of the yield stresses for $\phi \geq 0.40$. Another attempt has been made using Casson's model and gives similar data. The Bingham model was found to give less accurate values. The values of the yield stresses σ_s and shear plateau moduli G_0 (value of G' at a typical frequency f=1 Hz) are plotted in Fig. 4.8 as a function of volume concentration. This plot shows power law dependences of the form $\sigma_s \sim \phi^{m_1}$ and $G_0 \sim \phi^{m_2}$ and reminds previous results [Snabre

1996] obtained in the case of the rheology of RBCs suspensions, at least for the yield stress σ_s. From Fig. 4.8 we find that $m_1 \sim 8.4$ and $m_2 \sim 11.6$. The m_1 exponent is quite different from the one obtained in the case of RBCs suspensions ($m_1 \sim 3$) as this will be discussed below.

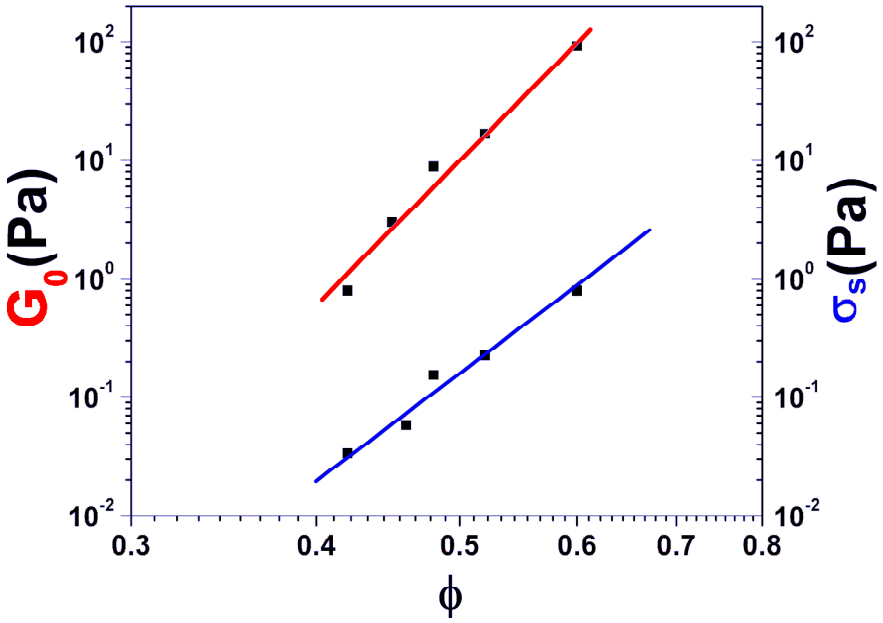

Fig. 4.8. Yield stress σ_s and Shear elastic modulus $G_0 = G'(f=1\ Hz)$, vs. volume fraction ϕ, log-scale

4.3.2 Microscopy

Cell suspensions correspond to aggregated systems. Fig. 4.9 shows microscopy images for four different suspensions (10%, 20%, 30% and 52% respectively).

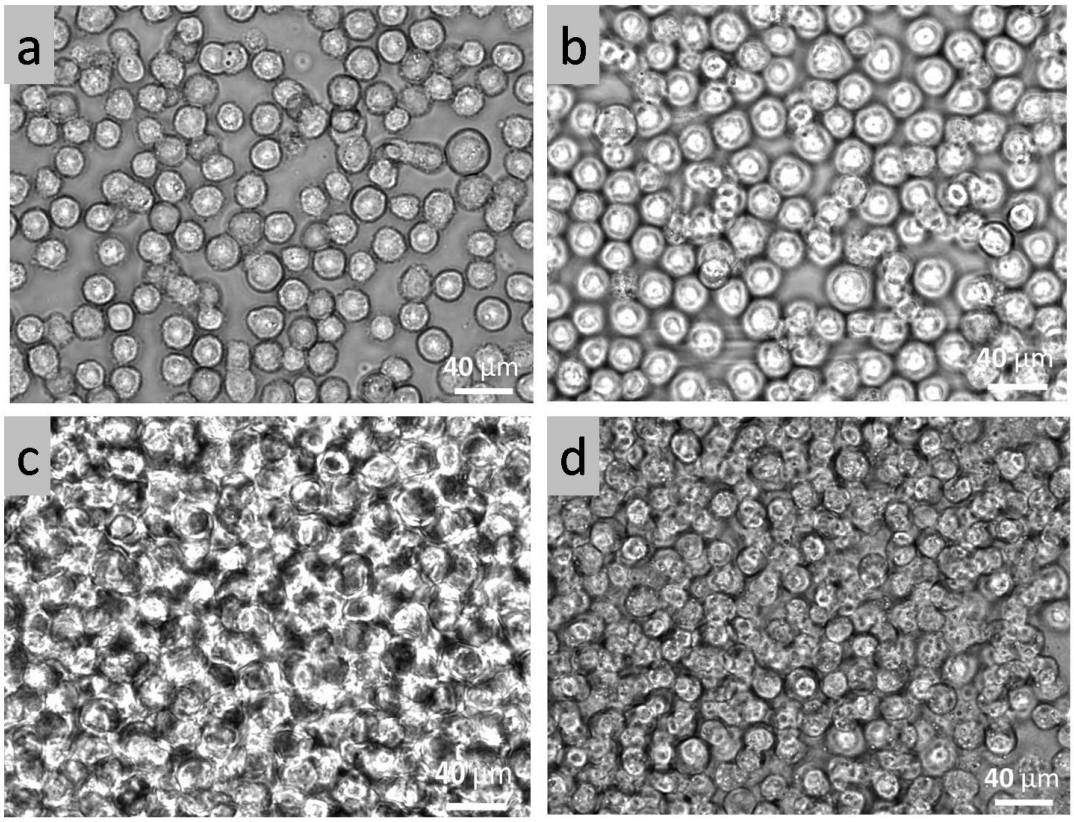

Fig. 4.9: Phase contrast microscopy of CHO cell suspensions, a) 10%, b) 20%, c) 30% d) 52%, Bar=40 µm for all images.

The method used is based on the image processing of clusters located between two glass plates after initial dispersion of the suspension.

4.4. Modelling

4.4.1 Fractal approach

As seen above, rheological modelling of such suspensions should therefore predict shear-thinning behaviour, as well as yield stress properties at low shear rates $\dot{\gamma} \to 0$ and a concentration dependence of σ_s and G_0.

Under flow, the structure of aggregated systems is based on the persistent remodelling of the cells with respect to each other as they exhibit deformations, rotations, possible rolling and/or separation. During such events, cells may form clusters of size R_f to be compared with the cell size a (radius). The formation and destruction of cell clusters is the major ingredient to understand the rheological properties of the cell system, in order to explain the data.

For example, when sheared under stress σ, clusters break into smaller ones, leading to shear-thinning effects. On the other hand, the possible encounter of clusters leads to the formation of larger structures, increasing the viscosity. Clusters are organized in a fractal way.

First, one needs to consider a cluster at rest. We have determined the fractal dimension of two-dimensional cell aggregates. The radius of the cluster is R_f and it contains N cells, linked by the following relationship [de Gennes 1979].

$$\frac{R_f}{a} = N^{1/D} \tag{4.4}$$

where D is the fractal dimension. To determine D, we follow a previous approach [Allain & Jouhier 1983] where an experimental simulation is made in two dimensions which allows studying the growth of clusters during an aggregation process. The existence of a critical surface fraction and of self similar geometrical properties of clusters is demonstrated. Based on this analysis, we considered circles (instead of rectangles) of radius R_f containing a cluster. Then cells (radius a) are counted for two rather small concentrations (10% and 20%). Clichés like a) in Fig. 4.9 are used to draw circles and count the number of cells N (see Fig. 4.10). For larger clusters containing more cells, we obtain a linear relationship between $log_{10}(R_f/a)$ and $log_{10}(N)$, as shown in Fig. 4.11.

Note that the two cases studied (10% and 20%) give the same slope for large values of N, this justifying the fractal hypothesis indicated by equation (4.4). For our system, we determine D ~ 1.47 from the 2D images. Thus, in three dimensions, we expect a fractal dimension of the order D~ 2 [Kolb 1984].

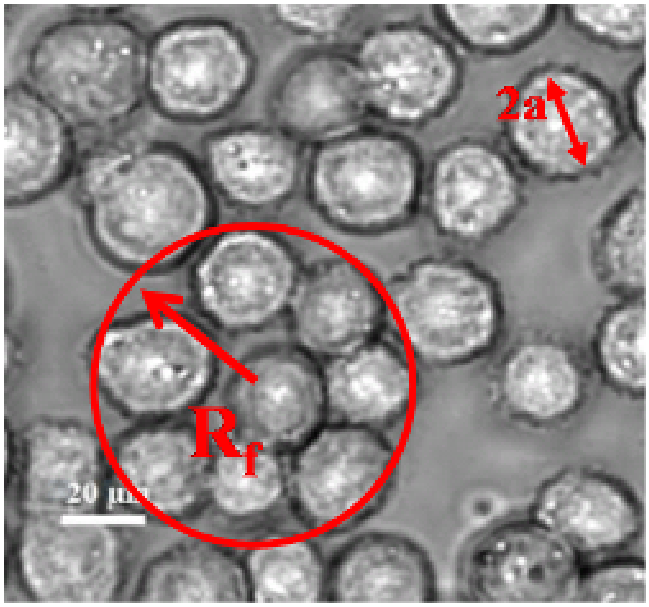

Fig. 4.10. Schematic representation for counting the number of cells N in a cluster of radius Rf

Kolb et al. proposed a model which interpolates between a diffusive and a chemical situation, where geometrical properties of clusters observed in aggregation have been investigated. They determined fractal exponents in two and three dimensions. In our case the fractal dimension in 3D is similar to the ones found for RBCs suspensions, although the scaling exponents for yield stresses are quite different. Two concentrations are used: 10% and 20%. There are noticeable differences at low values of N but there is an increased accuracy for large N, where the two concentrations give rise to the same slope D=1.47. In the semi-empirical model proposed by Snabre and Mills [Snabre 1996],

[Snabre 1999], the formation and dissociation of clusters under flow is taken into account. A change in R_f as a function of the applied shear stress is assumed:

$$\frac{R_f}{a} = 1 + \left(\frac{\sigma^*}{\sigma}\right)^m, \tag{4.5}$$

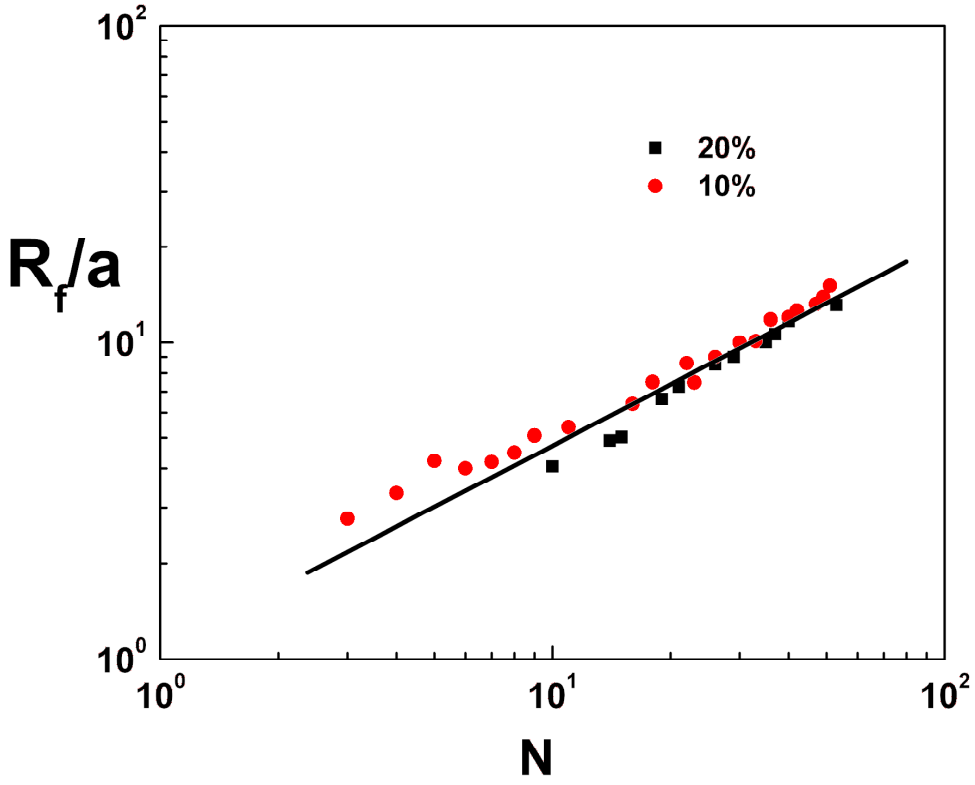

Fig. 4.11. Plot of R_f/a as a function of N to determine the fractal dimension D=1.47.

where m is a dimensionless parameter, σ^* is a critical stress related to the interfacial adhesion between cells: $\boldsymbol{\sigma^* = \frac{\Gamma}{a}}$, and $\boldsymbol{\Gamma}$ is the cell adhesion free energy.

Using the concept of effective medium with volume fraction

$$\phi_A = \phi\left(\frac{R_f}{a}\right)^{3-D}, \tag{4.6}$$

where ϕ_A is the effective particle volume fraction. We further assume an effective viscosity:

$$\eta(\sigma) = \eta \frac{1-\phi_A}{\left(1-\frac{\phi_A}{\phi_m}\right)^2}, \tag{4.7}$$

and one obtains the 1D-constitutive equation that is given by

$$\eta(\sigma) = \frac{\sigma}{\dot{\gamma}} = \eta_0 \frac{1-\phi\left(1+\left(\frac{\sigma^*}{\sigma}\right)^m\right)^{3-D}}{\left(1-\frac{\phi}{\phi_0}\left(1+\left(\frac{\sigma^*}{\sigma}\right)^m\right)^{3-D}\right)^2}, \tag{4.8}$$

which is implicit for σ but provides an explicit relation for $\dot{\gamma}$ in terms of σ. Letting $\dot{\gamma}\to 0$ allows one to determine the yield stress given by:

$$\sigma_s \sim \sigma^* \left(\frac{\phi}{\phi_0}\right)^{\frac{1}{m(3-D)}}. \tag{4.9}$$

The last parameter to be used in the formula $\boldsymbol{\phi_0}$ is the maximum packing concentration found previously. We use the previous model to explain our experimental data. The exponent $\boldsymbol{m_1} = 8.4$ found for the yield stress $\boldsymbol{\sigma_s}$ is plugged into the previous scaling law (4.9) for determination of the parameter $\boldsymbol{m = 0.078}$.

This is smaller than the values of m found for RBC suspensions (typically $m\sim 0.3$). This means that the size of clusters is not so sensitive to the applied stress, indeed one can consider that the cell aggregates are easy to form (or hard to break) because of the round shape of the cells, in contrast with RBCs which need to bind in a very special way to form 'rouleaux'. Thus, once broken by stress, 'rouleaux' are difficult to re-form.

We have obtained the value of the critical stress $\sigma^* = 1.4\, N/m^2$, and a corresponding value of $\Gamma = 1.4 * 10^{-5}\, N/m$. This value of σ^* is higher than the ones obtained for

RBCs [Snabre 1996] but the interfacial energy Γ is in the range of the small value indicated for vesicles [Guttenberg 2001]. This is in favour of the initial assumption that few adhesion molecules are involved in the region of contact between the cells.

Finally, we postulate a similar relationship for the shear elastic modulus:

$$G_0 \sim G^* \left(\frac{\phi}{\phi_0}\right)^{\frac{1}{p(3-D)}} \tag{4.10}$$

where G^* is an effective elastic modulus, but we include an additional exponent n to be determined. We come up with $p = 0.056$ and $G^* = 234$ Pa. This value of the reference modulus G^*, as explained in the concept of fractal exponents [de Gennes 1979], is to be related to typical values for single cells.

In particular, it corresponds to a Young's elastic modulus $E^* = 702$ Pa (assuming that the cell is incompressible) which is typical for adherent wild type CHO cells, of the order 0.5 – 1 kPa [Zhao 2006], and also already measured previously in the group using AFM [Canetta 2005].

4.4.2 An approach based on structural similarity

Another method for having access to parameters like the yield stress σ_s and the viscosity η of such suspensions has been proposed earlier [Coussot 1995]. Coussot shows that clay-water suspensions are shear-thinning yield stress fluids whose apparent viscosity increases with solid fraction. In a large solid fraction range, their behaviour is similar and goes through a transition from non-Newtonian to Newtonian behaviour when the nondimensional shear rate increases. It is shown experimentally that, in the ϕ range (5 - 50%), natural clay-water suspensions have similar simple shear behaviour

types, which suggest that their structures are similar. In a $\left(\frac{\sigma}{\sigma_s}, \dot{\gamma}\frac{\eta}{\sigma_s}\right)$ diagram (nondimensional shear stress and nondimensional shear rate), all shear data gather along a master curve composed of two parts: at low $\dot{\gamma}\frac{\eta}{\sigma_s}$ values, the rupture and restoration of particle links dissipate most of the energy leading to a shear thinning yield stress behaviour; at high $\dot{\gamma}\frac{\eta}{\sigma_s}$ values, hydrodynamic interactions are predominant, leading to a Newtonian behavior.

It can be of interest to mention such an approach since it is relevant to our case, in the context of concentration-dependent laws. The idea consists in assuming a dependence of the reduced shear stress $T = \frac{\sigma}{\sigma_s}$ as a function of the reduced shear rate $S = \frac{\eta\dot{\gamma}}{\sigma_s}$. This similarity is interesting because it can allow superposing the different curves onto a single master curve. The master curve is shown in our case for CHO cell suspensions (Fig. 4.12.) We note again a good superposition of the data, although the few available data points for low reduced shear rates do not allow very accurate results for the parameters under investigation. In an attempt to model the first part of the curve (low shear rates), a relationship of the following kind was found:

$$T = 1 + 6.13\, S^{0.47} \qquad (4.10)$$

The value of the exponent close to $1/2$ recalls the well-known Casson's equation but in a slightly different form. In fact, this form is a limiting case of Casson's equation, corresponding to an asymptotic expansion of equation equation (4.1) for small enough shear rates. The use of equation equation (4.1) instead of equation (4.10) does not fit the whole data. Proceeding further, we can obtain values of the yield stress σ_s and viscosity η from the 'ad-hoc' data reduction. This has led us to similar relationships for the yield stress dependence vs. concentration (as in Section 4.3.3). Similarly, the

analysis of the viscosity (η) dependence against concentration ϕ also shows that equation (4.2) and the following equation proposed by Chong [Chong 1971] :

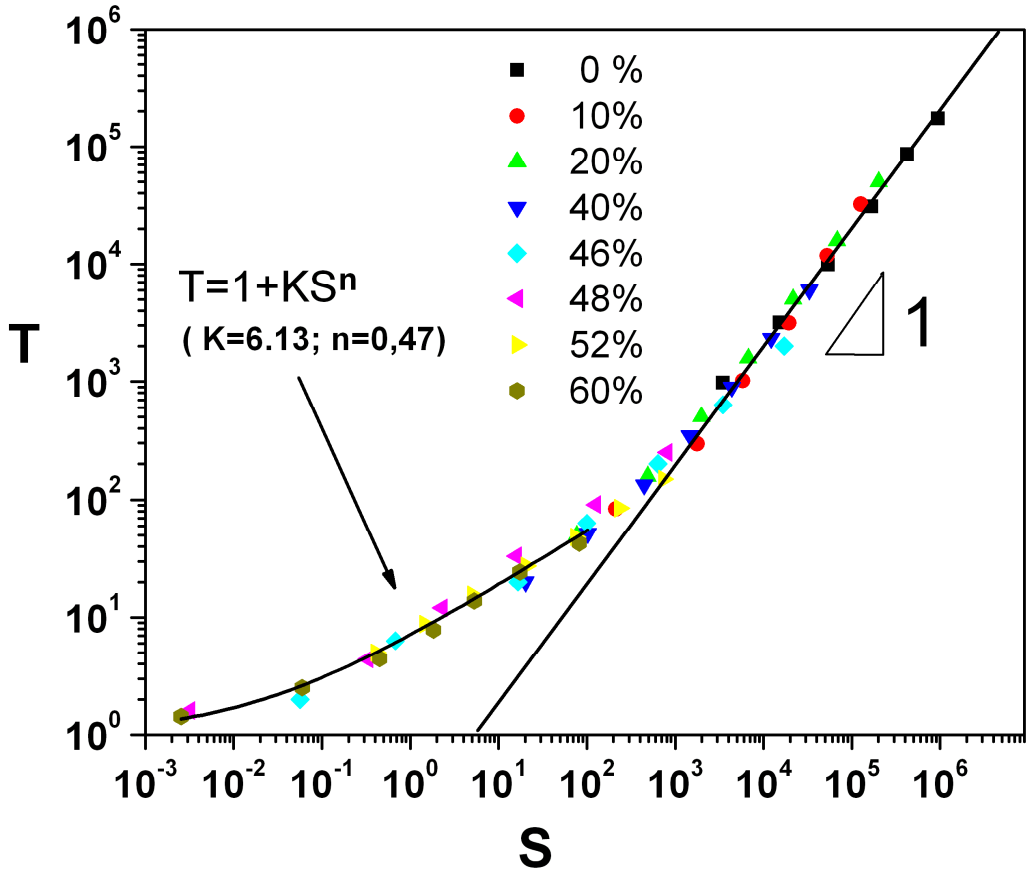

Fig. 4.12. Master curve of the reduced shear stress T vs. reduced shear rate S using the data for all concentrations.

$$\frac{\eta}{\eta_0} = \left[1 + \frac{0.75}{\left(\frac{\phi_0}{\phi - 1}\right)}\right]^2 \tag{4.11}$$

both predict a correct evolution of the viscosity η leading to a packing fraction of the order $\phi_0 = 0.65 - 0.7$. Therefore we can conclude that this approach is complementary to the previous one in the sense that it can lead to an increased

accuracy, when sufficient data is available, although it does not provide physical correlations between microscopic and macroscopic parameters, like the model that we chose to use in the above analysis [Snabre 1996].

4.4.3 Application of a elastic-visco-plastic model for cell suspensions

Finally we compare the results obtained above with the viscosity data for the CHO cell suspensions. Fig. 4.13 shows the comparison of the model with the above experiments.

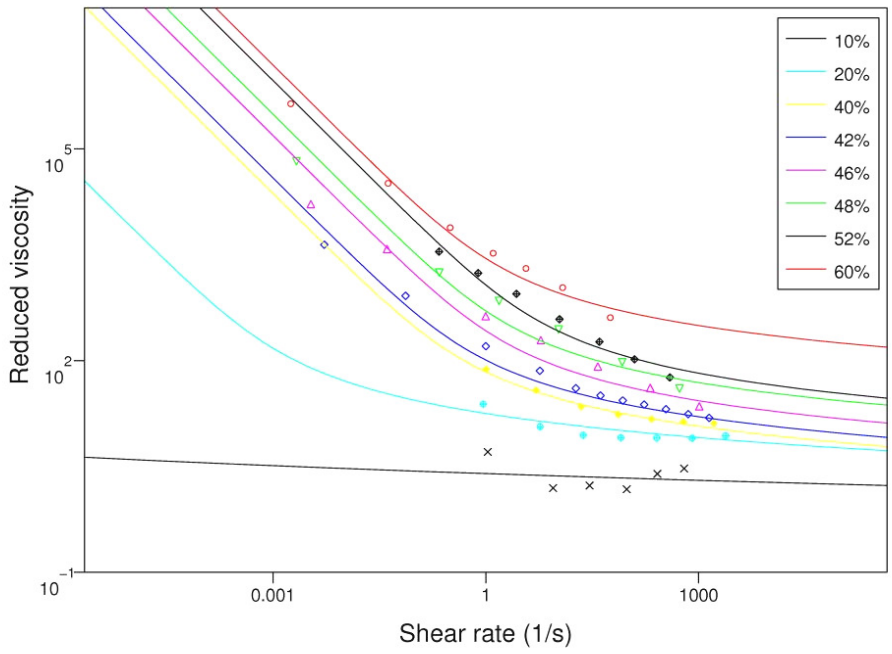

Fig. 4.13: Comparison of CHO cell suspensions with the elastico-visco-plastic model.

The results seem to be in good agreement with the data. Such results can allow the determination of the yield stress. In their simulations, Preziosi et al. [Preziosi 2008] found that α is very small: $\alpha \approx 0.01$, when using a constant limiting viscosity η=0.0013

Pa.s (the limiting value of our previous studies), and that the yield stress takes values slightly different from the previous ones (Fig. 4.14).

The exponent (14.4) describing the behaviour of the yield stress as a function of cell concentration $\sigma_s \approx \phi^{14.4}$, is higher than the previously found one. We do not draw any further conclusions here since more work is probably needed to conclude on the use of this complex model.

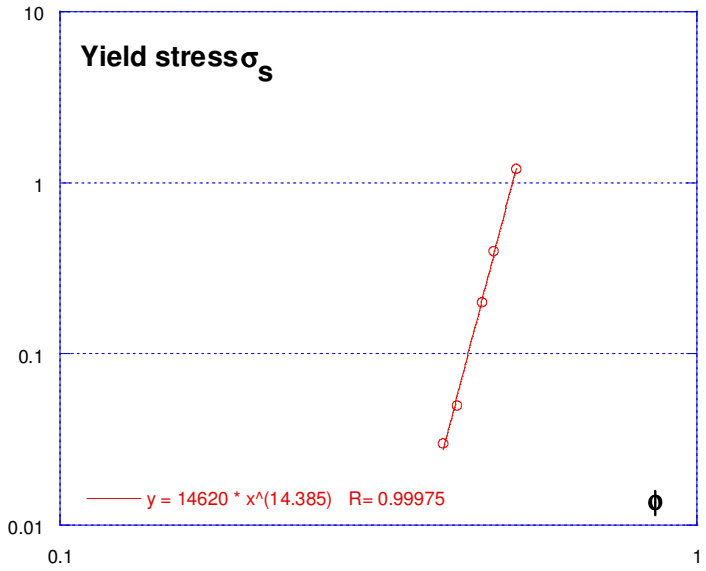

Fig. 4.14: Comparison of CHO cell suspensions with the model.

4.5 Conclusions

To sum up, the system studied here provides unique features important for the rheology of biological suspensions and tissues. These concentrated cell suspensions behave as yield stress fluids (also called elastico-visco-plastic materials), for which a fractal approach has been used. Under shear, the fractal structure changes and can be

modelled using a yield stress σ_s and elasticity modulus G_0 related to the fractal dimension D. Two other microscopic parameters of interest have been introduced in the model: the cell adhesion energy Γ, and the cell's effective elastic modulus E^* found to be:

$$\Gamma \sim 10^{-5} \frac{N}{m},\ E^* \sim 700Pa \tag{4.12}$$

The first is in the range of typical values of cell adhesion energies, and the second in agreement with previous microrheology experiments. We also found an amazing similarity between the dynamic shear moduli $G'(f)$ and $G''(f)$ in this study (at $\phi \geq 0.45$), and the ones obtained from microrheological studies on single cells [Fabry 2001], [Alcaraz 2003], [Hoffman 2006] using various techniques. All show slowly increasing dynamic moduli in terms of frequency, with the same relative positions. This idea probably deserves more attention and should be tested in the future; in particular further works may focus on the characterization of other cellular suspensions including cells with different elastic and adhesive properties.

Finally, such a study can naturally lead to the understanding of biological tissues, by including stronger adhesion properties between the cells, or by taking into account the addition of Extra-Cellular Matrix components, and this is considered in the next chapter.

Résumé français

Dans ce chapitre les résultats expérimentaux sur la rhéologie des suspensions de cellules CHO sont présentés et discutés. De nouveaux résultats sont proposés sur le comportement rhéologique de suspensions de cellules biologiques, du régime dilué jusqu'à des concentrations élevées. Les propriétés en écoulement mettent en évidence un comportement de fluide à seuil, comme dans le cas du sang. Les propriétés dynamiques font apparaître des régimes élastiques aux concentrations élevées. L'observation du seuil d'écoulement et du module de plateau démontre une variation en loi de puissance qui permet de prédire la rupture et la formation d'agrégats cellulaires.

Les paramètres utilisés dans ce modèle nous ont permis de remonter à des grandeurs microscopiques, l'adhésion intercellulaire et le module élastique des cellules individuelles. Par ailleurs ce système modèle devrait permettre de faire le lien entre suspensions concentrées et tissus biologiques.

Pour terminer, nous nous sommes intéressés à un travail récent de Preziosi, Ambrosi et Verdier : les auteurs utilisent un nouveau modèle visco-élasto-plastique pour analyser le comportement des suspensions cellulaires.

5. Viscoelastic properties of cells in 3D collagen gels[2]

5.1 Introduction

One of the goals of tissue engineering is to create artificial organs for patients who need organ transplant. Biomedical engineering and scientists are currently searching methods for creating such organs, which utilize both synthetic and biological components. Our aim was to develop a 3-dimensional cell culture system that mimics a normal tissue. An important aspect is the understanding of the tissue properties from a mechanical point of view. To undertake such investigations, we used a tissue model with is a concentration of collagen, high enough to link the cells together. The viscoelastic properties of these systems were investigated and compared with previous concentrated cell suspensions, to see the difference between cell aggregates and tissue. While rheometrical measurements can give us important information in quantitative terms, in general the structural changes responsible for the measured behaviour remain hidden.

Thus, rheometry was coupled with another experimental technique to characterize structural changes, i.e. confocal reflectance microscopy. This technique can provide 3D detailed images of both collagen structure and cell morphology in nearly real time.

[2] *The contents of this chapter forms the basis of a paper in preparation*

Previous experiments have shown that in collagen gels populated with cells, contraction can occur. Under specified conditions, the mechanical contributions of the fibroblasts in their matrix can be distinguished from those of the matrix [Wakatsuki 2000]. The stiffness of the extracellular matrix can profoundly influence cell and tissue behaviours, and conversely. A microrheometric assay to measure the mechanical properties of model extracellular matrix (type I collagen gel) has been previously developed to explore cytokine-induced, cell-mediated changes in matrix mechanical properties [Leung 2007]. The extra cellular matrix (ECM) provides a rich signalling environment, contributing both biochemically and mechanically to provide important information to morphogenesis or disease processes [Tomasek 2002]. Thus the mechanical properties of ECM are optimized for proper organ function, and these same properties strongly influence the function behaviours of resident cells [Discher 2005], [Engler 2006].

When pathophysiological changes in tissue mechanics appear, therapeutic approaches require a mechanistic understanding of the signals and cellular processes that regulate matrix mechanics. Sophisticated tools are available to study the global and local changes in matrix architecture mediated by cell-matrix interactions [Tomasek 2002]. Previous investigations of cell-mediated matrix remodelling have relied extensively on fibroblasts, the primary matrix regulatory cell, embedded within 3-dimensional scaffolds of purified reconstituted extracellular matrix proteins. Such models have underscored the distinct way cells interact with 3D matrices as opposed to traditional 2D tissue culture surfaces [Cukierman 2001].

Traditional engineering methods such as rotational shear [Zhu 1996], confined compression [Knapp 1997] and uniaxial tension testing have been used to directly assess the mechanical properties of extracellular matrix preparations.

In this respect, collagen gels are used extensively for studying cell-matrix mechanical interactions and for making tissue equivalents. The engineering of tissue analogs, such as bioartificial skin [Bell 1979] and artery based on entrapping cells in reconstituted type I collagen gel, has become an active area of research in recent years; they are named "tissue equivalents" and can be of great interest in fundamental studies of cell behaviour.

However, poor information about the viscoelastic properties of such model tissues can be found.

5.2 Materials and Methods

5.2.1 CHO cell line

We use the same cells as previously, a CHO line (Chinese Hamster Ovary) - an established line of fibroblast. Cells are grown in an adequate environment (typically, 37°C, 5% CO2) in a cell incubator. After first detaching them with trypsin from the box, cells are diluted. We diluted between 6 and 12 flasks with cells (depending on the desired concentration) and we obtained eventually 30-40 ml of culture medium with cells. The suspension was well homogenized and separated into two or three small tubes of 15 ml each. Then tubes containing the suspension were centrifuged for 5 min at 1200 rpm.

To determine cell concentration, a small amount of cell suspension is transferred (after pipeting with a 10 μL micropipette) to a Neubauer's cell chamber. The edge of the coverslip is covered with the suspension to allow each chamber to be filled by

capillarity. The cells are counted (objective x 10) using 16 large squares. Each square of the Neubauer's chamber represents a total volume of 10^{-4} cm^3. The subsequent cell concentration per mL (or the total number of cell) was then determined using the following calculations:

Cells/mL = average count per square x dilution factor x 10^4 (count 10 squares)

Number of cells = cells/mL x original fluid volume from which suspension was removed

5.2.2 Collagen Type I

Collagen is the most common protein in the human body (Fig. 5.1), and is the major component of the extracellular matrix that provides the tensile strength in tissues. The word "collagen" comes from the Greek, and means "glue producing". Because it has great tensile strength, it is the main component of ligaments and tendons. Therefore, it is natural that collagen is used as a scaffold for developing artificial materials in tissue engineering, particularly for blood vessels grafts, artificial skin, ligament and tendon, in which the first stage cells are dispersed into a collagen-based cell suspension and cast into gels.

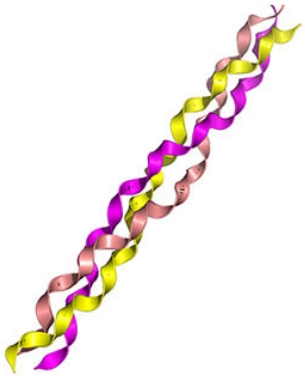

Fig. 5.1: Collagen structure [6].

In order to study cells embedded into a collagen matrix we prepare first collagen solutions (on ice, at 4°C):

1. A known volume of collagen solution (Type I) is added into a tube, depending on the desired concentration.
2. Next, we mix it with the corresponding volume of culture medium.
   (*Note*: The solution has a yellow colour.)
3. Finally we add the neutralization solution and immediately mix.
   (Note: The solution changes from pink to red colour.)
4. After mixing, the solution is still kept in ice, at 4°C.
5. The pH of collagen gel solution must be 7.4.

We next determine the collagen concentration. The initial collagen concentration was 3.45 mg/mL. In order to vary the concentration of collagen we use a volume v of collagen in a total volume V (collagen +culture medium). The desired collagen concentration is therefore:

$$\text{Collagen concentration} = \frac{(3.45\,\text{mg/mL})(\text{v(mL)})}{\text{V(mL)}}$$

Two types of solution were prepared:

a) Collagen gels alone at 4 different concentrations (1.8; 1.38; 0.95 and 0.42 mg/mL),

No.	Collagen Concentration (mg/mL)	Total Vol. (mL)	Collagen (mL)	Medium (mL)	Neutralization Solution 0.1 N NaOH (μL)
1	1.8	0.382	0.2	0.142	40
2	1.38	0.435	0.175	0.225	35
3	0.95	0.362	0.1	0.242	20
4	0.42	0.41	0.05	0.35	10

Table 5.1: Concentration of collagen solutions and component volumes used.

b) Four different collagen solutions including cells were also prepared, respecting the previous protocol. The only difference is the addition of cells following stage 5. A known volume of cell suspension (dilution ~9) was mixed with the collagen gel solution. Following this, the mixture was transferred immediately onto the rheometer at 37°C for 45 min., to initiate polymerization.

(Note: The polymerized gels with cells look cloudy)

No.	Collagen Concentration (mg/mL)	Total Vol. (mL)	Collagen (mL)	Medium (mL)	Neutralization Solution 0.1 N NaOH (μL)	Cells (mL)
1	1.8	0.382	0.2	0.1	40	0.042
2	1.38	0.435	0.175	0.175	35	0.05
3	0.95	0.362	0.1	0.2	20	0.042
4	0.42	0.41	0.05	0.3	10	0.05

Table 5.2: Concentration of collagen solutions with cells, and volumes used, corresponding to a cell concentration of 1.8 107 cells/mL.

Three different cell concentrations were tested: $1.8x10^7$; $1.17x10^7$; $0.7x10^7$ cells/mL. Therefore, the set of solutions will allow us to test the effect of collagen concentration first and of cell concentration in a second series of experiments.

The concentrations used correspond to about 12% volume concentration, since this represents already a large number of cells.

5.2.3 Rheological measurements

Several researchers have studied the rheology of Type I collagen using various techniques [Knapp 1997], [Kaufman 2005], [Velegol & Lanni 2001] but rheometry has not previously been used for collagen gels populated with cells. Rheological measurements of the collagen gels and model tissues have been conducted with the Bohlin Rheometer. After being neutralized, the cold collagen solution was brought to 37° C on the rheometer, under zero-shear conditions for 20 min., until the gels formed. The rheometer was equipped with a heating unit and samples were maintained at 37° C during testing. The viscoelastic properties (G', G'') of our materials were measured using parallel plate-plate geometry (diameter 20mm) and a 500 μm gap. After polymerization took place, the gap was set. We started the experiments immediately after polymerization. The linearity of the gels was checked and it was found that collagen is linear up to ~1% strain. The linear viscoelastic regime for reconstituted type I collagen gel has been established and characterized previously [Barocas 1995].

5.2.4 Microscopy

To characterize structural changes in our model tissues, rheometry was supplemented by another experimental method, microscopy. Confocal reflection microscopy and confocal fluorescence were used to identify and examine the organization of the cells within the matrix fibres. In the case of microscopy, model tissues were investigated at rest, after one day of preparation. The idea is to analyze cell shapes as well as their behaviour within the collagen network. Reflection is an intrinsic optical property of many biopolymers, including collagen. When combined with confocal microscopy, reflection images taken at sequential focal planes along the z axis can be reconstructed in 3D for visualization and for analytical purposes. Reflected light from the collagen matrix has been collected simultaneously with fluorescence for cells marked with GFP (green fluorescent protein) in a time-lapse mode to monitor the dynamic process of cell behaviour/migration through a 3D collagen matrix. We have used confocal reflection microscopy to quantify the cell deformations. Likewise, others used the method for visualization of 3D matrices prepared from natural biopolymers such as collagen [Brightman 2000], [Kaufman 2005].

5.3. Results

5.3.1. Rheometry

First, the collagen solutions were tested. The frequency dependence of G' and G'' at 1% deformation is shown in Fig. 5.2 for frequencies f ranging from 0.01 to 20 Hz at 37° C.

The elastic modulus is always larger than the loss modulus. Both moduli increase very slowly with f and are almost parallel. Similar results were obtained previously for collagen gels (2mg/mL) tested in oscillatory shear at a constant strain amplitude of 1% [Knapp 1997]. The viscoelastic moduli increase with collagen concentrations for solutions 0.42; 0.95; 1.38 and 1.8 mg/mL, as can be seen in Fig. 5.2.

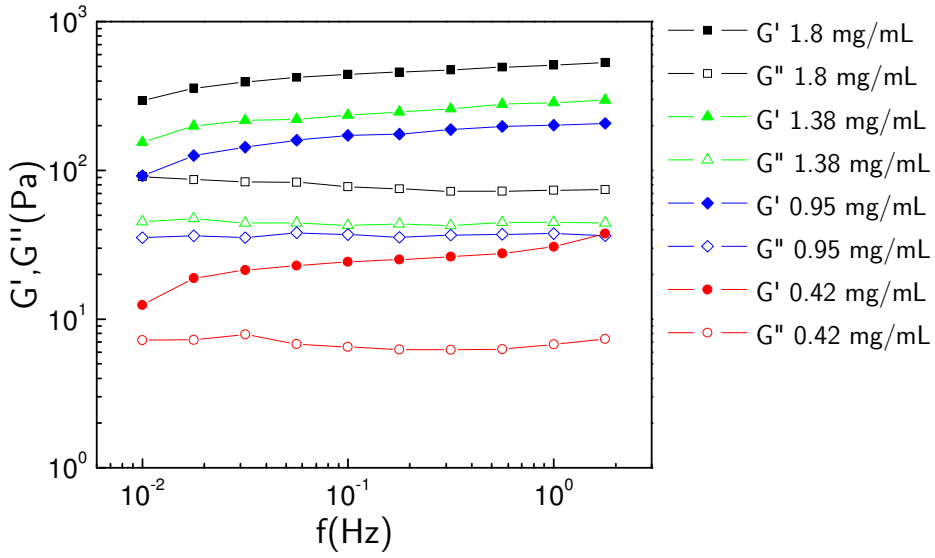

Fig. 5.2: Oscillation measurements: G'(f) (filled symbols) and G''(f) (open symbols) as a function of frequency f for collagen gel solutions at concentrations 0.42 mg/mL; 0.95 mg/mL; 1.38 mg/mL; 1.8 mg/mL.

The intrinsic properties of collagen gels result from the interactions between two component phases: a network of collagen fibrils and the interstitial solution, i.e. the culture medium. In shear, the network and the medium deform together and the resistance to the interstitial flow of the solution through the network can lead to high solution pressure, which allows the gel to withstand compressive load [Knapp 1997]. Our data for collagen gel solutions is comparable to the results obtained in laser trap microrheology [Velegol 2001]. The authors obtained an average shear modulus G which

increase with collagen concentration, but they found a variation in shear moduli using different samples at the same concentration.

Then the collagen gels with cells were characterized. Measurements of storage and loss moduli, $G'(f)$ and $G''(f)$, have been carried out in the frequency range f=0.01-10 Hz using three cell concentrations: $1.8\text{x}10^7$; $1.17\text{x}10^7$; $0.7\text{x}10^7$ cells/mL at each collagen concentration. The results are shown in Fig. 5.3.

a)

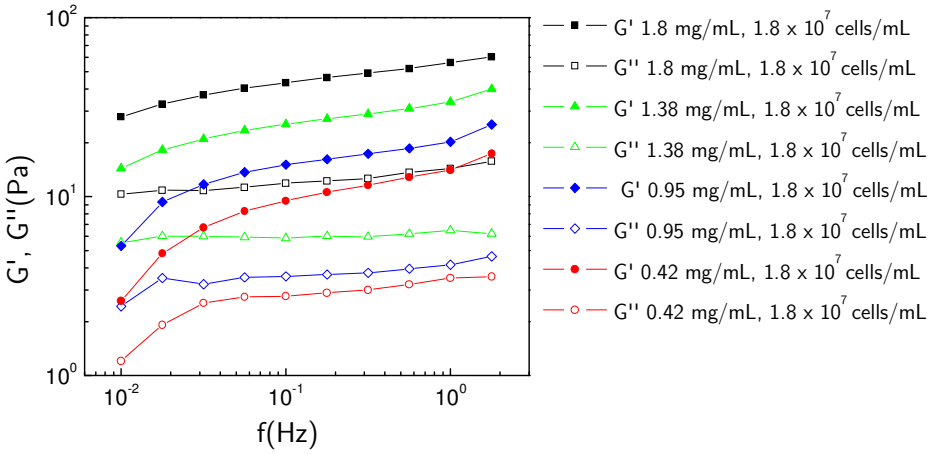

b)

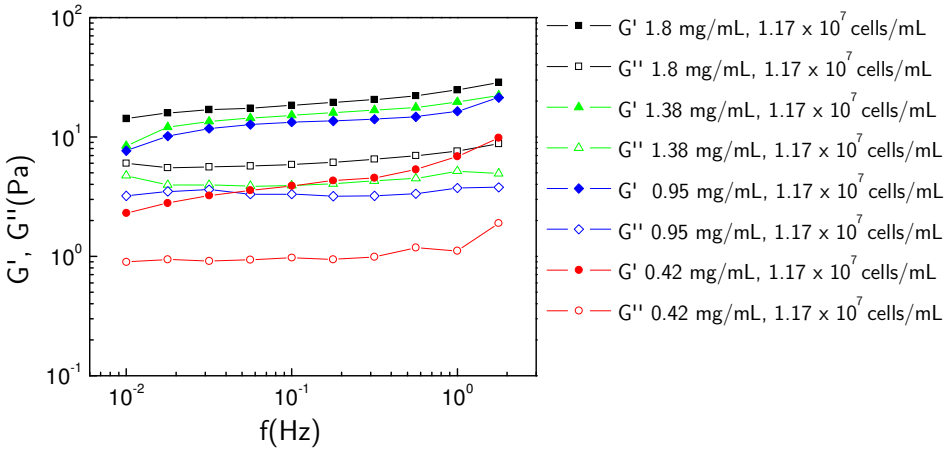

c)

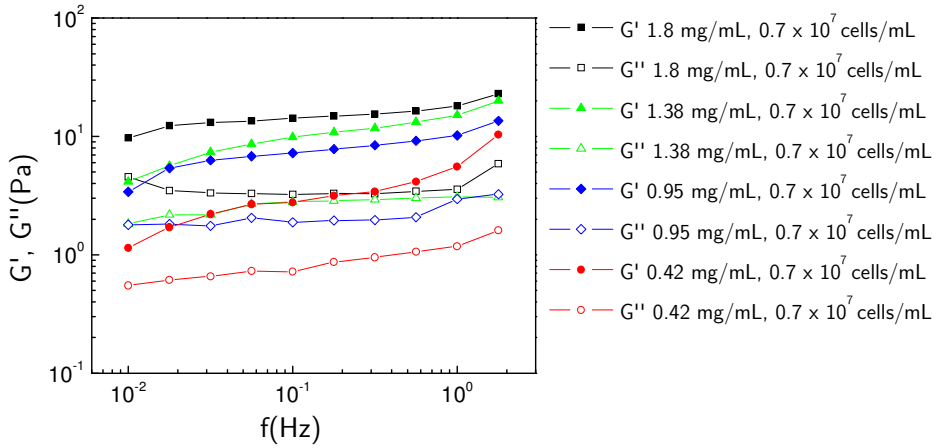

Fig. 5.3: G'(f) and G''(f) as functions of frequency for collagen gel solutions with cells at concentrations: a) 1.8x107 cells/mL; b) 1.17x107 cells/mL; c) 0.7x107 cells/mL for different collagen concentrations.

We observe that for both situations, with cells and in the absence of cells, the viscoelastic moduli increase with collagen concentration, when solutions with the same concentration of cells are compared. An interesting feature is found when solutions with different concentrations of cells are analyzed, as can be seen in Fig. 5.4.

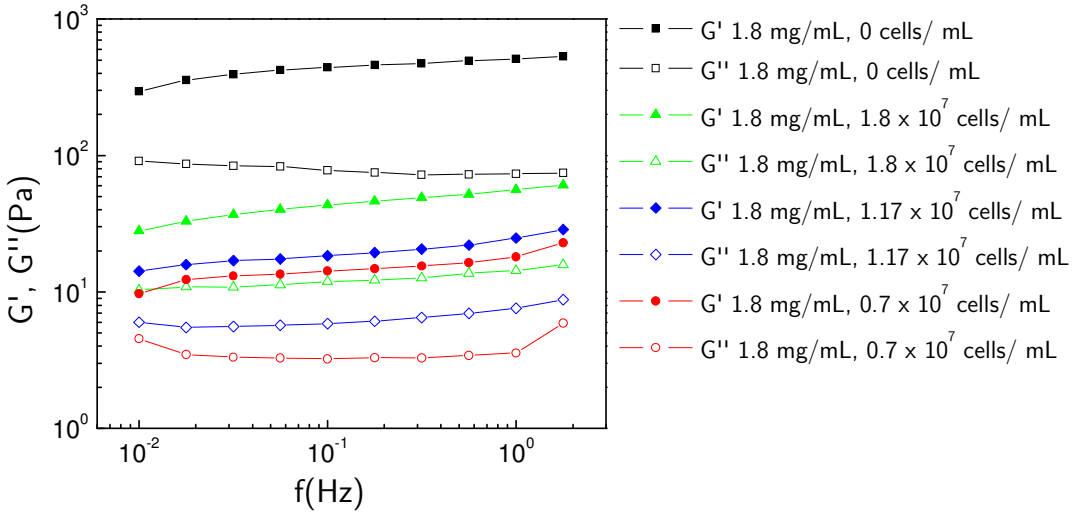

Fig. 5.4. Results of G'(f) and G''(f) as functions of frequency f for the 1.8 mg/mL collagen gel solution with cells at concentrations: 0 cells/mL; 1.8x107 cells/mL ; 1.17x107 cells/mL ; 0.7x107 cells/mL.

In the absence of cells the elasticity of the matrices is much higher. This was also observed using a different technique [Leung 2007]. In the presence of cells the viscoelastic properties increase directly with cell density. Leung *et al.* investigated matrix mechanic properties using microscale bead twisting microrheology with fibroblasts seeded in collagen gels and observed that the stiffness (measured after 1 day) varied inversely with cell density. Note that their cell densities (0.25 - $1*10^5$ cells/mL) were at the low end of those used in our experiments. On the contrary, we measured instantaneous properties of our collagen gels with cells and found a moduli decrease when cells are added and an increase when more cells are included. To analyze these results further, we made a parallel representation of the only *G'* modulus versus frequency *f* for each collagen concentration in the presence and absence of cells (Fig. 5.5).

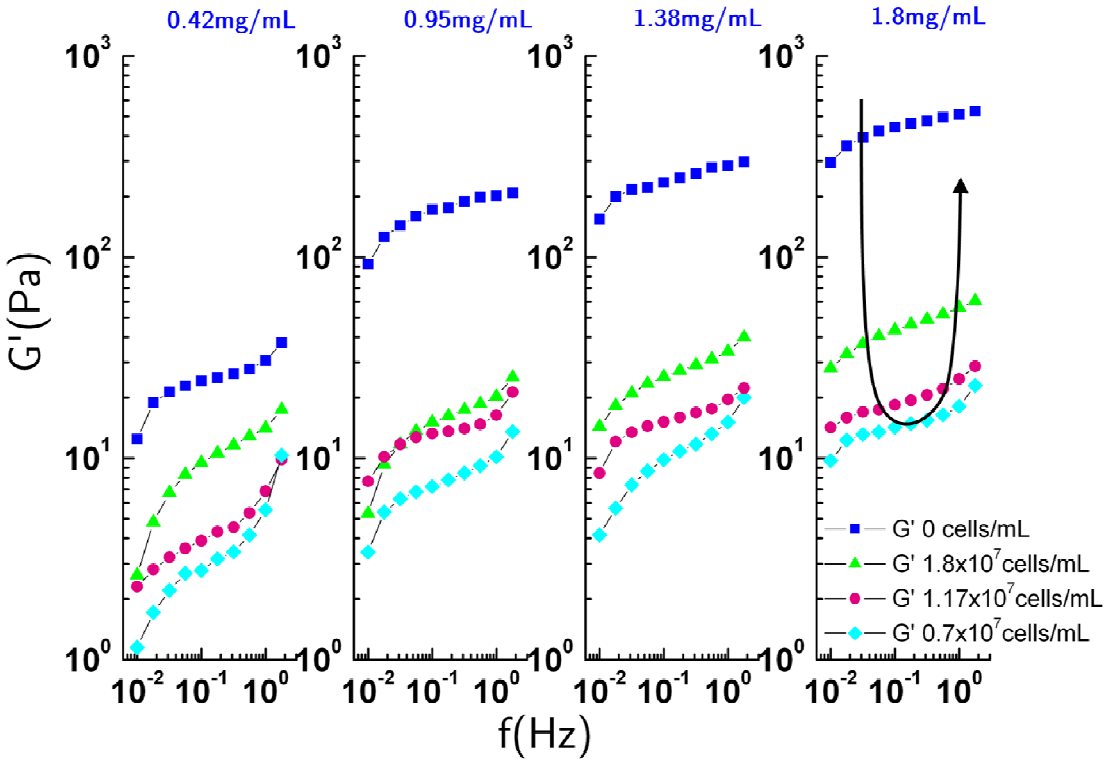

Fig. 5.5: Results of G'(f) as function of frequency f for 0.42; 0.95; 1.38; 1.8 mg/mL collagen concentrations with cells at concentrations: 0; 1.8x107; 1.17x107; 0.7x107 cells/mL. The arrow shows cell concentration increase.

The strongest value of G' was observed at the highest cell density (1.8×10^7 cells/mL) for all 4 collagen concentrations. When the same cell concentration is used at different collagen concentrations, G' increases with collagen density. On the other hand, at constant collagen concentration, we check that a very pronounced decrease in rigidities is present after cell incorporation, followed by an increase when more cells are added (Fig. 5.5). To confirm this analysis G' is presented as a function of frequency f for different cell densities (Fig. 5.6). The increase of the moduli as a function of collagen concentration is again clear. The concentration dependence of the plateau modulus G_0 has been examined by considering the value of $G'(f)$ at a fixed frequency $f = 0.1\,Hz$ (Fig. 5.7). This frequency lies within the plateau like region for all concentrations. Experimental data from various papers [Janmey 1991], [Schmidt 2000] have shown the concentration dependence of the shear modulus to vary from $c^{1.4}$ (virus solutions) [Janmey 1991] to $c^{2.2}$ (actin) [Schmidt 2000], and our case fits reasonably well with such data.

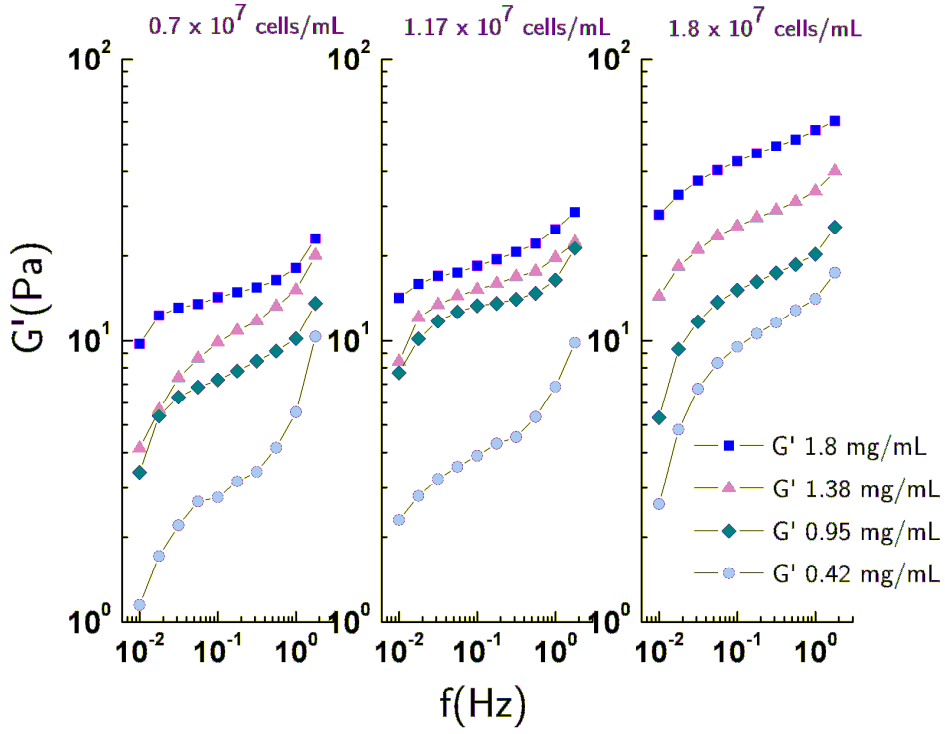

Fig. 5.6: Results of G'(f) as a function of frequency f for each cell density.

In both cases, the collagen gels in presence and absence of cells are sufficiently uniform, or their mechanical properties are dominated by a single structure. Such properties can be reasonably interpreted by existing models for synthetic materials. For example the mechanical properties of extracellular matrix are sufficiently dependent of their own polymer network, i.e. collagen [Storm 2005] and the rheology resembles that of gels of cross-linked polymers. Their relatively frequency- independent viscoelastic properties (G' and G'') as well as the scaling of elastic moduli with concentrations [Janmey 1991] resemble those of other semiflexible polymer networks. The similarity in rheology between some extracellular materials and synthetic polymers gels has motivated attempts to account for cell rheology using models developed for polymer networks [Storm 2005]. The rheology of soft biological materials indeed depends on the arrangement of long protein filaments into networks of different geometries.

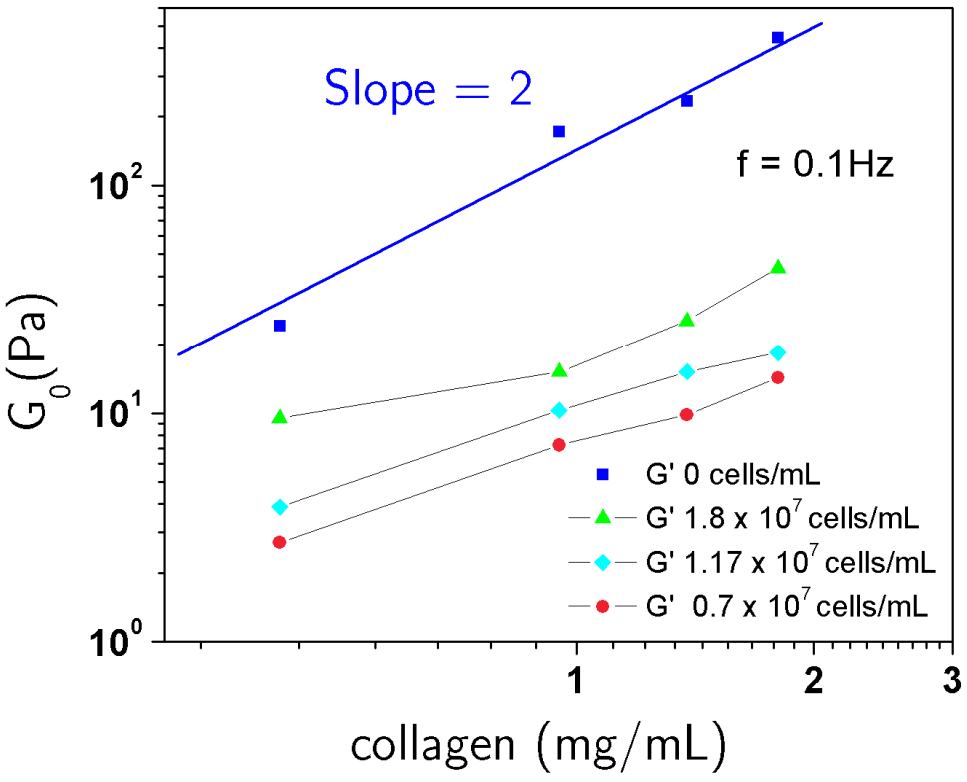

Fig. 5.7: Concentration dependence of the shear elastic modulus (0.1 Hz).

The specific geometries of these networks are determined by the chemical and mechanical properties of filaments, as well as those of the cross-links that hold the filaments together. Despite their chemical and structural differences, the most abundant protein filaments of extracellular matrices and intracellular cytoskeletons have the common property of being semiflexible filaments cross-linked into open meshworks. These mechanical properties likely contribute to the biological functions of cytoskeleton proteins in forming elastic networks with minimal protein production and networks with large mesh size that allow passage of large molecular assemblies and organelles.

The rheological properties of the networks formed *in vivo* are likely to differ in some aspects from those formed *in vitro*. *In vivo*, the production of filaments and networks is regulated by numerous cross-linking factors and is not yet capable of being produced from purified factors.

Based on these ideas, it seemed important for us to study the microstructure of such systems, and this is done in the next part.

5.3.2 Confocal reflection microscopy

To understand how cells remodel collagen matrices, collagen gels of various concentrations (c= 0.42 - 1.8 mg/mL) in absence and presence of cells are examined with microscopy. A confocal data set is similar to a book with many pages, and each page shows information only available if you move down to that page and read it (Fig. 5.8).

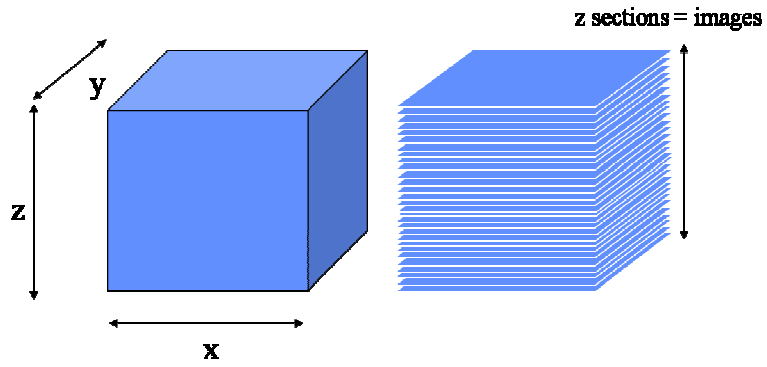

Fig. 5.8: 3D Image reconstruction.

First collagen matrices at the four concentrations (c= 0.42 - 1.8 mg/mL) are imaged with confocal reflectance microscopy (Fig. 5.9).

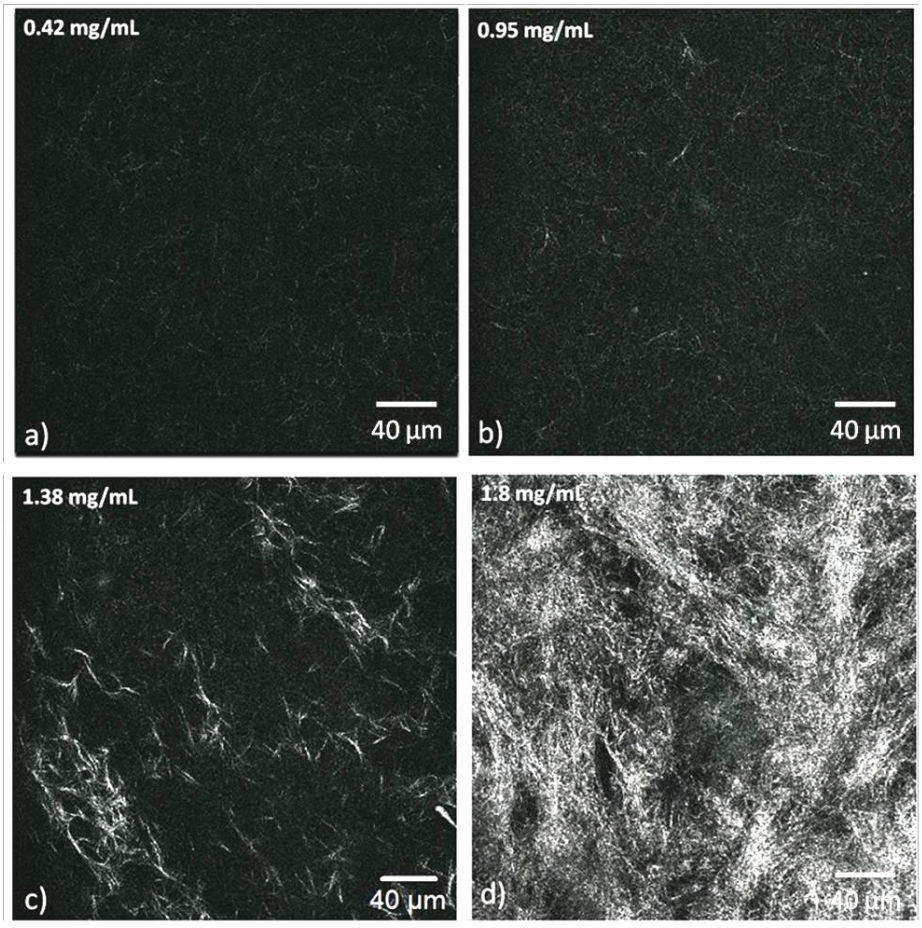

Fig. 5.9: Confocal reflection images at four collagen concentrations demonstrate the architectural differences between matrices prepared from type I collagen 24 h before microscopy experiments. Bar=40 µm for all images.

These images are taken ≈120 μm deep into the sample and a visual inspection suggests that the matrices present an increase in fibre density with increasing collagen concentration.

The advantage of confocal microscopy is that one can visualize frames from a 3D object even in planes that one does not image directly. This is called "slicing" an object and is an important advantage of confocal imaging.

The collagen within the entire block was extracted using the Metamorph software. The percentage of entire volume occupied by collagen was determined for each concentration (Fig. 5.10).

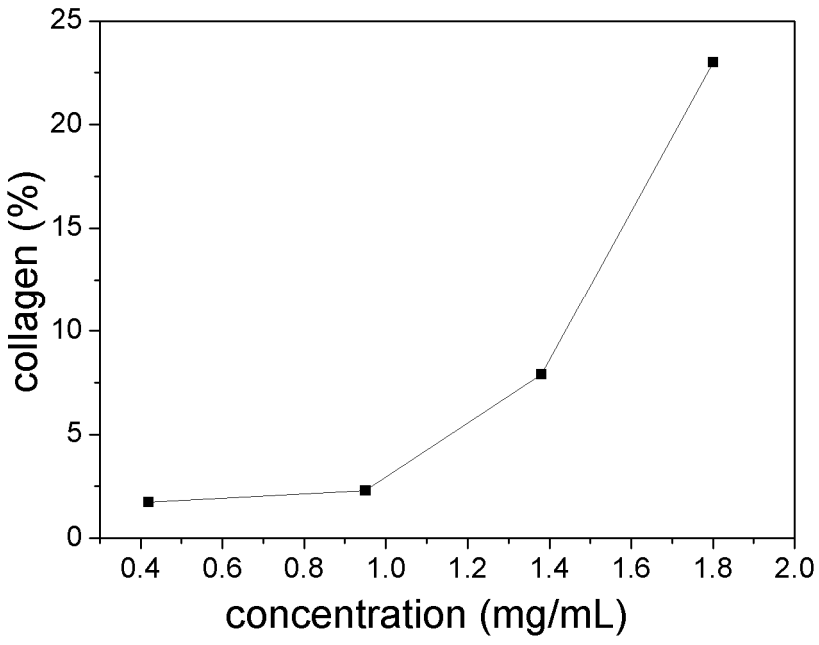

Fig. 5.10: The percentage of volume occupied by collagen fibres after polymerization versus real collagen concentration.

These results are not quantitative and this phenomenon is obviously inherent to the method. Still it shows a good correlation corresponding to collagen increase when going from a) to d) in Fig. 5.9.

To study the mechanical impact the cells have on their microenvironment, the cells ($1.8x10^7$ cells/mL) are placed within gels with collagen concentrations between 0.42 mg/ml and 1.8mg/mL. This is shown in Fig. 5.11.a-d.

It seems obvious that the expansion/elongation of the cells in Fig. 5.11.a (low concentration) is important. Cells adhere easily. Such cells seem to deform the collagen fibres in their surrounding areas and probably also bring collagen closer to them, i.e. they remodel it.

On the other hand, cells seem to be less elongated in the next two Fig. 5.11.b-c. Stiffer matrices have lower impact on cell shape.

Finally, at large collagen concentration (Fig. 5.11.d) cells seem to be stuck within the locally concentrated collagen and can hardly move. Meanwhile the solution between the collagen fibres seems to flow outwards. The idea being tested is that cell traction and outward pressure exerted by the fluid are two antagonistic forces and may play a role in the micro-environment of the 3D tissue model.

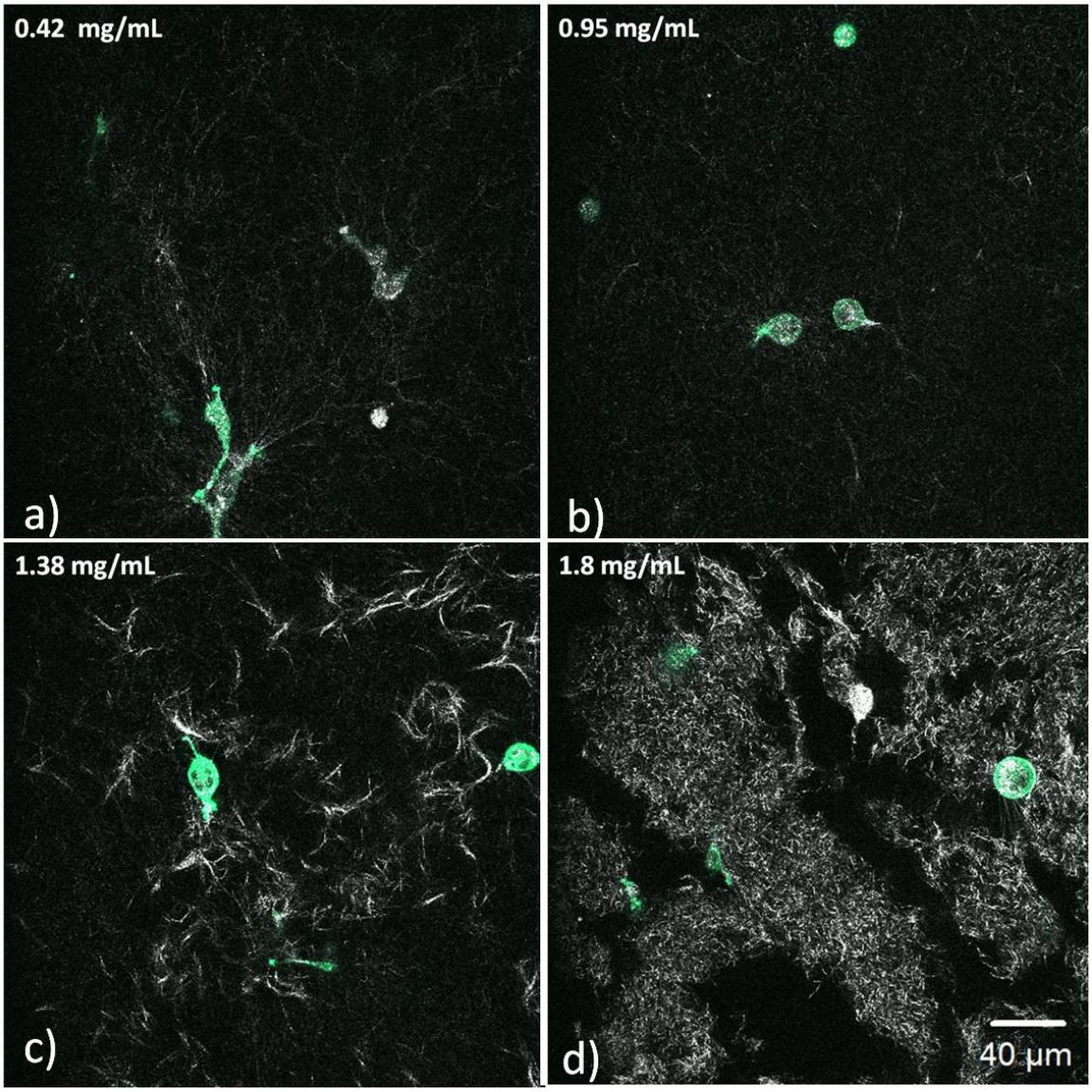

Fig. 5.11: Confocal reflectance and fluorescence microscopy for collagen gels with cells after 24h of incubation; (magnification 40x, 1µm z-slice, xy: 358 x 358µm, Zoom 0.7).

To verify these observations we analyzed a z-stack of images corresponding to single cells (zoom 3) embedded in collagen gels at different concentrations (c= 0.42 - 1.8 mg/mL). Fig. 5.12a confirms that in a less concentrated collagen gel the cell presents a large deformation, in opposition to higher collagen concentrations where cells retain the general shape (Fig. 5.12.b-d). In addition, Fig. 5.12.d shows a high density of fibres around the cell and low density areas elsewhere.

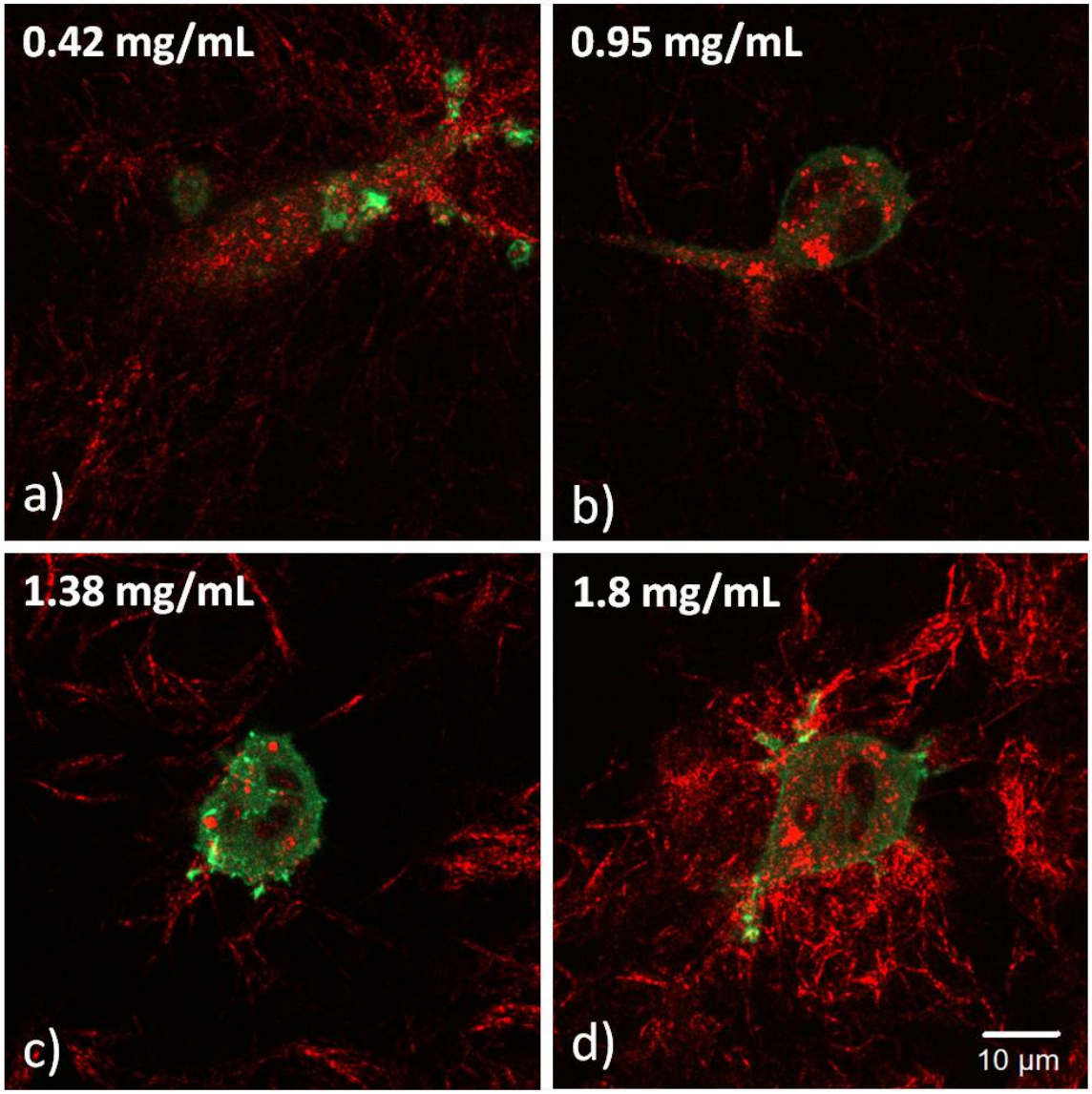

Fig. 5.12: Confocal reflectance and fluorescence microscopy for collagen gels with cells after 24h of implantation; (magnification 40x, 1µm z-slice, xy: 76.8 x 76.8 µm, Zoom 3).

However, there is no evidence in Fig. 5.11 and Fig. 5.12 that the pressure affects the environment of the cells and to complete the information of a "possible remodelling" of the collagen by the cells, we need to determine first the elongation of all the cells for each collagen concentration. To do that, cells from each model tissue were subdivided into many building blocks using Metamorph. To process the data for each cell we used the Edit3D_quanti software kindly provided by Yves Usson (TIMC-IMAG). The analysis

and 3D visualisation software were written in standard C language using the GL library (Silicon Graphics library) and the FORMS user interface library (courtesy of Marck Overmars, Department of Computer Science, Utrecht University, The Netherlands) [Wozniak 1996], [Parazza 1995], [Parazza 1993]. Details of the method are provided in the Appendix 1. The software does not account for the nucleus volume, so we obtain volumes of cells over the volume of cytoplasm (Example of such data in Appendix 2). To get the distribution of cells for each collagen concentration, cells were projected in 2D (Fig. 5.13).

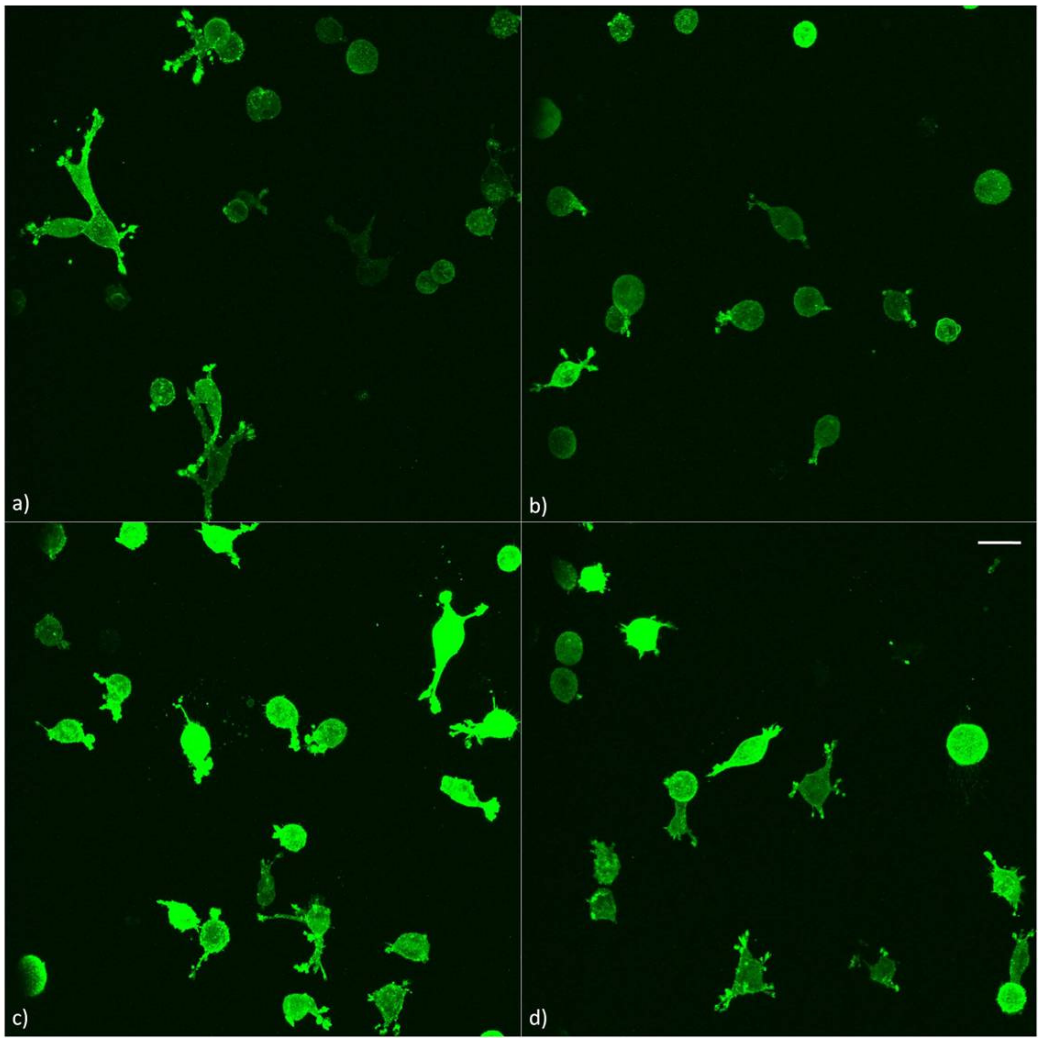

Fig. 5.13: Projection of cells in 2D for each collagen concentration. Bar= 20µm for all images. a) 0.42 mg/mL; b) 0.95 mg/mL; c) 1.38 mg/mL; d) 1.8 mg/mL.

All the cells in each block of images (Fig. 5.13) were processed using the plugin Edit3D. Elongation for each cell of each model tissue was calculated (Fig. 5.14) and we confirm our visual observations regarding the changing shape of cells at different collagen concentrations. The most elongated cells were found in less concentrated collagen (0.42 mg/mL)

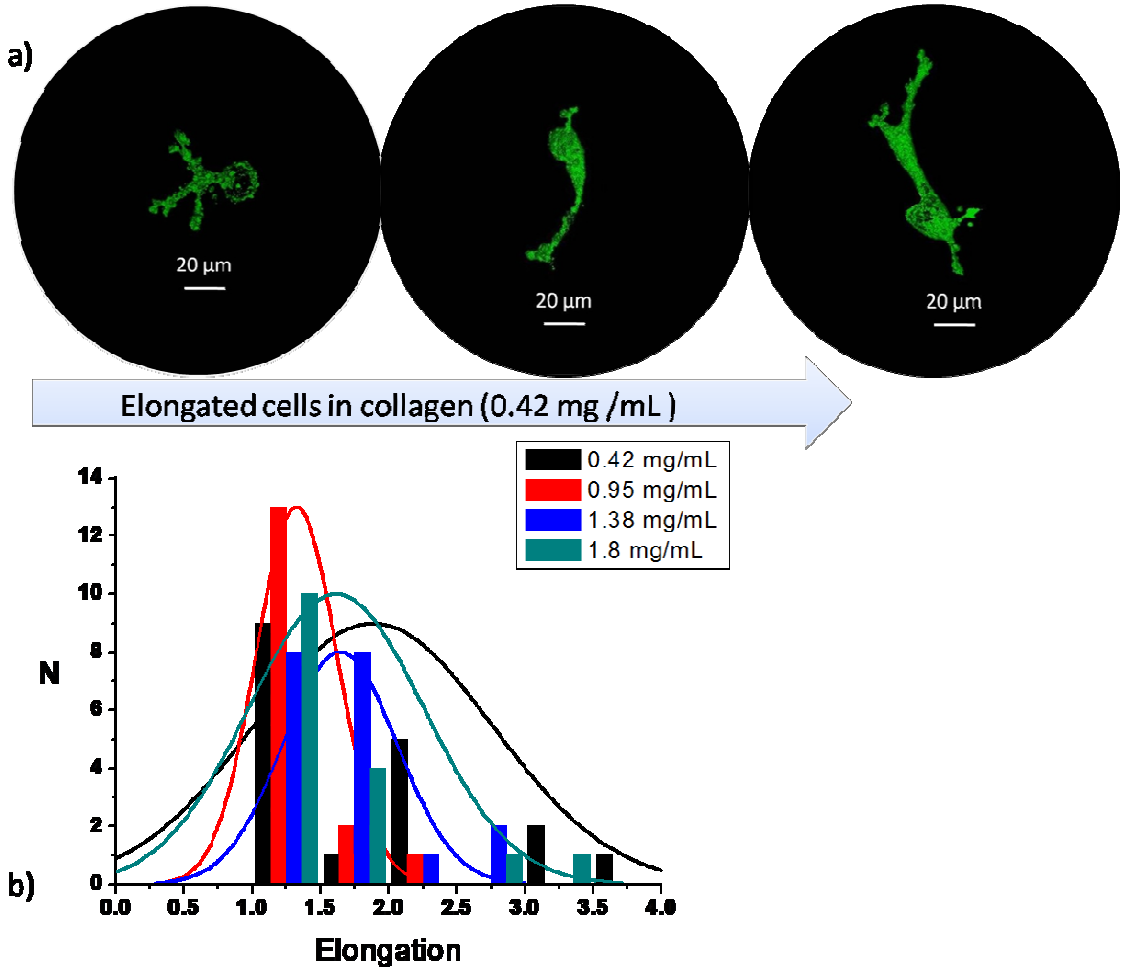

Fig. 5.14: a) Example of elongated cells in collagen gels (0.42 mg/mL), here surface representation of the cell with Edit3D; b) Histogram with elongation of cells for each collagen concentration, N number of cells.

In order to understand the range of elongation for each collagen concentration, the results from Fig. 5.14.b are portrayed as a box chart representation (Fig. 5.15).

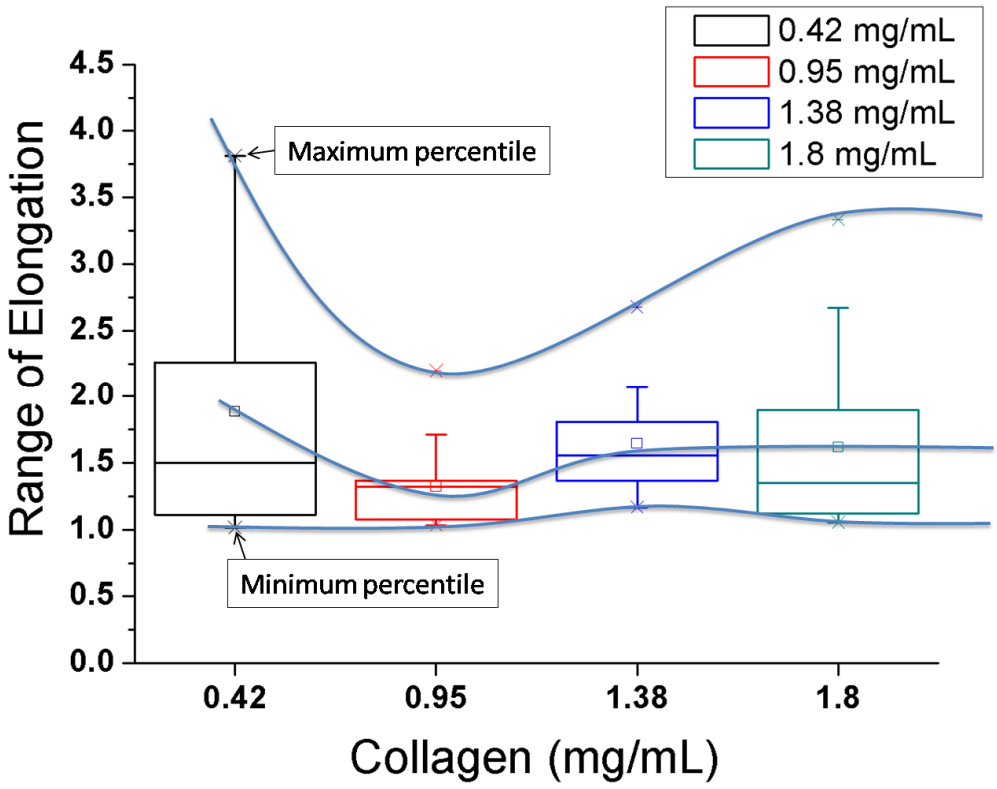

Fig. 5.15: Box chart representing range of elongation versus collagen concentration The Y-axis shows Range of elongation. The boxes outline the 25–75% data range, squares in the boxes correspond to the mean elongation value, crosses (x) delimit the 99% data range, and hyphens (-) represent minimum and maximum elongation values.

The box plot is a graphical representation of key values from summary statistics of elongation for cells in different collagen matrices. All parameters (mean, maximum, minimum) seem to indicate a maximum elongation for small concentration, then a minimum for intermediate collagen concentration, and finally a slow increase for larger concentrations.

5.4 Discussion

Fig. 5.15 is the starting point of the discussion regarding the effects of cell on the ECM (collagen) or conversely. It seems that tissue/cell reorganization is related to the existence of two effects competing together:

Effect 1 (collagen density):

- when collagen density is high, cells can adhere easily and elongate, and also migrate more easily, as long as the density is not too high. In such a case, they cannot move too much because they are well attached to the substrate. This corresponds to the migration velocity curve (in red in Fig. 5.16), shown in a famous paper [Palecek 1997],
- when collagen density is low, cells cannot move fast and do not elongate so much.

Effect 2 (size effects):

- when collagen density is high, cells do not have any space to move and elongate,
- when collagen density is low, cells have a lot of space, spread and migrate.

A third resulting effect can also affect the microstructure of this model tissue: cell attachment creates shrinking of the collagen filaments therefore they can be attracted by the cells; this creates larger aggregates in between which the interstitial fluid can circulate. This effect lowers the global rigidity of the tissue

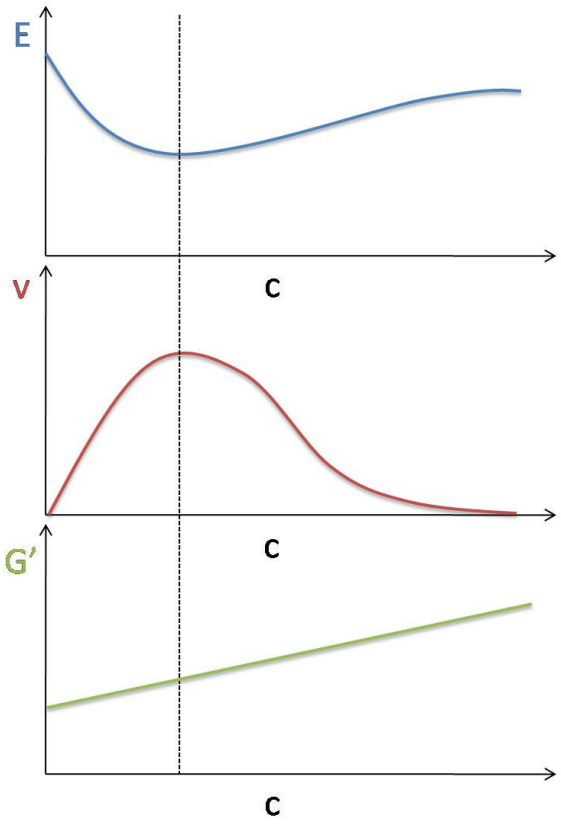

Fig. 5.16: Schematic representation of elongation of cells (E), speed of the cell (v) and elasticity of the collagen gels with cells (G') as function of collagen concentration (c).

Fig. 5.16 tries to model these features in the following way, under the above assumptions, considering a fixed cell concentration:

- *low collagen concentration:* more space and less material to adhere. It is the space effect which is dominant. Cells elongate and adhere strongly. They do not move fast. The rigidity of the tissue is high,
- *intermediate collagen concentration:* less space but more material. Cells do not have enough space to elongate. They remain round and are quite motile. Their movement is the amoeboid one, they move through the fibre network easily. Their elongation is small.

- *high collagen concentration:* hardly any space, but a lot of material to adhere to. Cells pull on the collagen but have no space. Eventually they remodel the network strongly. They are slightly elongated but do not move fast.

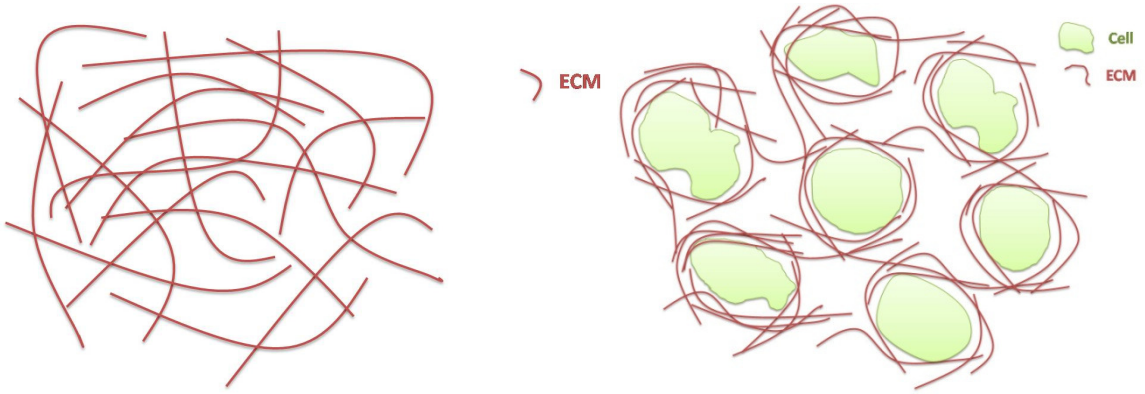

Fig. 5.17: Sketch of a possible new structure formed by the inclusion of cells in a 3D collagen network: Cells reorganize the collagen matrix by attracting collagen thus depriving other regions from collagen, thus creating less dense regions. The rigidity of the network on the right is smaller.

To be precise, we finally need to conclude on the drastic reduction of the elastic moduli obtained previously. All the ingredients are here now to explain that due to the ability of cells to attract collagen and bring filaments closer, the network can be reconstructed from its initial arrangement (Fig. 5.17a). There we can see a collagen network with strong interacting links which give a gel of high rigidity. After the addition of cells, which remodel the structure by attracting collagen, different sub-units can be formed and are networks of interacting cells, with the presence of less dense regions of collagen (as seen previously on the microscopic slides) like in Fig. 5.17b.

5.5 Conclusions

As a final point, we summarize our findings about the viscoelastic properties of cells embedded in collagen gels, obtained with two methods, namely rheology and microscopy. We focused here on the mechanical impact that CHO cells can have on their microenvironment, and reciprocally. We used a collagen type I gel for studying the behaviour of cells in networks submitted to diverse mechanical stress/strain regimes.

By means of a variety of techniques, including bulk rheology, and the simultaneous use of confocal reflectance and fluorescence microscopy, we were able to study both collagen matrices and collagen matrices including CHO cells.

Regarding collagen matrices, we found similar dependences of the elastic modulus as a function of collagen concentration, as predicted by previous theories and put down the basis of our analysis.

Concerning matrices including cells (i.e. tissues), we found that cells can affect the collagen microstructure drastically. This was evidenced by a strong decrease of the rigidity when adding cells, whatever their concentration, and whatever collagen concentration was used. Confocal microscopy (fluorescence and reflection) was found to be a very powerful tool for the investigations of such systems. It enabled us to determine the rate of elongation of cells in a tissue and to propose new ideas to investigate the interactions between cells and their micro-environment. These hypotheses can help predict the rheological properties of such biological systems.

Résumé français

Le chapitre 5 présente les principaux résultats obtenus avec les cellules CHO dans un réseau 3D de collagène. Un tissu modèle est réalisé, en incluant ces cellules dans une matrice de collagène. Pour mesurer les changements structurels, la microscopie confocale est utilisée. Un phénomène nouveau, la diminution de la rigidité du gel en présence de cellules, est observé. En effet, les cellules s'allongent dans le gel et peuvent le remodeler en fonction de la concentration : l'adhésion des cellules est facilitée lorsque la concentration en collagène est importante, mais l'espace est restreint. Ces deux effets s'opposent mais expliquent les comportements observés.

6. Conclusions

Cell suspensions and soft tissues interact mechanically in a variety of situations relevant to biomedicine and biotechnology. A key phenomenon in these interactions is the special behaviour of cells in a suspension or in a tissue model comprising cells entrapped in a gel.

In the case of concentrated suspensions, we have shown in this work that the system behaves as a yield stress fluids, for which a fractal approach has been suggested. Cell suspensions correspond to aggregated systems and under shear their structure is based on the remodelling of the cell units with respect to each other. Under flow, the fractal structure changes and can be modelled using a yield stress σ_s and elasticity modulus G_0 related to the fractal dimension D. Typical scaling behaviours for these two parameters have been investigated further as functions of concentration. By doing so, we also determined prefactors which can be compared to single microscopic properties, such as cell adhesion energy and the cell individual elastic modulus. It seems important to note that comparable qualitative results have been obtained previously through microrheological studies on single cells. All results show slowly increasing dynamic moduli in terms of frequency [Fabry 2001], [Alcaraz 2003], [Hoffman 2006]. This property probably deserves more attention in the future.

Finally, other models have also been proposed to investigate similar properties from another point of view, leading to satisfactory results.

We have kept the above description to carry on the second part of the work where the same suspensions were included in a collagen matrix. This network mimics normal tissues, such as connective tissues for example. To characterize structural changes in

our cell filled gels, rheometry was supplemented by another experimental method, confocal microscopy. The technique proved to be very powerful. The viscoelastic properties of these systems have been investigated. Similar behaviours between the dynamic shear moduli $G'(f)$ and $G''(f)$ were found for concentrated cell suspensions and tissue models. On the other hand, a very important feature has been observed, which shows that the collagen network architecture can be dramatically changed due to the presence of cells. This observation was not expected as we started this work. In order to explain the relevant physical mechanisms in presence, we measured a few parameters (both quantitative and qualitative) related to the way cells pull on their environment, how they move or migrate, and how elongated they are.

The elongation parameter revealed that cells are more elongated in less concentrated gels, whereas there is a minimum elongation, and the elongation rises again at higher concentrations. There is a biphasic behaviour which can be explained thanks to two few simple ideas: adhesion is easier when collagen concentration increases [Palecek 1997] and space is reduced as collagen concentration increases. These two mechanisms compete and can explain the bi-phasic dependence of the cell elongation curve. At the same time we can recover the biphasic migration curve but it is obtained here in 3D, and the elastic moduli strange behaviour is now understood.

Although this last part is rather qualitative, it can help understand the complex structure of tissues.

Naturally, one can think about further straight forward studies which we did not have time to carry out:

1. Following the work on cell suspensions, it seems interesting to investigate the effect of cell type, cell adhesion and cell rheological properties before we can think about a universal behaviour. As previously explained, the comparison between macrorheology

and microrheology seems to be surprisingly in agreement in the case of concentrated suspensions. This point needs further clarification.

2. Model tissues have revealed striking effects of cells on the collagen matrix and vice versa. It will be very interesting in the future to try to understand these features using these combined techniques (rheometry and confocal microscopy). For example, one possible extension of this work lies within the time dependent behaviour of cells. Migrating cells in such tissues can play a definite important role as they reorganize the ECM permanently. We only looked here at short times (24h) but other studies are concerned with much longer times of the order of several days. This time effect seems to have a more intricated effect [Leung 2007], which is possibly due to our observations, but this needs to be looked at in details.

3. Going back the technique used, this opens up a complete new field of study for the investigation of cell migration in such collagen matrices. The comparison between normal cells (CHO cells for examples) and tumour cells can now be made. Do tumour cells move in a different way? Is this a collagen concentration dependent mechanism? Do cells destroy the ECM or do they move using an amoeboid type of motion? It should be soon possible to find out more elements for answering these questions.

4. Finally we have provided several types of models to investigate cell suspensions. Another model is now available and more suited to the description of such tissues [Preziosi 2008]. This can again open up a new field of interesting applications. Probably the first questions would be to apply this model to the behaviour of the model tissues which we have determined in the present work.

Finally, we should mention that this work has been of importance during the collaborative years of our RTN Network. People have started to include cell interactions/adhesions in their models of tumour progression; they are now seriously

thinking about including also the environment resistance and we have proposed different tools to do so.

We hope that this work can serve as an important complementary tool for the investigation of cell behaviours, as well as the rheological properties of cell suspensions and tissues. It can lead naturally to other applications in cancer modelling, such as tumour modelling, and possibly in cancer therapy, if one thinks about differentiating different invasive tumours.

Résumé français

En conclusion de ce travail, nous pouvons espérer que les résultats (contrainte seuil, élasticité, approche fractale) sur les suspensions concentrées de cellules ont montré clairement le comportement visco-élasto-plastique de ces systèmes. Ils servent de base à la constitution de tissus 3D.

La caractéristaion rhéologique des suspensions cellulaires a été prolongée par l'étude un tissu biologique, où nous avons observé des résultats nouveaux et inattendus. Nous avons mis en évidence l'importance des propriétés cellule-matrice et du remodelage de la matrice pour expliquer ces propriétés rhéologiques.

En application de ce travail, nous pouvons proposer les perspectives suivantes :

- l'utilisation de lois de comportement pour prédire les propriétés rhéologiques de tissus et tumeurs,
- la corrélation entre micro- et macro-rhéologie demande à être précisée comme nous l'avons montré par des analogies,
- pour terminer, la technique optique développée permettra d'aborder la migration de cellules cancéreuses dans un environnement 3D, afin de mesurer les forces en présence, notamment grâce à la déformation locale des fibres de collagène autour de la cellule.

Appendix 1: Presentation of the software Edit_3D by Yves Usson

Interpolate

The *interpolation* function allows recreating an image with true dimensions. Indeed, a typical measured voxel is 0.32 µm in x and y, but 1 µm in z. In order to have cubic voxels, from which elongation can be calculated for instance, two slices have to be added in the z dimension, by interpolating the already existing slices.

3D filters - Noise removal

Random noise originating from low signal strength, which is the case in confocal microscopy, can usually be reduced by collecting more signals (temporal averaging) but this may not be practical. An often used approach to reducing random speckle noise in images is a neighbourhood smoothing operation. By averaging the value of each pixel with that of its neighbours (36 in our case), the random speckle noise in uniform regions tends to average out. However, this blurs edges and removes fine detail.

Dynamics - Compensate attenuation

The biological samples are in general transparent, but tend to absorb a slight amount of light. The curve of attenuation as a function of depth can be modelled (Fig. A1.1).

The image is a plot showing the number of pixels as a function of the pixel brightness value.

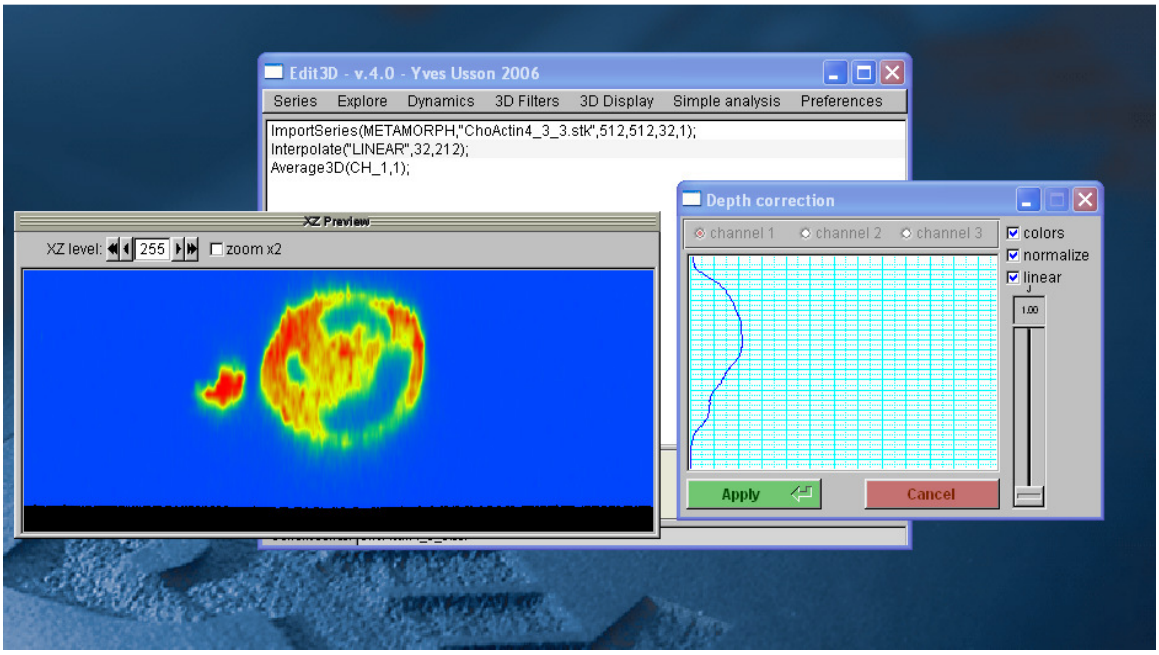

Fig. A1.1: Compensate attenuation step in Edit 3D_quanti processing.

Simple analyze - Binarize (Thresholding)

Thresholding is the simplest method of image segmentation. From a greyscale image, thresholding can be used to create binary images. A binary image is a digital image that has only two possible values for each pixel. Typically the two colours used for a binary image are black and white, though any two colours can be used. The colour used for the object(s) in the image is the foreground colour while the rest of the image is the background colour. During the thresholding process, individual pixels in an image are marked as "object" pixels if their value is greater than some threshold value (assuming

an object to be brighter than the background) and as "background" pixels otherwise (Fig. A1.2).

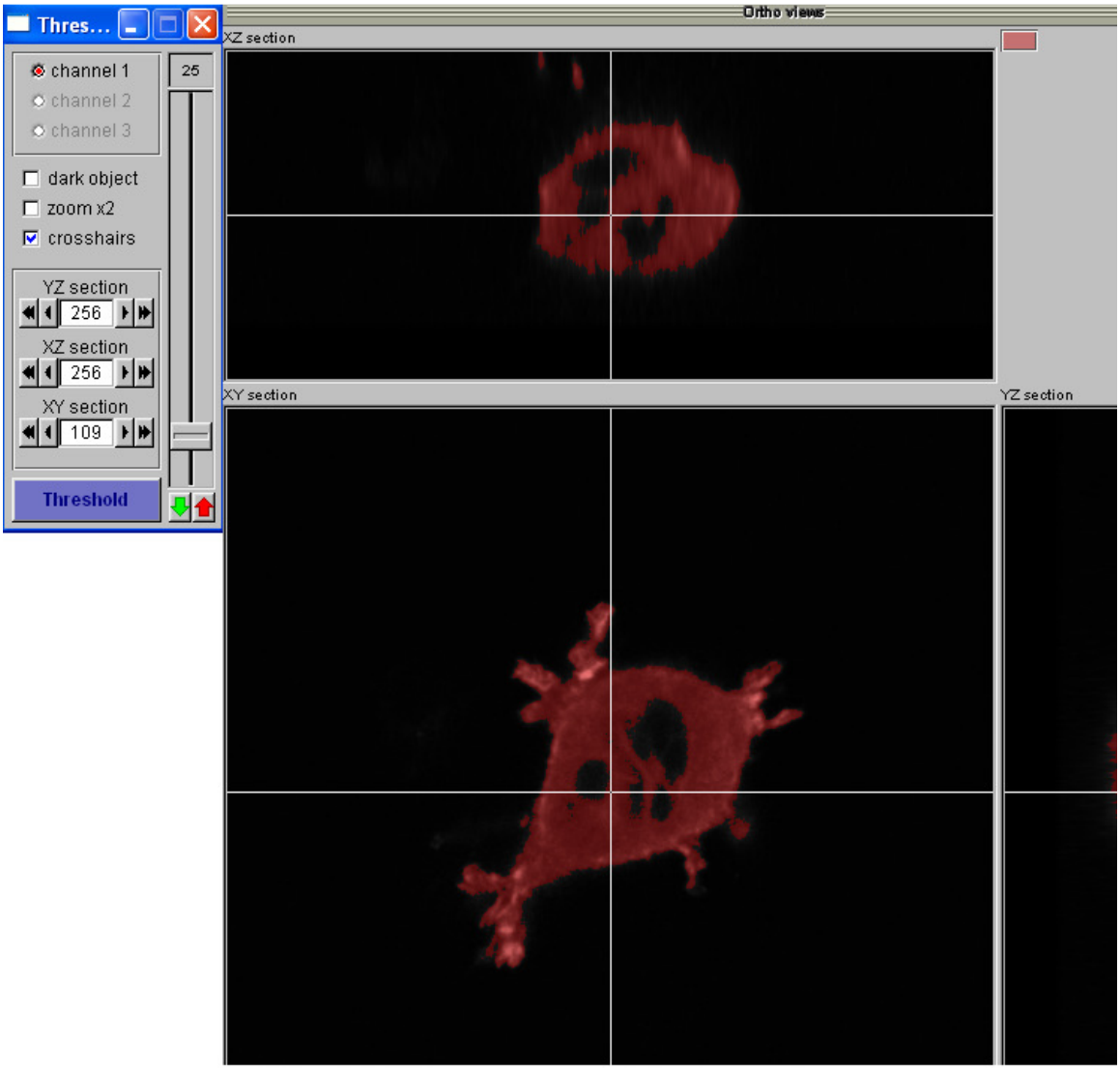

Fig. A1.2: Example of a threshold effect used on an image.

Simply Analysis - Labelling

Connected components labelling scans an image and groups its pixels into components based on pixel connectivity, i.e. all pixels in a connected component share similar pixel

intensity values and are in some way connected with each other. Once all groups have been determined, each pixel is labelled with a gray level or a colour (colour labelling) according to the component it was assigned to (Fig. A1.3).

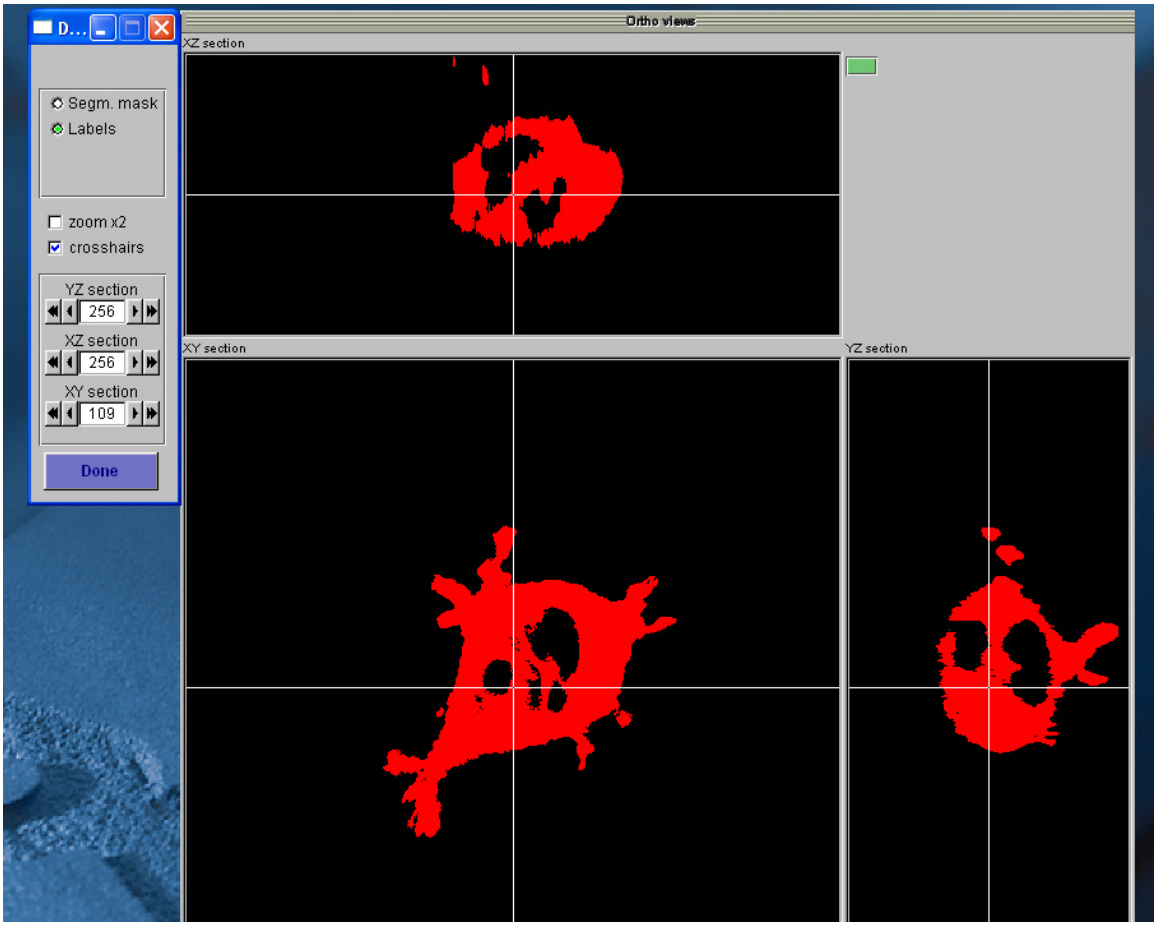

Fig. A1.3: An example of image analysis showed that the connected component labelling is a binary image which separates the objects from the background.

The cells are linked to an interactive spreadsheet of 3D object measurements, including volume, surface, and several other measurement parameters like vectors and radius projection.

Appendix 2: Example of data obtained after image processing

	A(X)	B(Y)	C(Y)	D(Y)	E(Y)	F(Y)	G(Y)	H(Y)	I(Y)	J(Y)	K(Y)	L(Y)	M(Y)	N(Y)
Long Name	Cells			RV	Volume	Surface	Shape	R1	R2	R3	Vector I	Vector J	Vector K	Elongation
Units				µm	µm3	µm2		µm						
Comments	Nr.	voxels	arccos(Vect. K)				RS/RV							R1/RV
1	1	373556	0.32052	14.21505	12025.8	5996.28	1.53696	14.9591	12.6033	11.9424	-0.05304	-0.31056	0.94907	1.05234
2	2	172345	1.9547	10.98405	5548.25	4581.43	1.73863	20.5858	13.8522	7.02228	-0.41892	0.82718	-0.37454	1.87415
3	3	92066	2.10084	8.91243	2963.85	2619.41	1.62022	23.7978	10.1872	4.63354	-0.03951	0.86188	-0.50558	2.67018
4	4	159848	0.87909	10.71187	5145.94	3507.12	1.55983	20.6066	10.8211	7.34118	0.44381	0.62943	0.63786	1.92372
5	5	93886	0.34522	8.97077	3022.44	3199.17	1.77892	17.6976	9.9843	6.44264	0.23035	0.24791	0.941	1.97281
6	6	166266	0.14797	10.85336	5352.55	3045.05	1.4345	11.5994	9.7775	9.29355	-0.14586	-0.02146	0.98907	1.06874
7	7	129714	0.29595	10.05054	4250.47	2454.73	1.39085	13.5666	9.62139	9.03875	0.20882	-0.20361	0.95652	1.34884
8	8	251425	0.52271	12.53131	8238.69	4786.07	1.55762	18.431	12.4271	10.9309	0.3812	-0.32236	0.86647	1.4708
9	9	85438	1.11781	8.74468	2799.63	2586.93	1.64103	11.4234	9.07985	6.63481	0.5472	0.71346	0.43765	1.30633
10	10	116052	0.69111	9.68452	3802.79	3747.02	1.78334	10.864	9.55763	7.62702	0.3743	0.51592	0.77054	1.12179
11	11	108528	1.60052	9.47054	3556.25	1892.15	1.2959	10.0009	8.90882	8.20586	0.05904	0.99781	-0.02972	1.056
12	12	197702	1.7635	11.49829	6364.56	5563.05	1.83017	21.7862	14.5897	9.22413	-0.3486	0.9175	-0.19152	1.89473
13	13	147889	0.62337	10.43779	4760.95	2253.58	1.28321	12.4964	10.418	9.58594	0.07961	0.57832	0.81192	1.19723
14	14	87630	1.73212	8.76693	2821.05	2643.09	1.65454	10.1369	8.91878	7.44309	-0.00103	0.98701	-0.16062	1.15627
15	15	69061	0.44513	8.09793	2223.26	1562.5	1.37722	11.421	7.15192	6.67119	-0.22406	-0.36768	0.90256	1.41036
16	16	131477	0.76419	10.03644	4232.6	3956.33	1.76822	33.44138	8.29522	5.00979	0.07825	-0.68751	0.72194	3.332
17														

Table 1: Example of data Edit_3D for gel solution, with cells obtained by microscopy.

Appendix 3: Article in Phys. Rev E (2008)

Fractal approach to the rheology of concentrated cell suspensions

A. Iordan,[1] A. Duperray,[2,3] and C. Verdier[1,*]
[1]*Laboratoire de Spectrométrie Physique, CNRS and Université Joseph-Fourier (UMR5588), 140 avenue de la physique, BP87 38402 Saint Martin d'Hères cedex, France*
[2]*INSERM, U823, Grenoble, France*
[3]*Université Grenoble I, Institut Albert Bonniot, Centre de Recherche Ontogénèse et Oncogénèse moléculaires, Grenoble, France*
(Received 20 September 2007; published 18 January 2008)

Results on the rheological behavior of Chinese hamster ovary cell suspensions in a large range of concentrations are reported. The concentration-dependent yield stress and elastic plateau modulus are formalized in the context of fractal aggregates under shear, and quite different exponents are found as compared to the case of red blood cell suspensions. This is explained in terms of intrinsic microscopic parameters such as the cell-cell adhesion energy and cell elasticity but also the cell's individual dynamic properties, found to correlate well with viscoelastic data at large concentrations ($\phi \geq 0.5$).

DOI: 10.1103/PhysRevE.77.011911 PACS number(s): 87.19.rh, 83.60.La, 47.57.Qk, 83.85.Cg

I. INTRODUCTION

The rheology of complex fluids has been studied extensively over the past decades [1] and has revealed very intriguing behaviors. In particular, properties of suspensions, either micronic or colloidal, are still a subject of interest [2–5]. Classical behaviors of suspensions usually reveal shear-thinning effects, but other unusual ones such as shear-thickening [6] (i.e., viscosity increase with shear rate) or yield stress have been observed [2,3]. The yield stress is the critical value of the shear stress needed to induce flow for a given fluid. It is closely related to the internal structure of the fluid therefore its ability to form (or break) particle clusters under flow. In this respect most studies have focused on solid sphere suspensions.

On the other hand, there is much less work dedicated to suspensions of deformable particles, such as biological cell suspensions. The main work can be found in the field of blood rheology. Suspensions of red blood cells (RBC) within plasma were investigated by Chien [7,8] and revealed a shear-thinning behavior, but a more detailed inspection of the viscosity-shear rate diagrams showed that at low shear rates, the stress level is close to a constant σ_s (Pa), called the yield stress. The well-known Casson's model [9] relating the shear stress σ to the shear rate $\dot{\gamma}$ (μ being a constant viscosity) can be used to determine the yield stress:

$$\sqrt{\sigma} = \sqrt{\sigma_s} + \sqrt{\mu \dot{\gamma}}. \quad (1)$$

Chien and co-authors obtained σ_s for a large range of hematocrit (H), i.e., the RBC volume concentration [10]. They showed a relationship of the type $\sigma_s \sim (H-b)^3$ (b being a constant hematocrit).

It is still not known yet whether this type of behavior is universal, or if it could depend on cell type, cell shape or other biological effects such as cell adhesion or cell elasticity. In particular, one proposed explanation of the yield stress in RBCs suspensions is based on the existence of "rouleaux" which build due to cell interactions and exhibit large shape aspect ratios [8] and a fractal dimension D. Therefore it is necessary to apply strong enough stresses in order to break such aggregates, in close relation with the yield stress.

In this work we propose to investigate the rheology of a cell suspension, consisting of CHO cells (Chinese hamster ovary cells) in a large range of concentrations. Such cells are commonly used in biology, easy to culture, and can be genetically modified to induce different adhesive properties. These cells are spherical when suspended in a culture medium, and organized in a specific manner leading to particular aggregation patterns of fractal type. This leads to the determination of scaling laws based on fractal exponents (for the yield stress σ_s and elastic modulus G_0) which are seen to be nonuniversal but dependent on cell type. The flow curves constitute a basis to test classical empirical models (Bingham, Casson, Herschel-Bulkley models) and other ones [11,12] based on kinetic theories describing the rupture and formation of particle clusters. The latter ones successfully relate macroscopic effects to microscopic parameters, such as the cell-cell adhesion energy and the cell elasticity. The microscopic parameters that we find match well the ones found in the literature using other techniques. This is important in the context of recent studies related to tumour growth [13–15] which consider cell assemblies with interactions as well as cell elastic deformations. Furthermore, this study emphasizes the relationship between the dynamic rheological properties of suspensions [16] and the single cell properties.

The paper is organized as follows. In Sec. II, we describe the materials and methods of investigation (i.e., mainly rheometry and microscopy). Then steady shear and dynamic oscillatory shear results are presented in Sec. III. In light of the typical scaling laws obtained, we suggest the use of the model of Snabre and Mills [11] presented in Sec. IV, to analyze our data, and find the corresponding microscopic parameters. Finally, we present an alternative approach based on structural similarity [17] in Sec. V.

II. MATERIALS AND METHODS

In our model system, adherent CHO cells are grown in culture medium [Dulbecco's Modified Eagle's Medium

*Author to whom correspondence should be addressed. FAX: 33-4-76-63-54-95. verdier@ujf-grenoble.fr

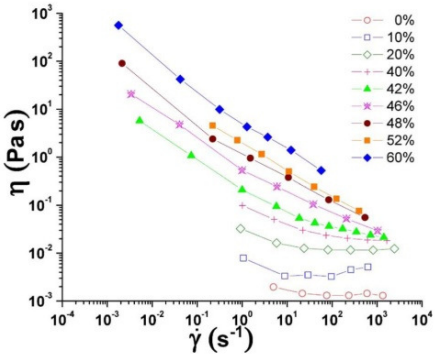

FIG. 1. (Color online) Viscosity η (Pa s) vs shear rate $\dot{\gamma}$ (s^{-1}) at different volume concentrations ϕ from 0 to 60%.

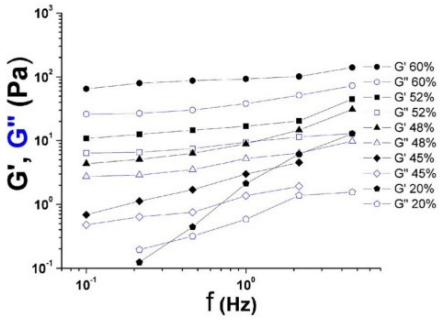

FIG. 2. (Color online) Shear moduli G' and G'' (Pa) vs frequency f at different volume concentrations ϕ ranging from 20% to 60%.

(DMEM) containing 10% fetal calf serum] using standard *T*75 boxes under proper conditions (37 °C, 5% CO_2), until they are detached using trypsin, when they reach a confluency of ~70%. Suspended cells are centrifuged at 1200 rpm, a high enough velocity to get a concentrated suspension, but slow enough in order to maintain the cells alive. Cell volume concentration ϕ (i.e., similar to the hematocrit *H*) is determined accurately after centrifugation in hematocrit tubes containing the CHO cells. Then the right amount of remaining supernatant is removed until the desired concentration is obtained (between 0 and 60%). Different experiments were carried out on a conventional rheometer (Bohlin Gemini 150). Both steady shear and oscillatory measurements were made at $T=20$ °C. Due to the large amount of cells needed (we usually require twelve *T*75 flasks in order to obtain a volume of roughly 0.3 mL of cells), we chose to use a plate-plate geometry (20 mm diameter) with a small gap (between 400 μm and 1 mm) for the concentrated suspensions whereas the smaller concentrations (below 10%) were tested using the 60 mm cone-plane geometry (2° angle). Typically in our fluid, the suspended cells are spherical and monodisperse with a radius $a \sim 10$ μm.

III. RESULTS

Experimental results for constant steady state shear rate $\dot{\gamma}$ are presented in Fig. 1. The viscosity η is shown to vary over several decades, within shear rates typically between 10^{-3} s^{-1} and 10^{3} s^{-1}. In some cases, we limited ourselves to the higher shear rates because of experimental reasons (i.e., steady state not reached). By a first inspection of the curves, we recognize the signature of a yield stress fluid as depicted by the slope close to -1 in the viscosity-shear rate diagram (or equivalently a constant shear stress at low shear rates), especially at the largest concentrations ϕ, which will be particularly of interest here. The existence of this yield stress is attributed to weak interactions which can exist after preparation of the system. Already existing proteins are available on cell membranes and can be recruited to form bonds, leading to particular structure arrangements. This explains the presence of a yield stress related to the formation of such structures. The yield stress is found to depend on volume concentration ϕ in a manner to be discussed later.

A second series of experiments was carried out in order to study the systems under oscillatory strains at frequency f. Small deformations (1% or less) within the linear regime were performed in order to characterize the elastic modulus $G'(f)$ and the loss modulus $G''(f)$. The frequency values were limited to the narrow range corresponding to fast modes, in order to limit a possible time dependence of the results, due to sedimentation, protein expression, cluster formation or destruction. We find an interesting behavior as shown in Fig. 2. Moduli $G''(f)$ usually prevails over $G'(f)$ at small concentrations (e.g. $\phi=0.2$), but as ϕ increases, the system becomes elastic with a much larger $G'(f)$. This behavior is the signature of a viscoelastic medium, due to the fact that interactions between elastic cells become effective at large concentrations ($\phi \geq 0.4$). The slow increase of the elastic modulus G' against frequency reveals the presence of a so-called "elastic plateau" modulus (G_0) determined by the value of $G'(f)$ at intermediate frequencies (1 Hz typically). The presence of elasticity has been observed previously for RBC suspensions [18], above a critical volume fraction around $\phi=0.2$, and is believed to come from the elasticity of the cells as they are packed more closely at large concentrations such as the ones also encountered in tumor spheroids [14]. Finally, we observe that the trends in the $G'-G''$ plots for large concentrations ($\phi \geq 0.5$) are remarkedly similar to previous microrheological results obtained on single cells [19–21]. Indeed, they show a slowly increasing G' and G'' (increasing slightly faster at frequencies above 1 Hz), where the elasticity dominates ($G' \geq G''$).

As in the case of suspensions, we define a maximum packing fraction ϕ_0 (which is usually 0.64 or even 0.74 for solid spheres in a face-centered-cubic crystal), depending on cell elasticity, i.e. their compactness [22]. Due to the presence of soft spherical cells, it is expected that the value of ϕ_0 will be in this range. ϕ_0 is determined using the reduced viscosity plot $\frac{\eta}{\eta_0}$ as a function of ϕ (η at a shear rate of 10^2 s^{-1}, $\eta_0=0.0014$ Pa s the solvent viscosity). In our case, this data (not shown) is found to match the well-known equation

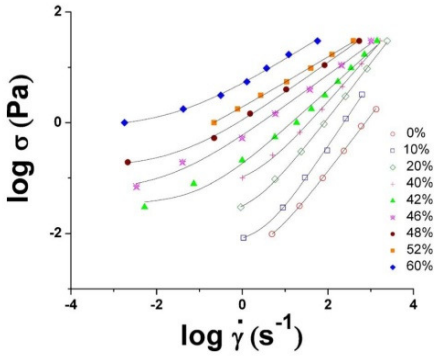

FIG. 3. (Color online) Determination of the yield stress σ_s using Herschel-Bulkley's model.

$$\frac{\eta}{\eta_0} = \left(1 - \frac{\phi}{\phi_0}\right)^{-2.5\phi_0} \tag{2}$$

proposed by Krieger and Dougherty [23], this providing the value $\phi_0 \sim 0.65$. Note that this relationship is interesting because it matches Einstein's viscosity for hard spheres [24,25] $\eta/\eta_0 = 1 + 2.5\phi$ as well as Batchelor's correction for non colloidal spherical particles [26] $\eta/\eta_0 = 1 + 2.5\phi + 5.2\phi^2$ [here an expansion of Eq. (2) for small ϕ gives a second coefficient in the expansion of ~5 instead of 5.2, when using $\phi_0 = 0.65$]. Finally, Eq. (2) diverges as expected when $\phi \to \phi_0$, the limiting packing fraction.

In order to investigate the effect of the volume concentration ϕ, we first need to obtain the flow curve $\sigma(\dot{\gamma})$ of the suspensions, as well as the relevant parameters, such as the yield stress σ_s. From the viscosity curve in Fig. 1, we plot the stress $\sigma = \eta(\dot{\gamma})\dot{\gamma}$ vs shear rate $\dot{\gamma}$ in Fig. 3, and fit the data with the Herschel-Bulkley law [2] $\sigma = \sigma_s + M\dot{\gamma}^n$, where M is a constant, and n is a shear-thinning exponent ranging between 0 and 1 (1 is for a Bingham fluid, and the case of the Newtonian fluid is recovered for $n=1$, $\sigma_s = 0$). Parameters have been optimized using a standard Newton-Raphson method. The parameter n is found to be very close to 1 at small concentrations (0,10,20%) and decreases with concentration, taking respective values of 0.89, 0.71, 0.57, 0.55, 0.47, 0.47 for concentrations of 40, 42, 46, 48, 52 and 60%. This point will be further discussed in Sec. V.

This leads to the determination of the yield stress σ_s as a function of volume fraction ϕ. Such measurements are usually difficult [10] because of possible slip, sedimentation and evaporation [27]. Care has been taken to avoid such problems, therefore only shear rates larger than 10^{-3} s^{-1} (lowest value) are considered. The empirical Herschel-Bulkley model (involving a yield stress) is then used when sufficient data points are available. The fits are in satisfactory agreement with the data which gives good confidence in the values of the yield stresses for $\phi \geq 0.42$. Another attempt has been made using Casson's model and gives similar data. The Bingham model was found to give less accurate values.

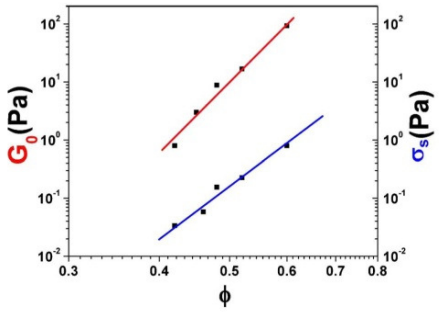

FIG. 4. (Color online) Yield stress σ_s and shear elastic modulus $G_0 = G'(f = 1\ \text{Hz})$, vs volume concentration ϕ, log scale.

The values of the yield stresses σ_s and shear plateau moduli G_0 (value of G' at a typical frequency $f = 1$ Hz) are plotted in Fig. 4 as a function of volume concentration. This plot shows power law dependences of the form $\sigma_s \sim \phi^{m_1}$ and $G_0 \sim \phi^{m_2}$ and recalls previous results [11] obtained in the case of the rheology of RBCs suspensions, at least for the yield stress σ_s. From Fig. 4 we find that $m_1 \sim 8.4$ and $m_2 \sim 11.6$. The m_1 exponent is quite different from the one obtained in the case of RBCs suspensions ($m_1 \sim 3$) as this will be discussed below.

IV. MODELING

As seen above, rheological modeling of such suspensions should therefore predict shear-thinning behavior, as well as yield stress properties at low shear rates $\dot{\gamma} \to 0$ and a concentration dependence of σ_s and G_0. In addition, cell suspensions correspond to aggregated systems (see Fig. 5). Under flow, their structure is based on the persistent remodeling of the cells with respect to each other as they exhibit deformations, rotations, possible rolling and/or separation. During such events, cells may form clusters of size R_f to be compared with the cell size a (radius). The formation and destruction of cell clusters is the major ingredient to understand the rheological properties of the cell system, in order to explain our data.

For example, when sheared under stress σ, clusters break into smaller ones, leading to shear-thinning effects. On the

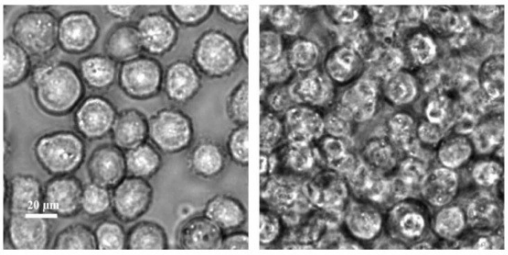

FIG. 5. Phase contrast microscopy of CHO cell suspension: 10% and 52%. Same scale for both images.

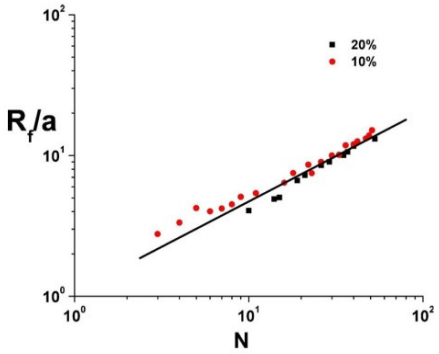

FIG. 6. (Color online) Plot of $\frac{R_f}{a}$ as a function of N to determine the fractal dimension D. Two concentrations are used: 10% and 20%. There are noticeable differences at low values of N but there is an increased accuracy for large N, where the two concentrations give rise to the same slope $D=1.47$.

other hand, the possible encounter of clusters leads to the formation of larger structures, increasing the viscosity. Clusters are organized in a fractal way. First, one needs to consider a cluster at rest. Its size is R_f and it contains N cells, linked by the following relationship [28]:

$$\frac{R_f}{a} \sim N^{1/D}, \tag{3}$$

where D is the fractal dimension. To determine D, we follow a previous approach [29] and consider circles (instead of rectangles) of radius R_f containing a cluster. Then cells (radius a) are counted for two rather small concentrations (10% and 20%). Clichés like the left one in Fig. 5 are used to draw circles and count the number of cells N. For larger clusters containing more cells, we obtain a linear relationship between $\log_{10}(R_f/a)$ and $\log_{10}(N)$, as shown in Fig. 6. Note that the two cases studied (10% and 20%) give the same slope for large values of N, this justifying the fractal hypothesis indicated by Eq. (3). For our system, we determine $D \sim 1.47$ from the two-dimensional (2D) images. Thus, in three dimensions, we expect a fractal dimension of the order $D \sim 2$ [30]. This number is similar to the ones found for RBCs suspensions, although the scaling exponents for yield stresses are quite different.

In the semi-empirical model proposed by Snabre and Mills [11,12], the formation and dissociation of clusters under flow is taken into account. A change in R_f as a function of the applied shear stress is assumed:

$$\frac{R_f}{a} = 1 + \left(\frac{\sigma^*}{\sigma}\right)^m, \tag{4}$$

where m is a dimensionless parameter, σ^* is a critical stress related to the interfacial adhesion between cells: $\sigma^* = \Gamma/a$, and Γ is the cell adhesion free energy. Using the concept of effective medium with volume fraction

$$\phi_A = \phi\left(\frac{R_f}{a}\right)^{3-D}, \tag{5}$$

one assumes an effective viscosity:

$$\eta(\sigma) = \eta_0 \frac{1-\phi_A}{\left(1-\frac{\phi_A}{\phi_0}\right)^2}, \tag{6}$$

and obtains the constitutive Eq. [31] which contains the yield stress given by

$$\sigma_s \sim \sigma^*\left(\frac{\phi}{\phi_0}\right)^{\frac{1}{m(3-D)}}. \tag{7}$$

The last parameter to be used in the formula, ϕ_0, is the maximum packing concentration found previously.

We use the previous model to explain our experimental data. The exponent $m_1=8.4$ found for the yield stress σ_s is plugged into the previous scaling law (7) for determination of the parameter $m=0.078$. This is smaller than the values of m found for RBC suspensions (typically $m \sim 0.3$). This means that the size of clusters is not so sensitive to the applied stress, indeed one can consider that the cell aggregates are easy to form (or hard to break) because of the round shape of the cells, in contrast with RBCs which need to bind in a very special way to form rouleaux. Thus, once broken by stress, rouleaux are difficult to re–form. We have obtained the value of the critical stress $\sigma^* = 1.4\ \mathrm{N/m^2}$, and a corresponding value of $\Gamma = 1.4 10^{-5}\ \mathrm{N/m}$. This value of σ^* is higher than the ones obtained for RBCs [11] but the interfacial energy Γ is in the range of the small values indicated for vesicles [32]. This is in favor of the initial assumption that few adhesion molecules are involved in the region of contact between the cells.

Finally, we postulate a similar relationship [28] for the shear elastic modulus

$$G_0 \sim G^*\left(\frac{\phi}{\phi_0}\right)^{\frac{1}{p(3-D)}}, \tag{8}$$

where G^* is an effective elastic modulus, but we include an additional exponent n to be determined. We come up with $p=0.056$ and $G^*=234$ Pa. This value of the reference modulus G^*, as explained in the concept of fractal exponents [28], is to be related to typical values for single cells. In particular, it corresponds to a Young's elastic modulus $E^*=702$ Pa (assuming that the cell is incompressible) which is typical for adherent wild type CHO cells, of the order 0.5–1 kPa as measured by AFM [33,34].

V. AN APPROACH BASED ON STRUCTURAL SIMILARITY

Another method for having access to parameters like the yield stress σ_s and the viscosity η of such suspensions has been proposed earlier [17]. It can be of interest to mention such an approach since it is relevant to our case, in the context of concentration-dependent laws. The idea consists in assuming a dependence of the reduced shear stress $T=\sigma/\sigma_s$

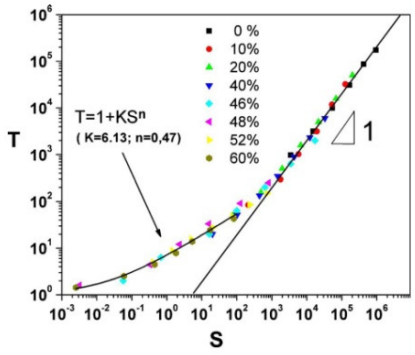

FIG. 7. (Color online) Master curve of the reduced shear stress T vs reduced shear-rate S.

as a function of the reduced shear rate $S=\eta\dot{\gamma}/\sigma_s$. This similarity is interesting because it can allow us to superpose the different curves onto a single master curve. Such an approach has been used previously with success in the case of clay-water suspensions. The master curve is shown in our case for CHO cell suspensions (Fig. 7).

We note again a good superposition of the data, although the few available data points for low reduced shear rates do not allow very accurate results for the parameters under investigation. In an attempt to model the first part of the curve (low shear rates), a relationship of the following kind was found:

$$T = 1 + 6.13S^{0.47}. \tag{9}$$

The value of the exponent close to $1/2$ recalls the well-known Casson's equation but in a slightly different form. In fact, this form is a limiting case of Casson's equation, corresponding to an asymptotic expansion of Eq. (1) for small enough shear rates. The use of Eq. (1) instead of Eq. (9) does not fit the whole data. Proceeding further, we can obtain values of the yield stress σ_s and viscosity η from the *ad hoc* data reduction. This has led us to similar relationships for the yield stress dependence vs concentration (as in Sec. IV). Similarly, the analysis of the viscosity (η) dependence against concentration ϕ also shows that Eq. (2) and the following equation $\eta/\eta_0=[1+0.75/(\phi_0/\phi-1)]^2$ from Chong and coauthors [35] both predict a correct evolution of the viscosity η leading to a packing fraction of the order $\phi_0\sim 0.65$. Therefore we can conclude that this approach is complementary to the previous one in the sense that it can lead to an increased accuracy, when sufficient data is available, although it does not provide physical correlations between microscopic and macroscopic parameters, such as the model that we chose to use in the above analysis [11].

VI. CONCLUSIONS AND PERSPECTIVES

To sum up, the system studied here provides unusual features important for the rheology of biological suspensions and tissues. These concentrated cell suspensions behave as yield stress fluids (also called visco-plastic materials), for which a fractal approach has been used. Under shear, the fractal structure changes and can be modeled using a yield stress σ_s and elasticity modulus G_0 related to the fractal dimension D. Two other microscopic parameters of interest have been introduced in the model: the cell adhesion energy Γ, and the cell's effective elastic modulus E^* found to be

$$\Gamma \sim 10^{-5}\ \text{N/m}, \quad E^* \sim 700\ \text{Pa}. \tag{10}$$

The first is in the range of typical values of cell adhesion energies, and the second in agreement with previous microrheology experiments. We also found a similar behavior between the dynamic shear moduli $G'(f)$ and $G''(f)$ in this study (at $\phi \geq 0.5$), and the ones obtained from microrheological studies on single cells [19–21] using various techniques. Both show slowly increasing dynamic moduli in terms of frequency, with the same relative positions. This idea probably deserves more attention and should be tested in the future, in particular further work may focus on the characterization of other cellular suspensions including cells with different elastic properties.

Finally, such a study can naturally lead to the understanding of biological tissues, by including stronger adhesion properties between the cells, or by taking into account the addition of extra-cellular matrix components.

ACKNOWLEDGMENTS

The authors wish to thank the EC Marie Curie Research Training Network MRTN-CT-2004-503661 on "Modelling, mathematical methods and computer simulation of tumour growth and therapy" (http://calvino.polito.it/~mcrtn/) for financial support, and C. Misbah for fruitful discussions about the manuscript.

[1] R. G. Larson, *The Structure and Rheology of Complex Fluids* (Oxford University Press, New York, 1999).
[2] P. Coussot, *Rheometry of Pastes, Suspensions and Granular Materials* (Wiley, New York, 2005).
[3] R. J. Flatt and P. Bowen, J. Am. Ceram. Soc. **89**, 1244 (2006).
[4] A. N. Alexandrou and G. Georgiou, J. Non-Newtonian Fluid Mech. **142**, 199 (2007).
[5] J. M. Brader, T. Voigtmann, M. E. Cates, and M. Fuchs, Phys. Rev. Lett. **98**, 058301 (2007).
[6] H. M. Laun, Angew. Makromol. Chem. **124-125**, 335 (1984).
[7] S. Chien, S. Usami, R. J. Dellenback, and M. I. Gregersen, Science **157**, 827 (1967).
[8] S. Chien, S. Usami, R. J. Dellenback, M. I. Gregersen, L. B. Nanninga, and M. Mason-Guest, Science **157**, 829 (1967).

[9] N. Casson, *A Flow Equation for Pigment-oil Suspensions of the Printing Ink Type* (Pergamon, London, 1959), Chap. 5.
[10] S. Chien, S. Usami, H. M. Taylor, J. L. Lundberg, and M. I. Gregersen, J. Appl. Physiol. **21**, 81 (1966).
[11] P. Snabre and P. Mills, J. Phys. III **6**, 1811 (1996).
[12] P. Snabre and P. Mills, Colloids Surf., A **152**, 79 (1999).
[13] D. Drasdo and S. Höhme, Phys. Biol. **2**, 133 (2005).
[14] J. Galle, M. Loeffler, and D. Drasdo, Biophys. J. **88**, 62 (2005).
[15] D. Ambrosi and L. Preziosi (unpublished).
[16] C. Verdier, J. Theor. Medicine **5**, 67 (2003).
[17] P. Coussot, Phys. Rev. Lett. **74**, 3971 (1995).
[18] G. B. Thurston, Biophys. J. **12**, 1205 (1972).
[19] B. Fabry, G. N. Maksym, J. P. Butler, M. Glogauer, D. Navajas, and J. J. Fredberg, Phys. Rev. Lett. **87**, 148102 (2001).
[20] J. Alcaraz, L. Buscemi, M. Grabulosa, X. Trepat, B. Fabry, R. Farré, and D. Navajas, Biophys. J. **84**, 2071 (2003).
[21] B. D. Hoffman, G. Massiera, K. M. V. Citters, and J. C. Crocker, Proc. Natl. Acad. Sci. U.S.A. **103**, 10259 (2006).
[22] D. Quemada, Eur. Phys. J. A **1**, 119 (1998).
[23] I. M. Krieger and T. J. Dougherty, Trans. Soc. Rheol. **3**, 137 (1959).
[24] A. Einstein, Ann. Phys. **19**, 289 (1906).
[25] A. Einstein, Ann. Phys. **34**, 591 (1911).
[26] G. K. Batchelor and J. T. Green, J. Fluid Mech. **56**, 401 (1972).
[27] Y. C. Fung, *Biomechanics. Mechanical Properties of Living Tissues* (Springer, New York, 1996).
[28] P. G. de Gennes, *Scaling Concepts in Polymer Physics* (Cornell University Press, New York, 1979).
[29] C. Allain and B. Jouhier, J. Phys. (France) Lett. **44**, 421 (1983).
[30] M. Kolb and R. Jullien, J. Phys. (France) Lett. **45**, 977 (1984).
[31] The 1D-constitutive equation is given by $\eta(\sigma)=\frac{\sigma}{\dot{\gamma}}=\eta_0\frac{1-\phi(1+(\sigma_s/\sigma)^m)^{3-D}}{(1-\phi/\phi_0(1+(\sigma_s/\sigma)^m)^{3-D})^2}$ which is implicit for σ but provides an explicit relation for $\dot{\gamma}$ in terms of σ. Letting $\dot{\gamma}\to 0$ allows us to determine the yield stress σ_s.
[32] Z. Guttenberg, B. Lorz, E. Sackmann, and A. Boulbitch, Europhys. Lett. **54**, 826 (2001).
[33] E. Canetta, A. Duperray, A. Leyrat, and C. Verdier, Biorheology **42**, 321 (2005).
[34] M. Zhao, C. Srinivasan, D. J. Burgess, and B. D. Huey, J. Mater. Res. **21**, 1906 (2006).
[35] J. S. Chong, E. B. Christiansen, and A. D. Baer, J. Appl. Polym. Sci. **15**, 2007 (1971).

Bibliography

[1] http://calvino.polito.it/~mcrtn/

[2] www.malvern.co.uk

[3] http://www.microscopyu.com

[4] http://rsbweb.nih.gov/ij/

[5] http://www.olympusfluoview.com/theory/confocalintro.htm

[6] http://www.3dchem.com/molecules.asp?ID=195

[Alcaraz 2003] J. Alcaraz, L. Buscemi, M. Grabulosa, X. Trepat, B. Fabry, R. Farre, and D. Navajas, Microrheology of human lung epithelial cells measured by atomic force microscopy. *Biophys J.* 84. 2071-2079 (2003).

[Alexandrou 2007] A.N.G. Alexandrou, G, On the early breakdown of semisolid suspensions. *J. Non-Newtonian Fluid Mech.* 142. 199-206 (2007).

[Allain 1983] C. Allain, and B. Jouhier, Simulation cinétique du phénomene d'agrégation. *J. Physique - Lettres* 44. L421-L428 (1983).

[Ambrosi 2008] D. Ambrosi, and L. Preziosi, On the closure of mass balance models for tumour growth *submitted (*2008).

[Barnes 1989] H.A. Barnes, J.F. Hutton, and K. Walters, An introduction to rheology, Elsevier, 1989.

[Barocas 1995] V.H. Barocas, A.G. Moon, and R.T. Tranquillo, The fibroblast-populated collagen microsphere assay of cell traction force-Part 2: Measurement of the cell traction parameter. *J Biomech Eng.* 117. 161-170 (1995).

[Batchelor 1977] G.K. Batchelor, The effect of Brownian motion on the bulk stress in a suspension of spherical particles. *Journal of Fluid Mechanics.* 83. 97-117 (1977).

[Batchelor 1972] G.K. Batchelor, Green, J.T. , The determination of the bulk stress in a suspension of spherical particles to order c^2. *J. Fluid Mech.* 56(3). 401-427 (1972).

[Bell 1979] E. Bell, B. Ivarsson, and C. Merrill, Production of a tissue-like structure by contraction of collagen lattices by human fibroblasts of different proliferative potential in vitro. *Proc Natl Acad Sci U S A.* 76. 1274-1278 (1979).

[Bellomo 2003] N. Bellomo, E. de Angelis, and L. Preziosi, Multiscale Modeling and Mathematical Problems Related to Tumor Evolution and Medical Therapy. *J. Theor. Medicine* 5(2). 111-136 (2003).

[Bird 1987] R.B. Bird, R.C. Armstrong, and O. Hassager, Dynamics of polymeric liquids, Wiley, New York ; Chichester, 1987.

[Bowden 1973] P.B. Bowden, The yield behaviour of glassy polymers, R.N. Haward (ed.), Appl. Sci. Publ., London, 1973.

[Brader 2007] J.M. Brader, T. Voigtmann, M.E. Cates, and M. Fuchs, Dense colloidal suspensions under time-dependent shear. *Phys Rev Lett.* 98. 058301 (2007).

[Brightman 2000] A.O. Brightman, B.P. Rajwa, J.E. Sturgis, M.E. McCallister, J.P. Robinson, and S.L. Voytik-Harbin, Time-lapse confocal reflection microscopy of collagen fibrillogenesis and extracellular matrix assembly in vitro. *Biopolymers.* 54. 222-234 (2000).

[Byrne 2003] H. Byrne, and L. Preziosi, Modelling solid tumour growth using the theory of mixtures. *Math Med Biol.* 20. 341-366 (2003).

[Canetta 2005] E. Canetta, A. Duperray, A. Leyrat, and C. Verdier, Measuring cell viscoelastic properties using a force-spectrometer: influence of protein-cytoplasm interactions. *Biorheology.* 42. 321-333 (2005).

[Casson 1959] N. Casson, A Flow Equation for Pigment-oil Suspensions of the Printing Ink Type, Chap. 5, Pergamon, London, 1959.

[Chien 1966] S. Chien, S. Usami, H.M. Taylor, J.L. Lundberg, and M.I. Gregersen, Effects of hematocrit and plasma proteins on human blood rheology at low shear rates. *J Appl Physiol.* 21. 81-87 (1966).

[Chien 1967a] S. Chien, S. Usami, R.J. Dellenback, and M.I. Gregersen, Blood Viscosity: Influence of Erythrocyte Deformation. *Science.* 157. 827-829 (1967a).

[Chien 1967b] S. Chien, S. Usami, R.J. Dellenback, M.I. Gregersen, L.B. Nanninga, and M.M. Guest, Blood Viscosity: Influence of Erythrocyte Aggregation. *Science.* 157. 829-831 (1967b).

[Chong 1971] J.S.C. Chong, E.B. & Baer, A.D. , Rheology of concentrated suspensions. *J. Appl. Polym. Sci.* 15. 2007-2021 (1971).

[Coussot 1995] P. Coussot, Structural Similarity and Transition from Newtonian to Non-Newtonian Behavior for Clay-Water Suspensions. *Phys Rev Lett.* 74. 3971-3974 (1995).

[Coussot 2002] P. Coussot, and J.L. Grossiord, Comprendre la Rhéologie - de la circulation du sang à la prise du béton, EDP Sciences, Les Ulis, 2002.

[Coussot 2005] P. Coussot, Rheometry of Pastes, Suspension and Granular Materials, Wiley, New York, 2005.

[Cukierman 2001] E. Cukierman, R. Pankov, D.R. Stevens, and K.M. Yamada, Taking cell-matrix adhesions to the third dimension. *Science.* 294. 1708-1712 (2001).

[de Gennes 1979] P.G. de Gennes, Scaling concepts in polymer physics, Cornell University Press, Ithaca, N.Y., 1979.

[Discher 2005] D.E. Discher, P. Janmey, and Y.L. Wang, Tissue cells feel and respond to the stiffness of their substrate. *Science.* 310. 1139-1143 (2005).

[Drasdo 2005] D. Drasdo, and S. Hohme, A single-cell-based model of tumor growth in vitro: monolayers and spheroids. *Phys Biol.* 2. 133-47 (2005).

[Einstein 1906] A. Einstein, Eine neue bestimmung der molek l-dimensionen. *Annals der Physik* 19. 289-306 (1906).

[Einstein 1911] A. Einstein, Berichtigung zu meiner arbeit: Eine neue bestimmung der molek l-dimensionen. *Annals der Physik* 34. 591-592 (1911).

[Engler 2006] A.J. Engler, S. Sen, H.L. Sweeney, and D.E. Discher, Matrix elasticity directs stem cell lineage specification. *Cell.* 126. 677-89 (2006).

[Fabry 2001] B. Fabry, G.N. Maksym, J.P. Butler, M. Glogauer, D. Navajas, and J.J. Fredberg, Scaling the microrheology of living cells. *Phys Rev Lett.* 87. 148102 (2001).

[Flatt 2006] R.J. Flatt, and P. Bowen, Yodel: A Yield Stress Model for Suspensions. 89. 1244-1256 (2006).

[Forgacs 1998] G.F. Forgacs, R.A.; Shafrir, Y. & Steinberg, M.S. , Viscoelastic properties of living embryonic tissues: a quantitative study. *Biophys J.* 74. 2227-2234 (1998).

[Fung 1996] Y.C. Fung, Biomechanics : mechanical properties of living tissues, Springer-Verlag, New York, 3rd edition, 1996.

[Galle 2005] J. Galle, M. Loeffler, and D. Drasdo, Modeling the effect of deregulated proliferation and apoptosis on the growth dynamics of epithelial cell populations in vitro. *Biophys J.* 88. 62-75 (2005).

[Guttenberg 2001] Z.L. Guttenberg, B.; Sackmann, E. & Boulbitch, A. , First-order transition between adhesion states in a system mimicking cell-tissue interaction. *Europhys. Lett.* . 54(6). 826-832 (2001).

[Hamilton 1998] G. Hamilton, Multicellular spheroids as an in vitro tumor model. *Cancer Lett.* 131. 29-34 (1998).

[Helmlinger 1997] G. Helmlinger, P.A. Netti, H.C. Lichtenbeld, R.J. Melder, and R.K. Jain, Solid stress inhibits the growth of multicellular tumor spheroids. *Nat Biotechnol.* 15. 778-783 (1997).

[Hirsch 1975] P.B. Hirsch, and N.F.S. Mott, The physics of metals. 2, Defects, Cambridge University Press, Cambridge, 1975.

[Hoffman 2006] B.D. Hoffman, G. Massiera, K.M. Van Citters, and J.C. Crocker, The consensus mechanics of cultured mammalian cells. *Proc Natl Acad Sci U S A.* 103. 10259-10264 (2006).

[Janmey 1991] P.A. Janmey, U. Euteneuer, P. Traub, and M. Schliwa, Viscoelastic properties of vimentin compared with other filamentous biopolymer networks. *J Cell Biol.* 113. 155-160 (1991).

[Kaufman 2005] L.J. Kaufman, C.P. Brangwynne, K.E. Kasza, E. Filippidi, V.D. Gordon, T.S. Deisboeck, and D.A. Weitz, Glioma expansion in collagen I matrices: analyzing collagen concentration-dependent growth and motility patterns. *Biophys J.* 89. 635-650 (2005).

[Knapp 1997] D.M. Knapp, V.H. Barocas, A.G. Moon, K. Yoo, L.R. Petzold, and R.T. Tranquillo, Rheology of reconstituted type I collagen gel in confined compression. *Journal of Rheology.* 41. 971-993 (1997).

[Kolb 1984] M.J. Kolb, R. , Chemically limited versus diffusion limited aggregation. *J. Physique Lett. .* 45. 977-981 (1984).

[Krieger 1959] I.M. Krieger, and T.J. Dougherty, A Mechanism for Non-Newtonian Flow in Suspensions of Rigid Spheres. *Journal of Rheology.* 3. 137-152 (1959).

[Larson 1999] R.G. Larson, The structure and rheology of complex fluids, Oxford University Press, New York, 1999.

[Laun 1984] H.M. Laun, Rheological properties of aqueous polymer dispersions. *Angew. Makromol. Chem. .* 124-125. 335–359 (1984).

[Leung 2007] L.Y. Leung, D. Tian, C.P. Brangwynne, D.A. Weitz, and D.J. Tschumperlin, A new microrheometric approach reveals individual and cooperative roles for TGF-beta1 and IL-1beta in fibroblast-mediated stiffening of collagen gels. *Faseb J.* 21. 2064-2073 (2007).

[Macosko 1994] C.W. Macosko, Rheology : principles, measurements, and applications, VCH, New York, NY ; Cambridge, 1994.

[Magnin 1990] A. Magnin, and J.M. Piau, Cone-and-plate rheometry of yield stress fluids study of an aqueous gel. *J. Non Newtonian Fluid Mech.* 36. 85-108 (1990).

[Moller 2006] P.C.F. Moller, J. Mewis, and D. Bonn, Yield stress and thixotropy: on the difficulty of measuring yield stresses in practice. 2. 274-283 (2006).

[Mollica 2007] F. Mollica, L. Preziosi, and K.R. Rajagopal, Modeling of biological materials, Birkhäuser ; Springer [distributor], Boston, Mass.London, 2007.

[Mooney 1951] M. Mooney, The viscosity of a concentrated suspension of spherical particles. *Journal of Colloid Science.* 6. 162–170 (1951).

[Pal 2003] R. Pal, Rheology of concentrated suspensions of deformable elastic particles such as human erythrocytes. *J Biomech.* 36. 981-989 (2003).

[Palecek 1997] S.P. Palecek, J.C. Loftus, M.H. Ginsberg, D.A. Lauffenburger, and A.F. Horwitz, Integrin-ligand binding properties govern cell migration

speed through cell-substratum adhesiveness. *Nature.* 385. 537-540 (1997).

[Parazza 1993] F. Parazza, C. Humbert, and Y. Usson, Method for 3D volumetric analysis of intranuclear fluorescence distribution in confocal microscopy. *Comput Med Imaging Graph.* 17. 189-200 (1993).

[Parazza 1995] F. Parazza, E. Bertin, Z.M. Wozniak, and Y. Usson, Analysis of the spatial distribution of AgNOR proteins in cell nuclei using simultaneous confocal scanning laser fluorescence and transmitted light microscopy. *Journal of Microscopy.* 178. 251-260 (1995).

[Picart 1998] C. Picart, J.M. Piau, H. Galliard, and P. Carpentier, Blood low shear rate rheometry: influence of fibrinogen level and hematocrit on slip and migrational effects. *Biorheology.* 35. 335-353 (1998).

[Preziosi 2003] L. Preziosi, Cancer modelling and simulation, Chapman & Hall/CRC, Boca Raton, Fla. ; London, 2003.

[Preziosi 2008] L. Preziosi , D. Ambrosi , and C. Verdier, Elasto-visco-plastic model of cell aggregates. *to be submitted (*2008).

[Quemada 1998] D. Quemada, Rheological modelling of complex fluids. I. The concept of effective volume fraction revisited. *The European Physical Journal Applied Physics.* 1. 119-127 (1998).

[Schmidt 2000] F.G. Schmidt, B. Hinner, and E. Sackmann, Microrheometry underestimates the values of the viscoelastic moduli in measurements on F-actin solutions compared to macrorheometry. *Phys Rev E Stat Phys Plasmas Fluids Relat Interdiscip Topics.* 61. 5646-5653 (2000).

[Snabre 1996] P. Snabre, and P. Mills, I. Rheology of Weakly Flocculated Suspensions of Rigid Particles. *Journal de Physique III.* 6. 1811-1834 (1996).

[Snabre 1999] P. Snabre, and P. Mills, Rheology of concentrated suspensions of viscoelastic particles. *Colloids and Surfaces A: Physicochemical and Engineering Aspects.* 152. 79-88 (1999).

[Storm 2005] C. Storm, J.J. Pastore, F.C. MacKintosh, T.C. Lubensky, and P.A. Janmey, Nonlinear elasticity in biological gels. *Nature.* 435. 191-194 (2005).

[Thurston 1972] G.B. Thurston, Viscoelasticity of human blood. *Biophys J.* 12. 1205-1217 (1972).

[Tomasek 2002] J.J. Tomasek, G. Gabbiani, B. Hinz, C. Chaponnier, and R.A. Brown, Myofibroblasts and mechano-regulation of connective tissue remodelling. *Nat Rev Mol Cell Biol.* 3. 349-363 (2002).

[Velegol 2001] D. Velegol, and F. Lanni, Cell traction forces on soft biomaterials. I. Microrheology of type I collagen gels. *Biophys J.* 81. 1786-1792 (2001).

[Verdier 2002] C. Verdier, Cours de viscoelasticité. *M1, Mécanique.* 35 pages (2002).

[Verdier 2003] C. Verdier, Review. Rheological properties of living materials: From cells to tissues. *J Theoretical Medicine.* 5. 67-91 (2003).

[Wagner 1990] N.J. Wagner, and W.B. Russel, Light scattering measurements of a hard-sphere suspension under shear. *Physics of Fluids A: Fluid Dynamics.* 2. 491-502 (1990).

[Wakatsuki 2000] T. Wakatsuki, M.S. Kolodney, G.I. Zahalak, and E.L. Elson, Cell mechanics studied by a reconstituted model tissue. *Biophys J.* 79. 2353-2368 (2000).

[Wozniak 1996] Z.M. Wozniak, Y. Usson, F. Parazza, P. Champelovier, D. Leroux, and D. Seigneurin, Quantitative analysis of three-dimensional distribution of AgNOR proteins during interphase in leukemic cells. *Cytometry.* 24. 14-26 (1996).

[Zhao 2006] M.S. Zhao, C.; Burgess, D.J. & Huey, B.D. , Rate- and depth-dependent nanomechanical behavior of individual living Chinese hamster ovary cells probed by atomic force microscopy. *J. Mater. Res. .* 21(8). 1906-1912 (2006).

[Zhu 1996] W. Zhu, J.C. Iatridis, V. Hlibczuk, A. Ratcliffe, and V.C. Mow, Determination of collagen-proteoglycan interactions in vitro. *J Biomech.* 29. 773-783 (1996).

Summary

We characterize the rheological properties of cell suspensions and tissues. The suspension concentration is varied over a wide range. CHO cell suspensions are used. In particular, we are able to characterize the flow properties of cells as well as their viscoelastic properties. The concentration-dependent yield stress and elastic plateau modulus are explained in the context of fractal aggregates under shear. These effects are related to intrinsic microscopic parameters.

Then a model tissue is constructed, by including the same cells in a collagen matrix. To characterize the structural changes, confocal microscopy is used. A new important feature is observed, which is the breakdown of the collagen network, due to the presence of cells. Indeed, cells elongate within the gel and can remodel it, in a concentration dependent manner: adhesion of cells is easier when collagen concentration increases, but space is reduced. These two mechanisms compete and can explain the behaviours observed.

Résumé

Les propriétés rhéologiques de suspensions cellulaires (CHO) et tissus sont étudiées. La concentration varie sur une large gamme. En particulier, nous avons caractérisé l'écoulement et les propriétés viscoélastiques. Le seuil d'écoulement et le module de plateau élastique varient avec la concentration et sont décrits par un modèle de structures fractales en écoulement. Ces effets sont reliés à des paramètres microscopiques.

Un tissu modèle est ensuite réalisé, en incluant ces cellules dans une matrice de collagène. Pour mesurer les changements structurels, la microscopie confocale est utilisée. Un phénomène nouveau est observé, la diminution de la rigidité du gel, en présence de cellules. En effet, les cellules s'allongent dans le gel et peuvent le remodeler, en fonction de la concentration : l'adhésion des cellules est facilitée lorsque la concentration en collagène est importante, mais l'espace est restreint. Ces deux effets s'opposent mais expliquent les comportements observés.